## INFORMATION TO USERS

This manuscript has been reproduced from the microfilm master. UMI films the text directly from the original or copy submitted. Thus, some thesis and dissertation copies are in typewriter face, while others may be from any type of computer printer.

**The quality of this reproduction is dependent upon the quality of the copy submitted.** Broken or indistinct print, colored or poor quality illustrations and photographs, print bleedthrough, substandard margins, and improper alignment can adversely affect reproduction.

In the unlikely event that the author did not send UMI a complete manuscript and there are missing pages, these will be noted. Also, if unauthorized copyright material had to be removed, a note will indicate the deletion.

Oversize materials (e.g., maps, drawings, charts) are reproduced by sectioning the original, beginning at the upper left-hand corner and continuing from left to right in equal sections with small overlaps. Each original is also photographed in one exposure and is included in reduced form at the back of the book.

Photographs included in the original manuscript have been reproduced xerographically in this copy. Higher quality 6" x 9" black and white photographic prints are available for any photographs or illustrations appearing in this copy for an additional charge. Contact UMI directly to order.

UMI

A Bell & Howell Information Company
300 North Zeeb Road, Ann Arbor MI 48106-1346 USA
313/761-4700 800/521-0600

Reproduced with permission of the copyright owner. Further reproduction prohibited without permission.

# NON-LINEAR FLOW IN POROUS MEDIA

by

SERGIO J. ROJAS

A Dissertation Submitted to the Graduate Faculty in Physics in Partial Fulfillment
of the Requirements for the Degree of Doctor of Philosophy
The City University of New York.
1998

UMI Number: 9820575

UMI
300 North Zeeb Road
Ann Arbor, MI 48103

This manuscript has been read and accepted for the Graduate Faculty in Physics in satisfaction of the dissertation requirement for the degree of Doctor of Philosophy.

1/15 98

Date Chairman of Examining Committee

1/15/98

Date Executive Officer

Prof. Andreas Acrivos

Prof. Herman Z. Cummins

Prof. Joseph L. Birman

Prof. Joel Koplik (Advisor)

Prof. Ronald Dickman

Supervisory Committee

**THE CITY UNIVERSITY OF NEW YORK**

# Abstract

## NON-LINEAR FLOW IN POROUS MEDIA

by

Sergio J. Rojas

Adviser: Professor Joel Koplik

Numerical solutions of the Navier-Stokes equations in two-dimensional quasi-periodic and quasi-isotropic random media were obtained to analyze the local and large scale aspects of finite Reynolds number flow. For Reynolds number less than one, the results show a first correction to Darcy's law which is cubic in the Darcy (averaged) velocity, while for Reynolds number greater than one, the results are in agreement with Forchheimer equation. That is, the correction to Darcy's law is quadratic in the average (Darcy) velocity. The cubic correction to Darcy's law support Mei and Auriault's (1991) theoretical study, based on *homogenization* theory. In addition, the results show support to an unifying empirical equation describing fluid flow in porous media of similar structure, first proposed by Beavers and Sparrow (1969). Also, the results show agreement, except by a multiplicative constant, with Sangani and Acrivos (1982) equation for the drag on dilute array of cylinders.

To my parents

# Acknowledgments

I would like to express my most sincere thanks to:

- Professor Joel Koplik for accepting me as his student, and for his financial support which allowed me to finish this work.
- The Benjamin Levich Institute of the City College of New York, under the direction of Professor Andreas Acrivos, where this work was done.
- INTEVEP, S.A., Research and Technological Support Center of Petróleos de Venezuela, S.A., for sponsoring my Doctoral studies through the program "Reto con Futuro".
- Cheryl Pahaham who had the patience to proofread this work.

# Contents

# List of Tables

# List of Figures

# Chapter 1

# Fluid Flow in Porous Media

## 1.1 Introduction

Fluid flow in porous media is a subject of widespread importance in areas such as: oil recovery, hydrology, agriculture, and chemical production processes. Examples of porous materials commonly found in everyday life include ordinary rocks, concrete, tissue paper, filter materials, and biological tissues (Scheidegger 1974; Dullien 1992).

In a general sense, the simplest and most important question to be inquired in a porous media flow is: what pressure drop is necessary in order to achieve a specific flow rate? In the limit of low fluid velocity or vanishing Reynolds number, more than a century of experimental studies and numerous convincing theoretical analyses have shown that Darcy's law (1856) describes with great precision the flow of fluid through a porous material. Therefore, for static and isotropic porous medium, the pressure drop ($\Delta P$) per unit length is then linear in the average flow velocity ($V$) with the fluid viscosity ($\mu$) divided by the permeability ($k$) of the porous medium as the proportionality factor. Darcy's law can be written in the form (Scheidegger 1974; Dullien 1992):

$$\nabla P = -(\frac{\mu}{k})\vec{V} \tag{1.1}$$

The permeability, or resistance to fluid flow, contains all of the dependence of the flow on the detailed structure of the porous material, and Darcy's law provides a simple empirical way to determine the medium's permeability.

At finite Reynolds number or high speed flow, however, the situation is far less clear. Only a relatively limited number of systematic experiments, and a few semi-empirical correlations can be found in the literature. Most studies only consider flows which are macroscopically one-dimensional, with constant average velocity. The available information supports the Forchheimer equation (1901) that considers a correction term to Darcy's law in which the pressure drop increases quadratically with the velocity. Thus, for one dimensional flows, the Forchheimer relation has the following form (Scheidegger 1974; Dullien 1992):

$$-\frac{\Delta P}{\Delta X} = (\frac{\mu}{k})V + b\rho V^2 \tag{1.2}$$

In words, this equation states that the flow resistance is the sum of a viscous resistance given by the linear term in V and the inertial resistance given by the quadratic term in V. This equation represents a competition between viscous forces and inertial forces in defining the flow resistance as the Reynolds number increases, in analogy with the well established fact that purely viscous flows around cylinders and spheres tend to disappear at $Re$ of order one and larger, when inertial forces dominate over viscous forces. However, the no-slip boundary condition at solid boundaries prevents the elimination of viscous effects around any object, even at very large values of $Re$. The coefficient ($b$) in equation (1.2) is an undefined parameter which, like the permeability (k), must be a function of the medium's geometry rather than a universal constant.

As was mentioned earlier, the available experimental work (Beavers and Sparrow 1969; Beavers et al. 1973, Macdonald et al. 1979, Dullien 1992) supports the validity of the Forchheimer's equation or any of its variants due to Burke & Plummer (1928) and Ergun (1952), which provide specific forms for the coefficients of the terms linear and quadratic in velocity. Moreover, some experimental investigations (Dybbs and

Edwards 1984, and references therein) indicate the existence of several flow regimes which can be roughly classified as follows: first, there is the Darcy (creeping) flow regime dominated by viscous forces at very low Reynolds number ($Re$). Then, starting at Reynolds number of about one, the influence of the non-linear term of the Navier-Stokes equations starts to be noticed by generating a non-linear laminar flow regime where the inertial forces become significant in the overall flow behavior and that is described, according to the analysis of the experimental data, by Forchheimer equation. After that, at larger values of the Reynolds number, an unsteady laminar flow regime has been observed and is characterized by the presence of laminar wake oscillations in the pores which take the form of traveling waves of distinct periods, amplitudes and growth rates. Finally, a highly unsteady and chaotic (turbulent) flow regime has been noticed for much higher Reynolds number. However, there is no consensus about the specific values of the Reynolds number between which each flow pattern can be found. The values of these transition Reynolds numbers are not unique, and seem to depend on the internal geometry of the porous media.

Although it is plausible that the quadratic nonlinearity in the Navier-Stokes equations generates the nonlinearity in the Forchheimer relation, there is no convincing, let alone rigorous, theoretical justification of any of these results. Nevertheless, some derivations of the Forchheimer equation can be found in the literature by using different theoretical approaches such as dimensional analysis, capillary models, and statistical theories (Ahmed and Sunada 1969; Bear 1972; Scheidegger 1974; Cvetkovic 1986; Dullien 1992, Whitaker 1996).

In the past two decades, a relatively new mathematical approach known as method of *homogenization* has successfully been applied in deriving, without cumbersome suppositions, the equations governing and characterizing many aspects of fluid flow through porous media, including Darcy's law (Sanchez-Palencia 1980, Keller

1980, Rubenstein and Torquato 1989, Hornung 1996). One of the merits of the *homogenization* approach is that, unlike other models, it provides a *microscale* boundary value problem for any constitutive coefficient that appears in the macroscopic law being derived. This boundary value problem can, in principle, be solved numerically (as in the work of Zick and Homsy 1982), and a complete macroscopic formulation of the initial problem can be given without assumption or hypothesis, which sometimes are hard to justify.

Based in a homogenization analysis, Mei and Auriault (1991) found a first correction to Darcy's law due to weak convective inertia of the pore fluid which, for an *isotropic* and *homogeneous* porous media, is cubic in the average (seepage or Darcy) velocity, while for the case of an *anisotropic* porous media, they found a quadratic term in the seepage velocity as leading correction term to Darcy's law. However, as pointed out by Mei and Auriault, they did not find any published experimental work supporting their cubic correction to Darcy's Law, mainly because such correction is predicted to be very small and the domain of validity of Darcy's law extends to Reynolds number not much smaller than unity.

In this work, we will use numerical solutions of the Navier-Stokes equations in two dimensional random and periodic media to obtain some qualitative insight into both the local and large scale aspects of finite Reynolds number flow in quasi-isotropic "samples" of porous media. Results will be presented which support the division of the non-linear inertial flow regime into two well defined regions: one where the correction to Darcy's law is dominated by a cubic correction term in the seepage (average) velocity, in agreement with the work of Mei and Auriault (1991), and a second region where the correction to Darcy's law is given by the Forchheimer equation. Finally, it should be mentioned that some of our results are in agreement with those found by Koch and Ladd (1997). In the rest of this chapter we will present a brief survey of some general ideas that have been useful in the understanding of the physics of complex systems, particularly in the area of fluid flow through porous media.

## 1.2 General Background

### 1.2.1 Permeability

The permeability $k$ is one of the most important transport coefficients of interest concerning porous materials, especially in the hydrology and oil industries. A knowledge of $k$ can be used to predict flow rate directly from Darcy's relation equation (1.1). Conversely, Darcy's equation provides the simplest and most precise direct way of knowing a medium's permeability (Darcy's law gives the operational definition of the permeability). However, direct measurements of $k$ are, in general, difficult and expensive. Therefore, it is desirable to have simple and inexpensive approaches for finding the permeability of a porous medium when detailed measurement and samples can not be obtained. Consequently, some theoretical models of porous medium structure have been devised which aim to predict good estimates of the macroscopic transport properties (long-scale behavior) of the medium from a knowledge of the small-scale dynamics. A commonly used semi-empirical relation for estimating permeability is the so-called Carman-Kozeny relation that relates $k$ to the porosity $\phi$ (fraction of the total volume occupied by the fluid) and the specific surface area based in solid's volume $S_o$ by the equation: $k = \frac{\phi^3}{k'(1-\phi)^2 S_o^2}$, where $k'$ is an adjustable parameter called the Kozeny constant (Scheidegger 1974; Dullien 1992). In addition, power laws relating $k$ with $\phi$ ($k \propto \phi^m, 1.3 < m < 4$) have been found or reinforced by using the network approach of porous media combined with effective medium and percolation theory ideas (Koplik 1982; Koplik et al. 1984; Chen and Koplik 1985; Dullien 1992; Matthews et al. 1993). Other calculations relating the permeability with the microscopic geometry of the medium have been carried out (Scheidegger 1974; Koplik et. al 1984; Lin et al. 1986; Thompson et al. 1987), and some insight about the appropriate length scales dominating the flow at the pores scales have been obtained (Johnson et al. 1986; Kostek et al. 1992; Martys and Garboczi 1992). Its relevance is based in the fact that $k$ has units of length squared and a dynamical length scale ($\ell$), based on the pore structure, can be used to define the permeability in the form $k = cF\ell^2$, where $F \equiv \frac{\sigma_f}{\sigma_0}$ is called the formation factor and $c$ is a constant scale factor; $\sigma_f$ is the conductivity of the conducting fluid (brine, for example) filling the porous matrix (considered as insulator) and $\sigma$ is the conductivity of the whole system. Furthermore, fractal ideas can be applied in order to study how and under what conditions the macroscopic properties of the system may be independent of its microscopic details. For instance, homogeneous porous media are characterized by well defined and unique pore-space properties such as porosity, pore size distribution and size independent transport properties (Adler 1992). In spite of these efforts of previous studies and their relative success in providing some insight about the deterministic behavior of flow through porous media, one should bear in mind that the complex structure of any porous material makes it very difficult to construct a general method for predicting the macroscopic transport properties of the medium. For example, it has been found that different rock samples with the same porosity have different transport properties, which may be a consequence of the history of the rock formation (Thompson et al. 1987).

### 1.2.2 Network Models and Effective Medium Theory

Roughly speaking, porous media consists of a solid matrix containing interconnected empty spaces constituted of throats (channels) and pores whose spatial distribution resembles an electrical random network. Consequently, porous media can be viewed as an electrical network (Fatt 1956; Koplik 1981; Koplik 1982; Bryant et al. 1993) of variable elements on which each node $\{i\}$ has an assigned voltage $\{v_i\}$ and the bonds $ij$, connecting node $\{i\}$ and node $\{j\}$, have an assigned random conductance $g_{ij}$. Non-existent bonds have $g_{ij} = 0$. Each bond has a current $I_{ij}$ satisfying the local equations:

$$I_{ij} = g_{ij}(v_i - v_j) \tag{1.3a}$$

$$\sum_{i \to j} I_{ij} = 0 \tag{1.3b}$$

The association with the fluid flow through a porous medium is accomplished by considering the nodes as the pores, the bonds as the throats connecting the pores, $v_i$ as the pressure at the pore $\{i\}$, $I_{ij}$ as a fluid flux, and the charge as the mass. The conductance $g_{ij}$ can be computed from the network geometry using, for instance, Poiseuille's law for cylindrical tubes (Fatt 1956; Kirkpatrick 1973; Koplik 1981; Koplik 1982). This idea can be illustrated by an example at low $Re$. Following Koplik et al. 1984, the calculation for the fluid flow problem involves the solution of the Stokes equations on each element (pores and throats) of the network and the match of the flow fields at the pore-throats boundaries. Neglecting the pore pressure drop, and considering the particular case of elliptically cylindrical throats of length (h) and semi-axis (a) and (b), it can be shown that the relation between the fluid flux and pressure drop across the throat $ij$ is given by the linear relation (Batchelor 1967; Happel and Brenner1983):

$$Q_{ij} = (\frac{g_{ij}}{\mu})(\Delta P)_{ij} \tag{1.4}$$

where $g_{ij} \equiv \frac{\pi a^3 b^3}{4h(a^2+b^2)}$ is the "conductance", function of the throat geometry only. In addition, mass conservation at the junctions (the pores) requires:

$$\sum_{i \to j} Q_{ij} = 0 \tag{1.5}$$

The analogy of equations (1.4) and (1.5) to equations (1.3$a$) and (1.3$b$) is rather clear. Furthermore, comparing equation (1.4), written in the form $A\mu(\frac{Q}{A}) = g(\frac{\Delta P}{h})h$, with equation (1.1), one can see that $k = (\frac{a}{A})h$ is the permeability of a solid matrix of cross section $A$ having one cylindrical pore on it.

Equations (1.3$a$) and (1.3$b$) can be rewritten in matrix form:

$$\mathbf{G} \cdot \mathbf{V} = \mathbf{S} \tag{1.6}$$

where $\mathbf{V} = (V_1, V_2, \cdots, V_n)^T$ is a column vector of nodes voltages, $\mathbf{G}$ is the conductance matrix, given by:

$$G_{ij} = \delta_{ij}(\sum_{k \to i} g_{ki}) - g_{ij} \tag{1.7}$$

and S containing the outside current supplied to nodes, usually through a prescribed voltage on two opposite edges of the network (Kirkpatrick 1973; Koplik 1981). The previous equations can be solved directly by setting up a set of cylindrical throats and finding the current(fluid flux) and voltages(pressure) everywhere and computing the over all permeability by using:

$$k = \mu(\frac{\frac{Q_{tot}}{A}}{\frac{\Delta P}{L}}) \tag{1.8}$$

where $Q_{tot}$, $\Delta P$, $A$, and $L$ are respectively the total flux, net pressure difference and cross sectional area and length of the sample. However, this would be awkward due to the amount of calculations that it involves. A better approach is provided by the so-called Effective Medium Approximation (EMA) which provides a more treatable recipe for computing the interesting unknown quantities in the network, based in the probability distribution function ($PDF$) of conductances that results from their random location in the network. The EMA recipe is as follows (Kirkpatrick 1973: Koplik 1981; Koplik et al. 1984; Koplik 1990): choose one conductor $g$ and suppose that the others random's $g$ of the network have been assigned a single effective medium value $g_m$. The voltage (pressure) across the distinguished conductance $g$ will differ from the field in the other conductances $g_m$ of the network by an amount depending on the particular value of $g$. This local fluctuation in the field is averaged over the probability distribution of $g$, and choosing $g_m$ such that the averaged fluctuation of the field is zero. This condition is satisfied by chosen $g_m$ as the solution of (Kirkpatrick 1973; Koplik 1981;Koplik 1990):

$$\langle\frac{(g_m - g)}{g + (\frac{\sigma}{2} - 1)g_m}\rangle_p = \int_0^\infty p(g)(\frac{(g_m - g)}{g + (\frac{\bar{\sigma}}{2} - 1)g_m})dg = 0 \qquad (1.9)$$

where $< \cdots >_p$ means average respect to $p(g)$, the PDF of local conductances $g$, and $\bar{\sigma}$ is the lattice average coordination number (number of bonds(throats) meeting at a node(pore)). Once $g_m$ is known, an "effective network" is obtained on which the averaged properties of the original flow problem remain unchanged. Each conductance of the "effective network" has the value $g_m$. Finally, the calculation of the over all permeability of the network can be found as follows (Koplik 1984): assume that an average pressure gradient $< \nabla P >$ across the network is produced by a fixed difference of pressure that is maintained at two ends of the network. Then, the total fluid flux across any plane **P** perpendicular to $< \nabla P >$ will be the sum of the individual fluxes $Q_b$ of each bond $b$ intercepting **P**. Each flux is $\frac{g_m}{\mu}$ times the pressure difference across the respective bond (see equation (1.4)). Therefore,

$$Q_{tot} = \sum_{b \bigcap \mathbf{P}} Q_b = \sum_{b \bigcap \mathbf{P}} (\frac{g_m}{\mu}) < \nabla p > \cdot \vec{L_b} \qquad (1.10)$$

where $\vec{L_b}$ is a vector in the direction of the bond $b$, with magnitude equal to the bond's length. The average velocity $\vec{V}$ is obtained dividing by the area $A(\mathbf{P})$ of the plane **P** ($\vec{V} = \frac{Q_{tot}}{A(\mathbf{P})}$), and using Darcy's law (equation (1.1)) the permeability is obtained to be:

$$k = g_m \langle \frac{1}{A(\mathbf{P})} \sum_{b \bigcap \mathbf{P}} \vec{L_b} \cdot \hat{n} \rangle \qquad (1.11)$$

where $\hat{n}$ is a unit vector along the pressure gradient, but to the extent that the material is statistically homogeneous and isotropic, any unit vector will do.

The comparison between EMA and the direct solutions of the matrix equation

(1.6) is accomplished by computing an effective bond conductance $g_{eff}$ by using:

$$g_{eff} = \frac{K(\{g_{ij}\})}{K(\{1\})} \tag{1.12}$$

where $K(\{g_{ij}\})$ is the overall conductance of the network with the randomly chosen $g_{ij}$ and $K(\{1\})$ is obtained by setting each $g_{ij} = 1$. The value of $K$ is computed by using:

$$K = \frac{I_{tot}}{V_L - V_R} \tag{1.13a}$$

$$I_{tot} = \sum_i (V_L - V_i) g_{iL} \tag{1.13b}$$

on which $V_L$ and $V_R$ represent the applied voltages to the left and right edges of a planar network (periodically boundary conditions is assumed on the other two edges). Then, to the extent that EMA is valid, it is expected that $g_{eff} = g_m$ (Koplik 1981). It has been found that satisfactory agreement (between 5% or better) is achieved, unless the PDF of conductances is near to the conduction threshold (appreciably near $g = 0$). Moreover, it was found that the details of $p(g)$, lattice size, and coordination number were irrelevant for the agreement. Consequently, EMA provides an inexpensive way to find the approximated averaged solutions of the network problem in relation to the considerable computation time required by a direct solution of equation (1.6) (Koplik 1981).

### 1.2.3 Percolation Theory

The network model of a porous media can be cast into the broad field of percolation theory (regular motion through a random medium), formally introduced in 1956 by Bradbent and Hammersley in order to study the spread of a hypothetical fluid through a random media. In some sense, percolation can be viewed as a theory that provides a probabilistic approach to study complex (disordered) systems where the connectedness properties of some components dominate the behavior of the system in consideration. Particular interest in percolation theory ideas in the field of fluid flow through porous materials may arise due to the similitude between scaling laws, characteristics of percolation problems, and some semi-empirical power-laws equations relating the transport coefficients (such as conductivity and permeability) with the porosity in flow through porous media. For instance, Archie's law links the conductivity and the porosity by a relation of the form: $\sigma = a\sigma_w\phi^m$, while $k = c\frac{\phi^3}{S_0^2}$ is the Kozeny equation that relates the permeability by a power of the porosity (Scheidegger 1974; Dullien 1992). These equations resemble the behavior in the usual percolation problem except that they suggest a threshold at $\phi = 0$. In addition, part of the understanding of the displacement and entrapment of one fluid by another in a porous matrix has been possible through the use of the so-called invasion percolation model (Lenormand and Boris 1980; Koplik and Lasseter 1985; Chen and Koplik 1985; Dullien 1992; Sahimi 1994).

Percolation models can be discrete or continuous. In general, discrete percolation problems are described in terms of d-dimensional grids divided in three main categories: bond, site and site-bond percolation problems. From the studies that have been carried out using these models, it seems that site percolation can be considered as more fundamental than bond percolation because it is always possible to convert a bond percolation problem into a site percolation problem in a different lattice (Shante and Kirkpatrick 1971; Stauffer 1992; Isichenko 1992).

For infinite lattice systems, the site(bond) percolation problem is defined by assigning a probability $p$ that any site(bond) be present in the network and, correspondingly, absent of the network with probability $1 - p$. Two nearest neighbor sites are connected if they are both occupied. A conglomeration of connected sites(bonds) bounded by vacant sites(bonds) is called a *cluster*. When $p$ is close to one, many sites(bonds) will be present and there should be a percolating cluster of sites(bonds) spanning the lattice in any direction. Conversely, when $p$ is small, only a few sites(bonds) will be present and it is expected to find only small isolates clusters with no connected path of sites(bonds) traversing the lattice in any direction. Consequently, there exists a critical(threshold) probability $p_c$, such that for $p < p_c$ there is no percolating cluster, while for $p > p_c$ it is ensured by the *fundamental theorem of percolation* that there will be only one percolating cluster (Kikuchi 1970; Newman and Schulman 1981). Monte-Carlo simulations and series expansion calculations together with some exact results, suggest that the critical percolation probability, for the case of bond percolation in planar and three-dimensional lattice, can be approximated by $p_c(b) \cong \frac{d}{(d-1)\sigma}$ (Ziman 1968; Kyazym-zade 1992), where $d$ represents the space dimensionality and $\sigma$ is the lattice coordination number (number of bonds meeting at a node). In the case of site percolation, the situation seems to be a little more complicated. Calculations on the square and the cubic lattice suggest that $p_c(s) = \frac{1}{2d-2}$, while for higher spatial dimensions, the results point in favor of having $p_c(s) = \frac{1}{2d-1}$. In general, $p_c(s) > p_c(b)$ (Essam 1980, Stauffer 1992).

In addition to the probability percolation threshold, it is also of interest to know whether a particular site(bond) is contained in the percolating (infinite) cluster. Hence, a probability $P(p)$ can be defined in order to describe such situation. For $p < p_c$ no percolating cluster exists, therefore $P(p) \equiv 0$. Just above $p_c$, it has been found that $P(p)$ follows the scaling behavior (Shante and Kirkpatrick 1971; Essam 1980;Stauffer 1992; Isichenko 1992):

$$P(p) \sim |p - p_c|^{-\beta} \tag{1.14}$$

where $\beta$ is one of the standard universal critical exponents that govern the behavior of different quantities near a critical point (Domb et al. 1972-1988). It depends only on the spatial dimension of the problem. In 2-dimensions(2D), $\beta = \frac{5}{36}$, while $\beta \cong 0.41$ in 3-dimensions(3D) (Stauffer 1992; Isichenko 1992). Similar behavior has been observed by the so-called *correlation length* $\xi$ of the problem, which represents the typical radius of the connected cluster for $p < p_c$. That is, it is the maximum size above which the clusters are exponentially rare. In addition, the correlation length $\xi$ can be considered as the length scale over which the percolating network is macroscopically homogeneous for $p > p_c$. In other words, for length scales $L$ larger than $\xi$, the system will be macroscopically homogeneous, while for length scales smaller than $\xi$ the system will not be homogeneous and its macroscopic properties will depend on $L$. Furthermore, at $p \cong p_c$, the correlation length $\xi$ becomes very large (being infinity at $p \equiv p_c$) and therefore, it will be the only characteristic length of the system in terms of which all other lengths should be measured (i.e. the system will be invariant under scale transformation because it does not have characteristic length). Defining by $g(r - r')$ the probability that points $r$ and $r'$ be connected by bonds, then, for large $|r - r'|$ and $p < p_c$ (Huang 1987):

$$g(r - r') \sim e^{-\frac{|r-r'|}{\xi}} \qquad (1.15)$$

while

$$\xi(p) \sim |p - p_c|^{-\nu} \quad p \cong p_c + 0^+ \qquad (1.16)$$

where $\nu$ is another universal exponent. It can be seen from (1.15) that regions separated by distances greater than the correlation length are essentially independent. In 2D $\nu = \frac{4}{3}$ and $\nu \cong 0.88$ in 3D.

Bond percolation can be illustrated by a random resistor network, where $p_c(b)$ separates a conductive phase from an insulating one. An example of site percolation may be a mixture of magnets and paramagnets. At $p_c(s)$ the system changes from a paramagnet to a magnet. One speaks of *site-bond* percolation model when both sites and bonds have, in general, unrelated occupancy probabilities $p_s$ and $p_b$ respectively. If $p_s = 1$( or $p_b = 1$), *site-bond* percolation reduces to bond (site) percolation. *Site-bond* can be used to study gelation and epidemic processes in diluted media

(Herrmann 1986).

Perhaps, the most realistic percolation model proposed to study natural phenomena is the so-called *continuum* percolation model, where the position of a random distribution of at least two kinds of components is not restricted to the discrete sites of a regular lattice. This model can be illustrated by randomly punching holes in a sheet of conducting material. More sophisticated models have been devised for modeling porous materials. It should be mentioned that all of the proposed percolation models predict a *universal* non-zero critical value for the porosity above which fluid could flow through the porous sample and that has not been observed.

Other applications of percolation theory to the realm of fluid flow through porous media are exemplified by its usefulness in studying: the transport of a dynamically neutral tracer injected into a fluid flowing in a porous medium (Koplik et al. 1988); the displacement, by capillary forces, of one immiscible fluid by another immiscible fluid, for example oil displaced by water (Chandler et al. 1982; Koplik and Lasseter 1985; Chen and Koplik 1985); the permeability of porous rocks (Wong et al. 1984; Thompson et al. 1987). Further and more detailed accounts of the applications and usefulness of percolation theory in describing a variety of disordered systems in others areas, as well as discussions of the extension of percolation theory in order to be applied to study finite and/or continuous systems, can be found in the reviews of Bunde and Havlin 1991; Stauffer 1992; Sahimi 1994.

# Chapter 2

# Homogenization, Multiple Scales Expansions, and Equations of Porous Media Flow

## 2.1 Introduction

Homogenization, a relatively new technique developed by mathematicians to study partial differential equations with rapidly oscillating coefficients (Bensoussan et all. 1978; Sanchez-Palencia 1980; Bakhvalov and Panasenko 1989), can be used in conjunction with the perturbative technique known as *Multiple Scale Analysis* (*expansions*) (Nayfeh 1973; Van Dyke 1975; Kevorkian and Cole 1996) in order to derive "homogenized" or averaged equations from more complicated ones. In particular, homogenization seems to be the most reliable tool used to obtain results consistent with the Navier-Stokes equations in an overall (macroscopic) sense without attempting to obtain detailed information of the field variables (velocity and pressure) everywhere in the domain of interest. For instance, Darcy's law, which represents a macroscopic balance of volumetric flow rates and global pressure gradient through a porous material at very low Reynolds number, is an example of an averaged equation which can be rigorously derived, without cumbersome suppositions, by applying the homogenization technique to the more complicated Navier-Stokes equations (Keller 1980; Rubenstein and Torquato 1989; Koplik 1990).

In deriving the equations governing the flow of fluid through porous media, the method takes into account the existence of two well defined contrasting length scales: the typical pore size $\ell$ representing a non-interesting short scale of variation which is to be eliminated, and the macro-scale $L$ that characterizes the averaged flow and represents the interesting long (macroscopic) scale of variation which is to be retained. As a consequence, two dimensionless space variables can then be naturally introduced: $\vec{x}^{\star}/L$, representing a *slow* (macroscopic) variable, and $\vec{x}^{\star}/\ell$, representing a *fast* (microscopic) variable. Both dimensionless quantities are related by the small parameter $\epsilon$ ($\epsilon \equiv \frac{\ell}{L} \ll 1$), in powers of which one may want to expand the variables of the original equation(s) when applying perturbation methods. The particular case of two well differentiated scales can also be found in numerous problems in mechanics where perturbation methods are the only suitable approach for finding satisfactory results that are amenable to further analysis (Cole 1968; Nayfeh 1973; Van Dyke 1975; Kevorkian and Cole 1996). Thus, starting from a "microscopic" description of a problem, one seeks a macroscopic, effective, description of it.

Phenomena characterized by the presence of a diversity of length scales seems to be one of the most conspicuous property of nature. Illustrative examples are given by ocean currents that persist for thousands of kilometers, ocean waves that range in size from less than a centimeter to several meters, and the great variety of granular materials, usually composed of particles of different sizes, found in our daily lives (Wilson 1979, Jaeger *et all.* 1996). In some cases, events distinguished by a great disparity in size have little influence on one another, and the phenomena associated with each scale can be treated independently. An example is the famous problem associated with low Reynolds number flow around an infinite cylinder (Stokes paradox) first solved by Oseen in 1910, and then, in 1956, by Proudman and Pearson using a somewhat, at that time, new perturbative approach known as *Matched Asymptotic Expansions*. The idea is that near the wall of the cylinder, the flow is described by a set of equations and boundary conditions which are essentially different from the ones governing the flow far from the wall. Each situation can be solved independent of the other, and the matching of both solutions at a certain distance (boundary layer) from the cylinder wall is then applied in order to have a uniform valid solution in the domain of interest (Van Dyke 1975). In contrast, *Multiple Scale Analysis* is a more general method which, in addition to the situations just described, can, in principle, be applied in the study of phenomena involving several physical processes evolving simultaneously in their own scales with each one influencing the overall (macroscopic) behavior of the phenomena in consideration. That is, fluctuations over all length scales are important.This situation is well illustrated by the behavior of a substance near its critical point where the scale of large density fluctuations becomes infinite, but the smaller fluctuations are in no way diminished (Wilson 1979). *Multiple Scale Analysis* is a so powerful technique that sometimes it is convenient to temporarily introduce, in an arbitrary thought way, the parameter $\epsilon$ into a difficult problem having no small parameters (Bender and Orstag 1978; Murdock 1991).

## 2.2 The Homogenization Method

The basic idea for the application of the homogenization technique is as follows (Keller 1980; Allaire 1992; Rubinstein and Torquato 1989). Assume we want to solve a physical problem which can be formulated in terms of partial differential equations with periodically oscillating coefficients with period $\epsilon$ (i.e.. heat conduction in a periodic composite medium), complemented by appropriate boundary conditions in some domain $\mathbf{D}$. Representing by $\mathbf{g}$ the partial differential operator and $\mathbf{u}$ the respective solution with a source $\mathbf{f}$, we have:

$$\mathbf{g} \cdot \mathbf{u} = \mathbf{f} \quad in \quad \mathbf{D}. \tag{2.1}$$

Assuming that the solution $\mathbf{u}$ converges to a limit $\mathbf{U}$, we look for a homogenized operator $\mathbf{G}$, such that $\mathbf{U}$ is the solution of:

$$\mathbf{G} \cdot \mathbf{U} = \mathbf{f} \quad in \quad \mathbf{D}. \tag{2.2}$$

Homogenization occurs in the steps leading from (2.1) to (2.2). The determination of the precise form of the homogenized operator $\mathbf{G}$ can be achieved through the application of the *Multiple Scale Analysis* perturbation technique. In particular, the so-called two-scales asymptotic expansion has been successfully applied to many problems involving fluid flow in porous media (Sanchez-Palencia1980; Bakhvalov and Panasenko 1989; Hornung 1996). A version of the method starts by identifying two (or more) well differentiated scales $\mathbf{x}$ and $\mathbf{y}$ related by a relation of the form $\mathbf{y} = \mathbf{x}/\epsilon$, with $\epsilon \ll 1$, and then postulating the following ansatz for $\mathbf{u}$:

$$\mathbf{u} = \mathbf{u}_0(\mathbf{x}, \mathbf{y}) + \epsilon \mathbf{u}_1(\mathbf{x}, \mathbf{y}) + \epsilon^2 \mathbf{u}_2(\mathbf{x}, \mathbf{y}) + \epsilon^3 \mathbf{u}_3(\mathbf{x}, \mathbf{y}) + \cdots \tag{2.3}$$

where each term $\mathbf{u}_i(\mathbf{x}, \mathbf{y})$ is considered to be periodic in $\mathbf{y}$ if the problem involves periodically oscillating operators.

Inserting (2.3) into (2.1) and collecting powers of $\epsilon$ leads to a set of equations for each term $\mathbf{u}_i(\mathbf{x}, \mathbf{y})$. Generally, the average with respect to $(\mathbf{y})$ of the corresponding equation for $\mathbf{u}_0(\mathbf{x}, \mathbf{y})$ leads to equation (2.2), and the precise form of $\mathbf{G}$ is computed with the so-called cell equation in the unit period (Bensoussan et all. 1978; Sanchez-Palencia 1980; Bakhvalov and Panasenko 1989). It should be noted, however, that the implementation of the method is not straightforward and mechanical as the recipe of its application may suggest. An arbitrary, not well thought selection of the scaling powers of $\epsilon$ may result in a set of inconsistent (unsolvable) equations. Therefore, a clear understanding of what is being sought is necessary for guessing the correct forms of the perturbative expansions which will lead to a satisfactory application of the procedure. After all, successful application of perturbation techniques is considered an art that involves a lot of ingenuity.

The theory of homogenization has been successfully applied in branches of applied physics involving composite media and micro-scale heterogeneities, in areas such as suspensions, sedimentation, plasticity, etc. (Sanchez-Palencia 1980; Bakhvalov and Panasenko 1989; Hornung 1996). Although homogenization has been mainly applied to problems with periodic structures, it is not restricted to those particular cases and can be applied to any kind of disordered media.

## 2.3 Equations governing flow through porous media

### 2.3.1 Navier-Stokes equations in dimensionless form

Before applying the homogenization approach to the set of equations governing a particular phenomena one needs to specify the equations in dimensionless form. This may allow the identification of dimensionless combinations of independent parameters that dominate the solution of the set of equations describing the physical process in consideration. For the case of the Navier-Stokes equations, such dimensionless quantity turns out to be the familiar fluid dynamics parameter known as the Reynolds Number, which is a measure of the strength of the fluid's inertia force relative to the fluid's viscous force.

To nondimensionalize the steady Navier-Stokes equations one should identify the appropriate length scale ($\mathcal{L}$) representing the physical distance over which the velocity changes by an amount proportional to the typical magnitude of the fluid velocity in the flow domain ($U$). In general, by setting $\vec{x^\star} = \mathcal{L}\vec{x}$, $p^\star(\vec{x^\star}) = \Delta P p(\vec{x})$, and $\vec{u}^\star(\vec{x}^\star) = U\vec{u}(\vec{x})$, the dimensional steady Navier-Stokes equations:

$$\begin{aligned} \rho(\vec{u}^\star(\vec{x}^\star) \cdot \nabla^\star)\vec{u}^\star(\vec{x}^\star) &= -\nabla^\star p^\star(\vec{x}^\star) + \mu {\nabla^\star}^2 \vec{u}^\star(\vec{x}^\star) \\ \nabla^\star \cdot \vec{u}^\star(\vec{x}^\star) &= 0 \end{aligned} \tag{2.4}$$

can be written in dimensionless form:

$$\begin{aligned} (\frac{\rho U^2}{\Delta P})(\vec{u}(\vec{x}) \cdot \nabla)\vec{u}(\vec{x}) &= -\nabla p(\vec{x}) + (\frac{\mu U}{\Delta P})(\frac{1}{\mathcal{L}})\nabla^2 \vec{u}(\vec{x}) \\ \nabla \cdot \vec{u}(\vec{x}) &= 0 \end{aligned} \tag{2.5}$$

At this point, the characteristic quantities $\mathcal{L}$, $\Delta P$, and $U$ are completely general and need to be associated with their respective counterparts in any specific problem. For fluid flow in porous media, it seems reasonable to consider that global variations in pressure $(\frac{\Delta P}{L})$, applied at the ends of the porous sample of length $(L)$, induce velocity variations at the pore scale $(\ell)$. In turn, this consideration provides a relation between $L$, $\ell$, $\Delta P$, and $U$ given by:

$$\frac{\Delta P}{L} = \frac{\mu U}{\ell^2} \tag{2.6}$$

However, it is still necessary to relate $U$ with a characteristic velocity in the flow, which can be chosen to be the Darcy (superficial) velocity $< \vec{u}(\vec{x}) >$ defined as the *mass flow rate* across a cross section of the porous media sample perpendicular to the macroscopic flow direction. With these considerations, one can arrives at the following dimensionless form of the steady Navier-Stokes equations:

$$\begin{aligned} (\frac{\rho < \vec{u}(\vec{x}) > \ell}{\mu})(\tfrac{\ell}{L})(\vec{u}(\vec{x}) \cdot \nabla)\vec{u}(\vec{x}) &= -\nabla p(\vec{x}) + (\frac{\ell}{\mathcal{L}})(\tfrac{\ell}{L})\nabla^2 \vec{u}(\vec{x}) \\ \nabla \cdot \vec{u}(\vec{x}) &= 0 \end{aligned} \tag{2.7}$$

Furthermore, there are two obvious possible choices for $\mathcal{L}$: the pore scale $(\ell)$ or the porous sample length $(L)$. Each choice defines a particular framework of analysis that may lead to a solvable set of equations when applying the homogenization process (Auriault 1991). If $\mathcal{L}$ is chosen to be equal to $(L)$, we will be adopting what can be called the *macroscopic* framework of analysis which implies the introduction of a new variable $\vec{y} = \vec{x^\star}/\ell = (\mathcal{L}/\ell)\vec{x} = \vec{x}/\epsilon$, $\epsilon \equiv \ell/L$. After the introduction of these new variables, the application of the homogenization process requires the expansion of the field variables in terms of functions of the new variables as in equation (2.3). This in turn implies, by applying the chain rule, the replacement of the operators $\nabla$ and $\nabla^2$ by:

$$\begin{aligned} \nabla &\to \nabla_{\vec{x}} + \frac{1}{\epsilon}\nabla_{\vec{y}} \\ \nabla^2 \equiv \nabla\cdot\nabla &\to \nabla^2_{\vec{x}} + \frac{1}{\epsilon}(\nabla_{\vec{x}}\cdot\nabla_{\vec{y}} + \nabla_{\vec{y}}\cdot\nabla_{\vec{x}}) + (\frac{1}{\epsilon})^2\nabla^2_{\vec{y}} \end{aligned} \tag{2.8}$$

where the subindex $\vec{x}$ or $\vec{y}$, labeling the Gradient or Laplacian operators, stand for derivation respect to the spatial variables $(x_1, x_2, x_3)$ or $(y_1, y_2, y_3)$ respectively. In this approach, $\vec{y}$ represents the microscopic or rapidly varying scale which is to be eliminated, while $\vec{x}$ represents the macroscopic or slowly varying scale which is to be retained. In addition, after applying $(\mathcal{L} = L)$, the dimensionless form of the Navier-Stokes equations (2.7) reads:

$$\begin{aligned} \epsilon Re(\vec{u}(\vec{x})\cdot\nabla)\vec{u}(\vec{x}) &= -\nabla p(\vec{x}) + \epsilon^2\nabla^2\vec{u}(\vec{x}) \\ \nabla\cdot\vec{u}(\vec{x}) &= 0 \end{aligned} \tag{2.9}$$

where $Re$ represent the Reynolds number given by (after using relation (2.6) with $U \equiv < \vec{u}(\vec{x}) >$):

$$Re \equiv \frac{\rho < \vec{u}(\vec{x}) > \ell}{\mu} = \epsilon\frac{\rho\Delta P\ell^2}{\mu^2} \tag{2.10}$$

On the other hand, the *microscopic* framework of analysis is adopted by choosing $\mathcal{L}$ to be equal to the pore scale $(\ell)$. In this case, consistency in the application of the homogenization process is obtained by introducing a new variable $\vec{y} = \vec{x^\star}/L = (\mathcal{L}/L)\vec{x} = \epsilon\vec{x}$, and replacing, as required by homogenization, the $\nabla$ and $\nabla^2$ operators by:

$$\begin{aligned} \nabla &\to \nabla_{\vec{x}} + \epsilon\nabla_{\vec{y}} \\ \nabla^2 \equiv \nabla\cdot\nabla &\to \nabla^2_{\vec{x}} + \epsilon(\nabla_{\vec{x}}\cdot\nabla_{\vec{y}} + \nabla_{\vec{y}}\cdot\nabla_{\vec{x}}) + \epsilon^2\nabla^2_{\vec{y}} \end{aligned} \tag{2.11}$$

In this context, the roles of $\vec{y}$ and $\vec{x}$ are reversed with respect to their definitions in the *macroscopic* framework of analysis. That is, $\vec{x}$ represents the microscopic or rapidly varying scale which is to be eliminated, while $\vec{y}$ represents the macroscopic or slowly varying scale which is to be retained. Moreover, the application of the choice ($\mathcal{L} = \ell$) to the dimensionless form of the Navier-Stokes equations (2.7) leads to the also dimensionless form of such equations:

$$\begin{aligned} \epsilon Re(\vec{u}(\vec{x}) \cdot \nabla)\vec{u}(\vec{x}) &= -\nabla p(\vec{x}) + \epsilon \nabla^2 \vec{u}(\vec{x}) \\ \nabla \cdot \vec{u}(\vec{x}) &= 0 \end{aligned} \tag{2.12}$$

with $Re$ defined as in equation (2.10).

Which framework of analysis (*macroscopic* or *microscopic*) should be adopted seems to be a matter of trial and error. The *microscopic* approach seems to be the most suitable for obtaining the governing equations of fluid flow through porous media. Notice that in the case where only one length scale is important (meaning that $\mathcal{L} \equiv \ell \equiv L$, and $\epsilon \equiv 1$), the previous equations (2.9) and (2.12) reduce to the familiar dimensionless form of the steady Navier-Stokes equations appropriated for analyzing low Reynolds number flow (Bachelor 1967, Tritton 1992):

$$\begin{aligned} Re(\vec{u}(\vec{x}) \cdot \nabla)\vec{u}(\vec{x}) &= -\nabla p(\vec{x}) + \nabla^2 \vec{u}(\vec{x}) \\ \nabla \cdot \vec{u}(\vec{x}) &= 0 \end{aligned} \tag{2.13}$$

where now the Reynolds number is given by $Re = (\frac{\rho <U> L}{\mu})$.

## 2.3.2 Derivation of Darcy's Law

In the limit of vanishing Reynolds number, Darcy's law (1.1) describes fluid flow through porous media with great precision. This fact together with the linearity of such relation suggest that the derivation of this important macroscopic relation could be obtained by the application of the homogenization technique to the steady Stokes equations which are obtained by dropping the non-linear inertial term in the general Navier-Stokes equations (2.13). Therefore, in the *microscopic* framework of analysis, the dimensionless form of the steady Stoke's equations can readily be obtained by dropping the left hand side of the equations (2.12), and can be written in the form:

$$\epsilon\nabla^2\vec{u}(\vec{x}) - \nabla p(\vec{x}) = 0 \tag{2.14a}$$

$$\nabla\cdot\vec{u}(\vec{x}) = 0 \tag{2.14b}$$

one seeks solution of the form:

$$\begin{aligned}\vec{u}(\vec{x}) &\to \vec{u}_0(\vec{x},\vec{y}) + \epsilon\vec{u}_1(\vec{x},\vec{y}) + \epsilon^2\vec{u}_2(\vec{x},\vec{y}) + \epsilon^3\vec{u}_3(\vec{x},\vec{y}) + \cdots\\ p(\vec{x}) &\to p_0(\vec{x},\vec{y}) + \epsilon p_1(\vec{x},\vec{y}) + \epsilon^2 p_2(\vec{x},\vec{y}) + \epsilon^3 p_3(\vec{x},\vec{y}) + \cdots\end{aligned} \tag{2.15}$$

Now, inserting (2.15) and (2.11) into (2.14), and collecting powers of $\epsilon$, the incompressibility (2.14*b*) condition yields the following equation as leading order terms:

$$\nabla_{\vec{x}}\cdot\vec{u}_0(\vec{x},\vec{y}) = 0 \tag{2.16a}$$

$$\nabla_{\vec{y}}\cdot\vec{u}_0(\vec{x},\vec{y}) + \nabla_{\vec{x}}\cdot\vec{u}_1(\vec{x},\vec{y}) = 0 \tag{2.16b}$$

while the momentum equation (2.14*a*) yields:

$$\nabla_{\vec{x}}p_0(\vec{x},\vec{y}) = 0 \quad\to\quad p_0(\vec{x},\vec{y}) = P(\vec{y}) \tag{2.17a}$$

$$\nabla_{\vec{x}}^2\vec{u}_0(\vec{x},\vec{y}) = \nabla_{\vec{x}}p_1(\vec{x},\vec{y}) + \nabla_{\vec{y}}P(\vec{y}) \tag{2.17b}$$

To proceed, it is necessary to average out the fluctuations at the pore scale ($\vec{x}$). To do that, the following average is defined:

$$\langle g\rangle_{\vec{x}} \equiv \frac{1}{V}\int_{V_f} g\; d^3x \tag{2.18}$$

which is taken over a large total volume $V$ in $\vec{x}$ with $V_f$ representing the volume available to the fluid phase. The volume $V$ can be taken as the volume of a period of the unit cell representing the porous sample in case of dealing with periodic structures. In the case of a random media, equation (2.18) represent an average over an ensemble of representatives realizations of the porous medium.

Then, averaging equation (2.16$b$) over an ensemble of realizations of the porous medium on the micro-scale ($\vec{x}$), and defining $\vec{U}(\vec{y}) \equiv \langle \vec{u}_0(\vec{x}, \vec{y}) \rangle_{\vec{x}}$ one obtains:

$$\nabla_{\vec{y}} \cdot \vec{U}(\vec{y}) + \langle \nabla_{\vec{x}} \cdot \vec{u}_1(\vec{x}, \vec{y}) \rangle_{\vec{x}} = 0 \tag{2.19}$$

By assuming that the ensemble average is stationary on the x-scale ( meaning that the averages are x-independent), the second term is given by:

$$\langle \nabla_{\vec{x}} \cdot \vec{u}_1(\vec{x}, \vec{y}) \rangle_{\vec{x}} \equiv \frac{1}{V} \int_{V_f} d^3x \nabla_{\vec{x}} \cdot \vec{u}_1(\vec{x}, \vec{y}) = \langle \frac{1}{V} \left[ \int_{\partial V} + \int_{\partial V_i} \right] d\vec{S}(\vec{x}) \cdot \vec{u}_1(\vec{x}, \vec{y}) \rangle \tag{2.20}$$

where the average is taken over a large volume $V$ in $x$, with outer boundary $\partial V$ and internal grain boundaries $\partial V_i$. In the last equation $S \propto V^{2/3}$, then the first term is $O(V^{-1/3})$ and is negligible as $V \to \infty$. Moreover, the second term vanished identically because $\vec{u}_1(\vec{x}, \vec{y}) = 0$ on the boundaries $\partial V_i$. Consequently, $\langle \nabla_{\vec{x}} \cdot \vec{u}_1(\vec{x}, \vec{y}) \rangle_{\vec{x}} = 0$ and therefore,

$$\nabla_{\vec{y}} \cdot \vec{U}(\vec{y}) \equiv \nabla_{\vec{y}} \cdot \langle \vec{u}_0(\vec{x}, \vec{y}) \rangle_{\vec{x}} = 0 \tag{2.21}$$

By the same token, $\langle \nabla_{\vec{x}} \cdot \vec{u}_0(\vec{x}, \vec{y}) \rangle_{\vec{x}} = 0$ and the average of equation (2.16$a$) lead to an identity $(0 = 0)$.

On the other hand, the solution of the momentum equation (2.17$b$) can be written in the form:

$$\vec{u}_0(\vec{x}, \vec{y}) = -\overset{\leftrightarrow}{w}(\vec{x}, \vec{y}) \cdot \nabla_{\vec{y}} P(\vec{y}) \tag{2.22a}$$

$$p_1(\vec{x}, \vec{y}) = -\vec{\pi}(\vec{x}, \vec{y}) \cdot \nabla_{\vec{y}} P(\vec{y}) \tag{2.22b}$$

where $\overset{\leftrightarrow}{w}(\vec{x}, \vec{y})$ and $\vec{\pi}(\vec{x}, \vec{y})$ are solution of the following boundary value problem, obtained after plugging (2.22$a$) into (2.17$b$) and (2.16$a$):

$$\begin{aligned} \nabla^2_{\vec{x}} \overset{\leftrightarrow}{w}(\vec{x}, \vec{y}) &= \nabla_{\vec{x}} \vec{\pi}(\vec{x}, \vec{y}) - \overset{\leftrightarrow}{I} \\ \nabla_{\vec{x}} \cdot \overset{\leftrightarrow}{w}(\vec{x}, \vec{y}) &= 0 \end{aligned} \tag{2.23}$$

or in components:

$$
\begin{aligned}
\nabla^2_{\vec{x}} w_{ij} &= \frac{\partial \pi_j}{\partial x_i} - \delta_{ij} \\
\frac{\partial w_{ij}}{\partial x_i} &= 0
\end{aligned}
\tag{2.24}
$$

with boundary condition $\overleftrightarrow{w}\,(\vec{x},\vec{y}) = 0$ on $\partial V_i$. Averaging equation (2.22$a$) gives:

$$\vec{U}(\vec{y}) = -\langle \overleftrightarrow{w}(\vec{x},\vec{y})\rangle_{\vec{x}} \cdot \nabla_{\vec{y}} P(\vec{y}) \equiv -\overleftrightarrow{K}(\vec{y}) \cdot \nabla_{\vec{y}} P(\vec{y}) \tag{2.25}$$

This is the equation we were looking for (Darcy's relation), which is to be supplemented by the incompressibility condition given by equation (2.21). Also, equations (2.21) and (2.25) lead to:

$$\nabla_{\vec{y}} \cdot (\overleftrightarrow{K}(\vec{y}) \cdot \nabla_{\vec{y}} P(\vec{y})) = \frac{\partial}{\partial y_i}\left(K_{ij}\frac{\partial P}{\partial y_j}\right) = 0 \tag{2.26}$$

The permeability tensor $\overleftrightarrow{K}(\vec{y}) = \langle \overleftrightarrow{w}(\vec{x},\vec{y})\rangle_{\vec{x}}$ is defined by the boundary value problem (2.24) and can be proved to be positive definite and symmetrical (Sanchez-Palencia 1980). For the special case where the medium is statistically homogeneous and isotropic, the permeability tensor takes the usual form $\overleftrightarrow{K}(\vec{y}) = k\overleftrightarrow{I}$, with $k$ constant.

Dimensional form of Darcy's relation can be obtained from its dimensionless form (2.25) by using equation (2.6) together with the fact that $\vec{y} = \vec{x^\star}/L$, $P^\star(\vec{x^\star}) = \Delta P P(\vec{y})$, and $\vec{U^\star}(\vec{x^\star}) = U\vec{U}(\vec{y})$. With this considerations one obtains:

$$\vec{U^\star}(\vec{x^\star}) = -\frac{1}{\mu}\overleftrightarrow{K}^\star(\vec{x^\star}) \cdot \nabla^\star P^\star(\vec{x^\star}) \tag{2.27}$$

with $\overleftrightarrow{K}^\star(\vec{x^\star}) = \ell^2 \overleftrightarrow{K}(\vec{x^\star}/L)$, which suggests the use of the square root of the permeability as the characteristic length representing the pore scale.

### 2.3.3 First Correction to Darcy's Law

In order to find corrections to Darcy's Law in the limit of vanishing (but finite) Reynolds number, Mei and Auriault (1991) considered the situation in which the

Reynolds number (2.10) is in the interval $\epsilon \ll Re \ll 1$. In particular, they took $Re = O(\sqrt{\epsilon})$ in (2.12) obtaining (after using $\epsilon = \beta^2$):

$$\beta^3(\vec{u}(\vec{x}) \cdot \nabla)\vec{u}(\vec{x}) = -\nabla p(\vec{x}) + \beta^2\nabla^2\vec{u}(\vec{x}) \qquad (2.28a)$$

$$\nabla \cdot \vec{u}(\vec{x}) = 0 \qquad (2.28b)$$

supplemented by the no-slip boundary condition ($\vec{u}(\vec{x}) = 0$) at each solid surface. Consequently, the application of the homogenization technique proceeds, following Mei and Auriault (1991), by introducing $\vec{y} = \beta^2\vec{x}$ and considering :

$$\begin{aligned} \vec{u}(\vec{x}) &\rightarrow \vec{u}_0(\vec{x},\vec{y}) + \beta\vec{u}_1(\vec{x},\vec{y}) + \beta^2\vec{u}_2(\vec{x},\vec{y}) + \beta^3\vec{u}_3(\vec{x},\vec{y}) + \cdots \\ p(\vec{x}) &\rightarrow p_0(\vec{x},\vec{y}) + \beta p_1(\vec{x},\vec{y}) + \beta^2 p_2(\vec{x},\vec{y}) + \beta^3 p_3(\vec{x},\vec{y}) + \cdots \end{aligned} \qquad (2.29)$$

Now, by applying equations (2.11), with $\epsilon$ changed by $\beta$, and (2.29) to equation (2.28) and collecting powers of $\beta$, one obtains up to order $O(\beta^4)$ from (2.28*a*):

$$-\nabla_{\vec{x}} p_0(\vec{x},\vec{y}) = 0 \qquad (2.30a)$$

$$-\nabla_{\vec{x}} p_1(\vec{x},\vec{y}) = 0 \qquad (2.30b)$$

$$-\nabla_{\vec{y}} p_0(\vec{x},\vec{y}) - \nabla_{\vec{x}} p_2(\vec{x},\vec{y}) + \nabla^2_{\vec{x}}\vec{u}_0(\vec{x},\vec{y}) = 0 \qquad (2.30c)$$

$$(\vec{u}_0(\vec{x},\vec{y}) \cdot \nabla_{\vec{x}})\vec{u}_0(\vec{x},\vec{y}) = -\nabla_{\vec{y}} p_1(\vec{x},\vec{y}) - \nabla_{\vec{x}} p_3(\vec{x},\vec{y}) + \nabla^2_{\vec{x}}\vec{u}_1(\vec{x},\vec{y}) \qquad (2.30d)$$

$$\begin{aligned} &(\vec{u}_0(\vec{x},\vec{y}) \cdot \nabla_{\vec{x}})\vec{u}_1(\vec{x},\vec{y}) + (\vec{u}_1(\vec{x},\vec{y}) \cdot \nabla_{\vec{x}})\vec{u}_0(\vec{x},\vec{y}) = \\ &-\nabla_{\vec{y}} p_2(\vec{x},\vec{y}) - \nabla_{\vec{x}} p_4(\vec{x},\vec{y}) + \nabla^2_{\vec{x}}\vec{u}_2(\vec{x},\vec{y}) + 2(\nabla_{\vec{y}} \cdot \nabla_{\vec{x}})\vec{u}_0(\vec{x},\vec{y}) \end{aligned} \qquad (2.30e)$$

from the continuity relation (2.28*b*) one gets:

$$\nabla_{\vec{x}} \cdot \vec{u}_0(\vec{x},\vec{y}) = 0 \qquad (2.31a)$$

$$\nabla_{\vec{x}} \cdot \vec{u}_1(\vec{x},\vec{y}) = 0 \qquad (2.31b)$$

$$\nabla_{\vec{x}} \cdot \vec{u}_2(\vec{x},\vec{y}) + \nabla_{\vec{y}} \cdot \vec{u}_0(\vec{x},\vec{y}) = 0 \qquad (2.31c)$$

$$\nabla_{\vec{x}} \cdot \vec{u}_3(\vec{x},\vec{y}) + \nabla_{\vec{y}} \cdot \vec{u}_1(\vec{x},\vec{y}) = 0 \qquad (2.31d)$$

$$\nabla_{\vec{x}} \cdot \vec{u}_4(\vec{x},\vec{y}) + \nabla_{\vec{y}} \cdot \vec{u}_2(\vec{x},\vec{y}) = 0 \qquad (2.31e)$$

Also, on each solid surface, the no-slip boundary condition implies $\vec{u}_i(\vec{x},\vec{y}) = 0$ for each $i = 0, 1, 2, \cdots$.

Now, equations (2.30*a*, *b*) imply that:

$$p_0(\vec{x},\vec{y}) = P_0(\vec{y}) \tag{2.32a}$$

$$p_1(\vec{x},\vec{y}) = P_1(\vec{y}) \tag{2.32b}$$

while the general solution of (2.30*c*) can be written in the form:

$$\vec{u}_0(\vec{x},\vec{y}) = -\overleftrightarrow{K}(\vec{x},\vec{y}) \cdot \nabla_{\vec{y}} P_0(\vec{y}) \tag{2.33a}$$

$$p_2(\vec{x},\vec{y}) = -\vec{A}(\vec{x},\vec{y}) \cdot \nabla_{\vec{y}} P_0(\vec{y}) + P_2(\vec{y}) \tag{2.33b}$$

Following the discussion given when deriving Darcy's law in section (2.3.2), it can be seen that (2.33*a*, *b*), (2.32*a*), and (2.30*c*) are identical to the problem posed by $\vec{u}_0(\vec{x},\vec{y})$ and $p_1(\vec{x},\vec{y})$ in that section (compare with equations (2.22*a*, *b*), (2.17*a*, *b*)), and hence will lead, after averaging according to (2.18), to the same result, namely Darcy's law. For the sake of completeness, some results of section (2.3.2) will be rewritten below using notation of the present section:

$$\nabla_{\vec{x}}^2 \overleftrightarrow{K}(\vec{x},\vec{y}) = \nabla_{\vec{x}} \vec{A}(\vec{x},\vec{y}) - \overleftrightarrow{I} \tag{2.34a}$$

$$\nabla_{\vec{x}} \cdot \overleftrightarrow{K}(\vec{x},\vec{y}) = 0 \tag{2.34b}$$

$$\langle \vec{u}_0(\vec{x},\vec{y}) \rangle_{\vec{x}} = -\langle \overleftrightarrow{K}(\vec{x},\vec{y}) \rangle_{\vec{x}} \cdot \nabla_{\vec{y}} P_0(\vec{y}) \tag{2.34c}$$

$$\langle p_2(\vec{x},\vec{y}) \rangle_{\vec{x}} = -\langle \vec{A}(\vec{x},\vec{y}) \rangle_{\vec{x}} \cdot \nabla_{\vec{y}} P_0(\vec{y}) + \phi P_2(\vec{y}) \tag{2.34d}$$

$$\nabla_{\vec{y}} \cdot \langle \vec{u}_0(\vec{x},\vec{y}) \rangle_{\vec{x}} = 0 \tag{2.34e}$$

$$\nabla_{\vec{y}} \cdot \left( \langle \overleftrightarrow{K}(\vec{x},\vec{y}) \rangle_{\vec{x}} \cdot \nabla_{\vec{y}} P_0(\vec{y}) \right) = \frac{\partial}{\partial y_i} \left( \langle K_{ij} \rangle_{\vec{x}} \frac{\partial P_0}{\partial y_j} \right) = 0 \tag{2.34f}$$

where $\phi = V/V_f$ is the porosity. To continue, Mei & Auriault (1991) assumed the solution of (2.30*d*) has the general form:

$$\vec{u}_1(\vec{x},\vec{y}) = -(\overset{3}{\overleftrightarrow{L}}(\vec{x},\vec{y})\cdot\nabla_{\vec{y}}P_0(\vec{y}))\cdot\nabla_{\vec{y}}P_0(\vec{y}) - \overleftrightarrow{K}(\vec{x},\vec{y})\cdot\nabla_{\vec{y}}P_1(\vec{y}) \tag{2.35a}$$

$$p_3(\vec{x},\vec{y}) = -(\overleftrightarrow{B}(\vec{x},\vec{y})\cdot\nabla_{\vec{y}}P_0(\vec{y}))\cdot\nabla_{\vec{y}}P_0(\vec{y}) - \vec{A}(\vec{x},\vec{y})\cdot\nabla_{\vec{y}}P_1(\vec{y}) + P_3(\vec{y}) \tag{2.35b}$$

Where the symbol $\overset{n}{\leftrightarrow}$ means Cartesian tensor of rank n. Using indicial notation the equation reads:

$$u_1^{(i)} = -L_{ijk}\frac{\partial P_0}{\partial y_j}\frac{\partial P_0}{\partial y_k} - K_{ij}\frac{\partial P_1}{\partial y_j} \tag{2.36a}$$

$$p_3 = B_{jk}\frac{\partial P_0}{\partial y_j}\frac{\partial P_0}{\partial y_k} - A_j\frac{\partial P_1}{\partial y_j} + P_3(\vec{y}) \tag{2.36b}$$

Then, substitution into (2.31*b*) and (2.30*d*) leads to the following boundary value problem for $\overset{3}{\overleftrightarrow{L}}(\vec{x},\vec{y})$ and $\overleftrightarrow{B}(\vec{x},\vec{y})$ (after using (2.31*b*), (2.30*d*), (2.33), and (2.34*a*, *b*)):

$$\begin{aligned} &\nabla_{\vec{x}}^2\overset{3}{\overleftrightarrow{L}}(\vec{x},\vec{y}) = \nabla_{\vec{x}}\overleftrightarrow{B}(\vec{x},\vec{y}) - (\overleftrightarrow{K}(\vec{x},\vec{y})\cdot\nabla_{\vec{x}})\overleftrightarrow{K}(\vec{x},\vec{y}) \\ &\nabla_{\vec{x}}\cdot\overset{3}{\overleftrightarrow{L}}(\vec{x},\vec{y}) = 0 \end{aligned} \tag{2.37}$$

or equivalently,

$$\begin{aligned} \nabla_{\vec{x}}^2 L_{ijk} &= \frac{\partial B_{jk}}{\partial x_i} - K_{lj}\frac{\partial K_{ik}}{\partial x_l} \\ \frac{\partial L_{ijk}}{\partial x_i} &= 0 \end{aligned} \tag{2.38}$$

complemented with boundary condition $\overset{3}{\overleftrightarrow{L}}(\vec{x},\vec{y}) = 0$ (or $L_{ijk} = 0$) on any solid boundary. As can be seen, this problem is of the same type as that for $\overleftrightarrow{K}(\vec{x},\vec{y})$ and $\vec{A}(\vec{x},\vec{y})$ defined by (2.33) and (2.34*a*, *b*) and both problems can be solved using the same technique. Averaging equations (2.35) and (2.31*d*) according to (2.18) and

(2.20) leads to:

$$\langle u_1^{(i)}\rangle_{\vec{x}} = \langle L_{ijk}\rangle_{\vec{x}}\frac{\partial P_0}{\partial y_j}\frac{\partial P_0}{\partial y_k} - \langle K_{ij}\rangle_{\vec{x}}\frac{\partial P_1}{\partial y_j} \qquad (2.39a)$$

$$\langle p_3\rangle_{\vec{x}} = \langle B_{jk}\rangle_{\vec{x}}\frac{\partial P_0}{\partial y_j}\frac{\partial P_0}{\partial y_k} - \langle A_j\rangle_{\vec{x}}\frac{\partial P_1}{\partial y_j} + \phi P_3(\vec{y}) \qquad (2.39b)$$

$$\nabla_{\vec{y}}\cdot\langle\vec{u}_1(\vec{x},\vec{y})\rangle_{\vec{x}} = \frac{\partial}{\partial y_i}\langle u_1^{(i)}\rangle_{\vec{x}} = 0 \qquad (2.39c)$$

Equation (2.39*c*) can be used to obtain a governing equation for $P_1(\vec{y})$ after averaging equations (2.35) and given by:

$$\frac{\partial}{\partial y_i}(\langle L_{ijk}\rangle_{\vec{x}}\frac{\partial P_0}{\partial y_j}\frac{\partial P_0}{\partial y_k}) = \frac{\partial}{\partial y_i}(\langle K_{ij}\rangle_{\vec{x}}\frac{\partial P_1}{\partial y_j}) \qquad (2.40)$$

Now, for an *isotropic* and *homogeneous* media with respect to $\vec{y}$:

$$\langle\overset{3}{\overleftrightarrow{L}}(\vec{x},\vec{y})\rangle_{\vec{x}} = L\epsilon_{ijk}\hat{e}_i\hat{e}_j\hat{e}_k \qquad (2.41a)$$

$$\langle\overleftrightarrow{B}(\vec{x},\vec{y})\rangle_{\vec{x}} = B\delta_{ij}\hat{e}_i\hat{e}_j = B\overleftrightarrow{I} \qquad (2.41b)$$

$$\langle\overleftrightarrow{K}(\vec{x},\vec{y})\rangle_{\vec{x}} = k\delta_{ij}\hat{e}_i\hat{e}_j = k\overleftrightarrow{I} \qquad (2.41c)$$

where $L$, $B$, $k$ are constants. The symbols $\delta_{ij}$ and $\epsilon_{ijk}$ represent the Kronecker delta and the Levi-Civita symbols respectively, which are defined by:

$$\begin{gathered} \delta_{ij} = 1 \text{ if } i = j \\ \delta_{ij} = 0 \text{ otherwise} \\ \epsilon_{123} = \epsilon_{231} = \epsilon_{312} = 1 \text{ ; } \epsilon_{132} = \epsilon_{213} = \epsilon_{321} = -1 \\ \epsilon_{ijk} = 0 \text{ otherwise} \end{gathered} \qquad (2.42)$$

Then, it can be seen that for an *isotropic* and *homogeneous* media:

$$\langle L_{ijk}\rangle_{\vec{x}}\frac{\partial P_0}{\partial y_j}\frac{\partial P_0}{\partial y_k} = 0 \qquad (2.43)$$

In addition, due to the fact that both $P_0(\vec{y})$ and $P_1(\vec{y})$ satisfy the Laplace equation equation when the medium is *isotropic* and *homogeneous* , Mei and Auriault assumed that $P_1(\vec{y}) = 0$ which leads to $\langle u_1^{(i)} \rangle_{\vec{x}} = 0$, after using (2.43). Furthermore, they derived the identity:

$$\langle L_{ijk} \rangle_{\vec{x}} + \langle L_{kji} \rangle_{\vec{x}} = 0 \tag{2.44}$$

which leads to the conclusion that when the global pressure gradient is in one direction only, say for example only $\frac{\partial P_0}{\partial y_1} \neq 0$, then $\langle L_{111} \rangle_{\vec{x}} = 0$ which implies $\langle u_1^{(i)} \rangle_{\vec{x}} = 0$. However, $\langle L_{211} \rangle_{\vec{x}}$ and $\langle L_{311} \rangle_{\vec{x}}$ are in general non-zero, given the quadratic correction to Darcy's law to be valid for anisotropic media.

Next, Mei and Auriault proceed to find the next correction term given in terms of $\vec{u}_2(\vec{x}, \vec{y})$ and $p_4(\vec{x}, \vec{y})$ and defined by equations (2.30*e*) and (2.31*c*). From (2.33) and (2.31*c*) one obtains:

$$\frac{\partial u_2^{(i)}}{\partial x_i} = \frac{\partial}{\partial y_j}\left(K_{jk}\frac{\partial P_0}{\partial y_k}\right) = \frac{\partial K_{jk}}{\partial y_j}\frac{\partial P_0}{\partial y_k} + K_{jk}\frac{\partial^2 P_0}{\partial y_j \partial y_k} \tag{2.45}$$

while from (2.33), (2.36), and (2.30*e*)) it is found that:

$$\begin{aligned} -\frac{\partial}{\partial x_i}\left( p_4(\vec{x}, \vec{y})\right) + \nabla_{\vec{x}}^2\, u_2^{(i)}(\vec{x}, \vec{y}) = \frac{\partial}{\partial y_i} P_2(\vec{y}) + F'_{ijkl}\frac{\partial P_0}{\partial y_j}\frac{\partial P_0}{\partial y_k}\frac{\partial P_0}{\partial y_l} + \\ F''_{ijk}\frac{\partial^2 P_0}{\partial y_j \partial y_k} + F'''_{ijk}\left(\frac{\partial P_0}{\partial y_k}\frac{\partial P_1}{\partial y_j} + \frac{\partial P_1}{\partial y_k}\frac{\partial P_0}{\partial y_j}\right) + F^{iv}_{ik}\frac{\partial P_0}{\partial y_k} \end{aligned} \tag{2.46}$$

where:

$$\begin{aligned} F'_{ijkl} &= K_{ml}\frac{\partial L_{ijk}}{\partial x_m} + L_{mjk}\frac{\partial K_{il}}{\partial x_m} \\ F''_{ijk} &= -A_k \delta_{ij} + 2\frac{\partial K_{ik}}{\partial x_j} \\ F'''_{ijk} &= K_{mk}\frac{\partial K_{ij}}{\partial x_m} \\ F^{iv}_{ik} &= -\delta_{ij}\frac{\partial A_k}{\partial y_j} + 2\frac{\partial}{\partial y_j}\left(\frac{\partial K_{ik}}{\partial x_j}\right) \end{aligned} \tag{2.47}$$

Then, expressing the solution of of (2.45) and (2.46) in the form:

$$\begin{aligned} u_2^{(i)} = -K_{ij}\frac{\partial P_2}{\partial y_j} - M'_{ijkl}\frac{\partial P_0}{\partial y_j}\frac{\partial P_0}{\partial y_k}\frac{\partial P_0}{\partial y_l} - M''_{ijk}\frac{\partial^2 P_0}{\partial y_j \partial y_k} - \\ M'''_{ijk}\left(\frac{\partial P_0}{\partial y_k}\frac{\partial P_1}{\partial y_j} + \frac{\partial P_1}{\partial y_k}\frac{\partial P_0}{\partial y_j}\right) - M^{iv}_{ij}\frac{\partial P_0}{\partial y_j} \end{aligned} \tag{2.48a}$$

$$\begin{aligned} p_4 = -A_j\frac{\partial P_2}{\partial y_j} - C'_{jkl}\frac{\partial P_0}{\partial y_j}\frac{\partial P_0}{\partial y_k}\frac{\partial P_0}{\partial y_l} - C''_{jk}\frac{\partial^2 P_0}{\partial y_j \partial y_k} - \\ C'''_{jk}\left(\frac{\partial P_0}{\partial y_k}\frac{\partial P_1}{\partial y_j} + \frac{\partial P_1}{\partial y_k}\frac{\partial P_0}{\partial y_j}\right) - C^{iv}_{j}\frac{\partial P_0}{\partial y_j} + P_4(\vec{y}) \end{aligned} \tag{2.48b}$$

where the tensor components $M'_{ijkl}$, $M''_{ijk}$, $M'''_{ijk}$, $M^{iv}_{ij}$, $C'_{jkl}$, $C''_{jk}$, $C'''_{jk}$, and $C^{iv}_{j}$ are obtained by solving the boundary value problem;

$$\frac{\partial}{\partial x_i} M'_{ijkl} = 0 \tag{2.49a}$$

$$\frac{\partial}{\partial x_i} M''_{ijk} = -K_{jk} \tag{2.49b}$$

$$\frac{\partial}{\partial x_i} M'''_{ijkl} = 0 \tag{2.49c}$$

$$\frac{\partial}{\partial x_i} M^{iv}_{ik} = -\frac{\partial}{\partial y_j} K_{jk} \tag{2.49d}$$

$$-\frac{\partial}{\partial x_i} C'_{jkl} + \nabla^2_{\vec{x}} M'_{ijkl} = -F'_{ijkl} \tag{2.49e}$$

$$-\frac{\partial}{\partial x_i} C''_{jk} + \nabla^2_{\vec{x}} M''_{ijk} = -F''_{ijk} \tag{2.49f}$$

$$-\frac{\partial}{\partial x_i} C'''_{jk} + \nabla^2_{\vec{x}} M'''_{ijk} = -F'''_{ijk} \tag{2.49g}$$

$$-\frac{\partial}{\partial x_i} C^{iv}_{k} + \nabla^2_{\vec{x}} M^{iv}_{ik} = -F^{iv}_{ik} \tag{2.49h}$$

complemented by no-slip boundary condition. Now, after averaging (2.31$e$) one obtains:

$$\frac{\partial}{\partial y_i} \langle u^{(i)}_2(\vec{x}, \vec{y}) \rangle_{\vec{x}} = 0 \tag{2.50}$$

and by (2.48$a$) the following governing equation for $P_2(\vec{y})$ is obtained;

$$\frac{\partial}{\partial y_i}(\langle K_{ij} \rangle_{\vec{x}} \frac{\partial P_2}{\partial y_j}) = \frac{\partial}{\partial y_i}(-\langle M'_{ijkl} \rangle_{\vec{x}} \frac{\partial P_0}{\partial y_j}\frac{\partial P_0}{\partial y_k}\frac{\partial P_0}{\partial y_l} - \langle M''_{ijk} \rangle_{\vec{x}} \frac{\partial^2 P_0}{\partial y_j \partial y_k}$$
$$- \langle M'''_{ijk} \rangle_{\vec{x}} (\frac{\partial P_0}{\partial y_k}\frac{\partial P_1}{\partial y_j} + \frac{\partial P_1}{\partial y_k}\frac{\partial P_0}{\partial y_j}) - \langle M^{iv}_{ij} \rangle_{\vec{x}} \frac{\partial P_0}{\partial y_j}) \tag{2.51}$$

The average of equation (2.48) according to (2.18) gives $\langle u^{(i)}_2 \rangle_{\vec{x}}$ and $\langle p_4 \rangle_{\vec{x}}$ in terms of the macroscale gradients $P_0(\vec{y})$, $P_1(\vec{y})$, and $P_2(\vec{y})$ which, in the general anisotropic situation, are given by (2.34$f$), (2.40), and (2.51). Consequently, it can be concluded that for a general *anisotropic* and *inhomogeneous* medium, the macroscopic field equations are known up to order $\beta^2$.

Now, for the special case of *isotropic* and *homogeneous media* with respect to $\vec{y}$, it is found from (2.49$g$, $h$), because of the homogeneity assumption in $\vec{y}$, that:

$$M^{iv}_{ik} = \frac{\partial}{\partial x_i} M^{iv}_{ik} \equiv 0 \tag{2.52}$$

Therefore, according to (2.48*a*) the only nonzero contribution to the average $\langle u_2^{(i)}(\vec{x},\vec{y})\rangle_{\vec{x}}$ is due to the first two terms of the right hand side of such equation. The contribution of $\langle M'''_{ijk}\rangle_{\vec{x}}$ and $\langle C'''_{jk}\rangle_{\vec{x}}$ are zero because $P_1(\vec{y}) = 0$, while the contribution of the *isotropic* third-rank tensor $\langle M''_{ijk}\rangle_{\vec{x}}$ vanishes because of its proportionality to the Levi-Civita symbol. Furthermore, the most general *isotropic* fourth-rank tensor has the form:

$$\langle M'_{ijkl}\rangle_{\vec{x}} = \lambda\delta_{ij}\delta_{kl} + \mu(\delta_{ik}\delta_{jl} + \delta_{il}\delta_{jk}) + \nu(\delta_{ik}\delta_{jl} - \delta_{il}\delta_{jk}) \tag{2.53}$$

which leads to:

$$\langle u_2^{(i)}(\vec{x},\vec{y})\rangle_{\vec{x}} = -k\frac{\partial P_2(\vec{y})}{\partial y_i} - \gamma\frac{\partial P_0}{\partial y_i}\frac{\partial P_0}{\partial y_k}\frac{\partial P_0}{\partial y_k} \tag{2.54}$$

where $\gamma = \lambda + 2\mu = \langle M'_{iiii}\rangle_{\vec{x}}$ and after combining (2.54) with (2.50) the governing equation for $P_2(\vec{y})$ is obtained:

$$K\frac{\partial^2 P_0}{\partial y_i \partial y_i} = -\gamma\frac{\partial}{\partial y_i}\left(\frac{\partial P_0}{\partial y_i}\frac{\partial P_0}{\partial y_k}\frac{\partial P_0}{\partial y_k}\right) \tag{2.55}$$

Likewise,

$$\langle p_4(\vec{x},\vec{y})\rangle_{\vec{x}} = -C''\frac{\partial^2 P_0}{\partial y_k \partial y_k} \tag{2.56}$$

with $C''_{ik} = C''\delta_{ij}$.

Finally, after combining (2.34*c*), (2.39*a*), and (2.54) one gets:

$$\begin{aligned}\langle u^{(i)}(\vec{x},\vec{y})\rangle_{\vec{x}} &= \langle u_0^{(i)}(\vec{x},\vec{y})\rangle_{\vec{x}} + \beta\langle u_1^{(i)}(\vec{x},\vec{y})\rangle_{\vec{x}} + \beta^2\langle u_2^{(i)}(\vec{x},\vec{y})\rangle_{\vec{x}} + O(\beta^3)\\ &= -k\left(\frac{\partial P_0}{\partial y_i} + \beta^2\frac{\partial P_2}{\partial y_i}\right) - \gamma\beta^2\frac{\partial P_0}{\partial y_i}\frac{\partial P_0}{\partial y_k}\frac{\partial P_0}{\partial y_k} + O(\beta^3)\end{aligned} \tag{2.57}$$

Similarly, after using (2.34*d*) one gets for the pressure:

$$\begin{aligned}\langle p(\vec{x},\vec{y})\rangle_{\vec{x}} &= \langle p_0(\vec{x},\vec{y})\rangle_{\vec{x}} + \beta\langle p_1(\vec{x},\vec{y})\rangle_{\vec{x}} + \beta^2\langle p_2(\vec{x},\vec{y})\rangle_{\vec{x}} + O(\beta^3)\\ &= P_0(\vec{y}) + \beta^2(\langle A_j(\vec{x},\vec{y})\rangle_{\vec{x}}\frac{\partial P_0}{\partial y_j} + \phi P_2(\vec{y})) + O(\beta^3)\end{aligned} \tag{2.58}$$

By taking $\langle A_j(\vec{x},\vec{y})\rangle_{\vec{x}} = 0$, equation (2.58) can be rewritten in the form:

$$\langle p(\vec{x},\vec{y})\rangle_{\vec{x}} = P_0(\vec{y}) + \beta^2 P_2(\vec{y}) + O(\beta^3) \tag{2.59}$$

and then equation (2.57) takes the form:

$$\langle u_i\rangle_{\vec{x}} = -K\frac{\partial\langle p\rangle_{\vec{x}}}{\partial y_i} - \beta^2\gamma\frac{\partial\langle p\rangle_{\vec{x}}}{\partial y_i}\frac{\partial\langle p\rangle_{\vec{x}}}{\partial y_k}\frac{\partial\langle p\rangle_{\vec{x}}}{\partial y_k} + O(\beta^3) \tag{2.60}$$

or alternatively,

$$\langle u_i\rangle_{\vec{x}}(1 - \frac{\beta^2\gamma}{K^3}\langle u_k\rangle_{\vec{x}}\langle u_k\rangle_{\vec{x}}) = -K\frac{\partial\langle p\rangle_{\vec{x}}}{\partial y_i} + O(\beta^3) \tag{2.61}$$

which explicitly shows a term cubic in the mean velocity as the leading order correction to Darcy's law for low Reynolds number flow in a *isotropic* and *homogeneous* medium. The coefficients $K$ and $\gamma$ are defined by their respective boundary value problems (2.34*b*) and (2.49*a*, *b*). Also, $K$ can be proved to be positive defined (Sanchez-Palencia 1980), while $\gamma$ is proved to be non-positive by Mei and Auriault, 1991. This results are in agreement with the intuitive, and general accepted, idea that higher pressure gradient is needed to maintain certain flow rate. Finally, either equations (2.60) or (2.61) need to be combined with the incompressibility condition:

$$\nabla_{\vec{y}}\cdot\langle\vec{u}(\vec{x},\vec{y})\rangle_{\vec{x}} = 0 \tag{2.62}$$

# Chapter 3

# Numerical Results

## 3.1 Introduction

The main part of this work is based on obtaining computer solutions of the Navier-Stokes equations at low and finite Reynolds number for flow through two-dimensional ($2D$) quasi-periodic and quasi-isotropic random stationary porous matrix. Attention is given to 2D flowes through porous media in order to reduce computational work, and in the belief that the results can be extended to 3D flows through isotropic porous materials. This assumption is reasonable, since Darcy's law is applicable to both two and three-dimensional porous media. The Quasi-periodic geometries are included due to the fact that Mei and Auriault's (1991) theoretical results are based on assuming a porous media composes of a collection of periodic unit cells on which a boundary value problem, like the one defined by (2.34$b$) and (2.34$a$), needs to be solved to find the undefined coefficients and have a complete solution of the problem. However, our main goal is to find some insight in the general behavior of fluid flow through random porous structures, and to see whether our results can be justified by Mei and Auriault's (1991) theoretical results.

Numerical solutions of the Navier-Stokes equation were obtained by using the commercial Computational Fluid Dynamics software called NEKTON, a brief discussion of which is given in the Appendix. In each calculation, the fluid viscosity ($\mu$) and its density ($\rho$) were taken to be one in CGS units. Also, the calculations were carried out until the results were essentially independent of the number of macroelements used in defining the sample geometry, and of the number of internal nodes defined by NEKTON, when defining the computational domain, on each macroelement.

## 3.2 Problem Setup

Using the NEKTON graphical interface, we were able to set up a suitable geometry emulating a porous medium inserted between the walls of a channel as shown in Fig.-3.1 through Fig-3.10, which resemble the setup used by Beavers and Sparrow (1969) in their experimental work. Then, the *simulated experiment* proceeds by specifying a desired flow rate at both ends of the channel, and measuring, after equilibrium has been reached, the corresponding pressure gradient necessary to achieve such flow rate. A prescribed flow rate along the channel is achieved by specifying a Poiseuille parabolic velocity profile at both ends of the channel. The rationality of such a boundary condition is based in the expectation that far from the porous medium "sample", the flow will be of the corresponding Poiseuille type, as is corroborated by the streamlines shown in Fig-3.11 and Fig-3.12. This information allows us to find the corresponding pressure drop at the porous media sample. Then, the permeability $k$ is obtained through its operational definition given by Darcy's law in equation (1.1) and using data corresponding to low flow rate. An example is given in Fig.-3.16. The pressure drop ($\Delta P$) across the porous media sample is obtained by noting that the total pressure drop across the entire channel is equal to the pressure drop across the porous media sample plus the pressure drop across the two channel regions located at both sides of the porous media sample (see for example Fig-3.11), where the pressure drop is given by the well known Poiseuille equation for flow in a channel. Therefore, the pressure drop in the porous media sample is given by:

$$\Delta P = (p_2 - p_1) - (\Delta x - \Delta X)\frac{\Delta P_{Poiseuille}}{\Delta x} \tag{3.1}$$

where: $p_{1,2}$ is the "measured" pressure at $x = x_{1,2}$, $\Delta x = |x_2 - x_1|$ is the length of the channel, and $\Delta X$ is the length of the porous medium sample. $\Delta P_{Poiseuille}$ represents the Poiseuille pressure drop in a channel, given by:

$$\frac{\Delta P_{Poiseuille}}{\Delta x} = -8(\frac{\mu}{w^2})v_{max} \tag{3.2}$$

in which: $w$ represent the channel width, and $v_{max}$ is the maximum value of the parabolic velocity profile specified as boundary condition at both ends of the channel in the form:

$$v_x = v_{max}(1 - (\frac{y}{\frac{w}{2}})^2) \ ; \ v_y = 0 \tag{3.3}$$

which gives for the averaged velocity (or rate of fluid flow per unit area) $V$:

$$V = (\frac{2}{3})v_{max} \tag{3.4}$$

The analysis of our results will be based in fitting the data using the following equation:

$$-\frac{\Delta P}{\Delta X} = (\frac{\mu}{k})V + b\rho V^2 + CV^3 \tag{3.5}$$

which can be cast in the following dimensionless form after using $Re = \frac{\rho \mathcal{L} V}{\mu}$:

$$F \equiv \frac{\rho \mathcal{L} k}{\mu^2 Re}(-\frac{\Delta P}{\Delta X}) = 1 + (\frac{k}{\mathcal{L}})bRe + (\frac{k}{\mathcal{L}^2})(\frac{\mu}{\rho^2})CRe^2 \tag{3.6}$$

The following particular cases of the above equation are of interest:

$$F_3 \equiv \frac{\rho \mathcal{L} k}{\mu^2 Re}(-\frac{\Delta P}{\Delta X}) = 1 + (\frac{k}{\mathcal{L}^2})(\frac{\mu}{\rho^2})CRe^2 \tag{3.7a}$$

$$F_2 \equiv \frac{\rho \mathcal{L} k}{\mu^2 Re}(-\frac{\Delta P}{\Delta X}) = 1 + (\frac{k}{\mathcal{L}})bRe \tag{3.7b}$$

Notice that $F_3$ only includes a cubic correction term to Darcy's law, while $F_2$ only includes a quadratic correction term to Darcy's law. The undefined coefficient $C$ must be non-negative in order to have a positive pressure drop at higher flow rates.

These equations will be used to compare our numerical results with theoretical (Mei and Auriault (1991)) and experimental (Beavers and Sparrow (1969), Macdonald *et al.* (1979), Dybbs and Edwards (1984)) work, which respectively predicts and show the existence of two flow regimes at low and moderated values of the Reynolds number ($Re$). Specifically, the arrangement of equation (3.7$a$) is useful to see the applicability of Mei and Auriault's 1991 theoretical results. To reach this goal and be consistent with the theoretical work, the length scale $\mathcal{L}$ needs to be chosen equal to a microscale $\ell$ characterizing the porous material. Furthermore, to compare, through $F_2$, our results with the experimental work of Beavers and Sparrow (1969), the length scale $\ell$ need to be chosen equal to the $\sqrt{k}$. One should notice that the arrangements of terms in equation (3.7$b$) defining $F_2$ is slightly different from the one used by Beavers and Sparrow (1969) which has the form:

$$f \equiv \frac{\rho\mathcal{L}^2\sqrt{k}}{\mu^2 Re^2}\left(-\frac{\Delta P}{\Delta X}\right) = \frac{\mathcal{L}}{\sqrt{k}}\frac{1}{Re} + b\sqrt{k} \tag{3.8}$$

However, when $\mathcal{L} = \sqrt{k}$, $f = \frac{F_2}{Re}$. In this situation, the independent coefficient of equation (3.8) and the coefficient multiplying $Re$ in equation (3.7$b$) are the same, and we will be interested in this parameter.

One of the reasons for choosing the experimental work of Beavers and Sparrow (1969) is because they worked with a set of porous media samples (made up of metallic fibers) which, besides having high porosity, were of similar structure. Their conclusion was that equation (3.8) can be considered as a unifying equation for fibrous porous materials of similar structure with $b\sqrt{k} = 0.074$ in the average. Our simulations can be considered as an emulation of such porous materials. In particular, the quasi-isotropic random samples shown in Fig.-3.5 through Fig.-3.10 were built starting from the one shown in Fig.-3.4 by keeping the center of the obstacles in the same place and shrinking the obstacles. This makes each sample have the same structure while increasing the porosity. As already indicated, the porous samples were not completely isotropic, but, to be precise, were isotropic under finite rotations of ninety degree. This was verified by first finding the permeability of the sample shown in Fig.-3.4 with fluid flowing in a particular orientation of the porous medium sample. Posteriorly, other set of data was taken after rotating the porous media sample ninety degrees respect to the previous orientation. Comparing the permeability obtained in both orientations of the sample, it was found that the sample permeability was the same in both directions by less than three percent respect to the average.

## 3.3 Presentation of the Results and Discussion

Let's start with Fig.-3.13 to Fig.-3.15 where we show how $F$ looks when plotted against the whole range of $Re$ that we were able to obtain. Then, in Fig.-3.16 it is shown an example of low flow rate used to find the permeability of the medium according to Darcy's law in equation (1.1). After that, typical deviation of the data from Darcy's law is shown in Fig.-3.17 and Fig.-3.18.

First, we consider the transition from Darcy's flow, which occurs for moderate Reynolds numbers, starting at $Re \cong \epsilon^{1/2}$, with $\epsilon = \frac{\sqrt{k}}{L}$, where $L = 0.8\,cm$ is the length of the porous sample. Some plots corresponding to data taken for such values of the Reynolds number and fitted according to $F_3$, in equation ($3.7a$), are shown in Fig.-3.19 through Fig.-3.21. As observed, the data is very well fitted by $F_3$ which can be justified by the theoretical work of Mei and Auriault (1991). However, the fit is not unique in the sense that the data can also be fitted by the equation (3.6), as shown in Fig.-3.22 through Fig.-3.24. Moreover, though the contribution of the quadratic correction to Darcy's law is smaller than the respective contribution due to the cubic correction term, this contribution is not completely negligible as one may expect according to Mei and Auriault (1991) work. Probably it is due to the fact that our sample is not totally isotropic. It should be noticed that this flow regime was observed to occur at values of the Reynolds number in the range $\epsilon^{1/2} < Re < \epsilon^0 = 1$, with $\epsilon = \sqrt{k}/L$, and $L$ being the size of the porous sample ($L = 0.8\,cm$ in this case). Later, below equation (3.9), we will compare the fit of the data in this flow regime according to $F_3$ and $F$ by looking at the value of the quantity $\chi^2$ shown in the captions of the corresponding figures.

Next we consider larger Reynolds number, $Re > 1$. Fits of some data corresponding to such Reynolds number according to $F_2$, in equation (3.7$b$), are shown in Fig.-3.25 through Fig.-3.27. This flow regime was observed to occur at values of the the Reynolds number actually starting at $Re > \epsilon^{-1/10}$. In addition, we also tried to verify if the data in this flow regime would be fitted by $F$, in equation (3.6). In this case, however, the fit of the data by $F$, some of which are shown in Fig.-3.28 through Fig.-3.30, clearly indicates that this fit can not be valid in this flow regime, because the additional (cubic correction) term, added by $F$, besides being negative, is very small. Consequently, in this flow regime, the $F$ fit need to be rejected and the data is best fitted by $F_2$, in agreement with Forchheimer relation, equation (1.2) on page 2.

It should be mentioned, that a transition region between the flow regime governed by $F_3$ to the flow regime dominated by $F_2$ was also observed. In this transitional region, for which the Reynolds number was found to be in the range $1 < Re < \epsilon^{-1/10}$, the data is best fitted by $F$ in equation (3.6). Some plots are shown in Fig.-3.31 through Fig.-3.33. The data's goodness of fit can be explored further by computing the quantity:

$$\chi^2 \equiv \sum_{i=1}^{N} (\frac{y_i - y(x_i)}{\sigma_i})^2 \tag{3.9}$$

called chi-square. This quantity should be a minimum when a set of $N$ data points $(x_i, y_i)$, with normally distributed measurement errors having standard deviation $\sigma_i$, are fitted by the function $y(x; a_1, ..., a_M)$ with the appropriated set of $M$ parameters $a_1, ..., a_M$ (Press, W.H. et al. 1992). By assuming $\sigma_i = \sigma$ for all points, $\chi^2$ was computed for the fits shown in Fig.-3.31 through Fig.-3.33. The value of $\chi^2$ for each fit is shown in the caption of the respective figure. As expected, it was found that the $\chi^2$ value corresponding to the fit given by $F$ in equation (3.6), $\chi_F^2$, has the lowest value compared with the $\chi^2$ values corresponding the fits according to equations (3.7*b*), $\chi_{F_2}^2$, and equation (3.7*a*), $\chi_{F_3}^2$. In addition, $\chi_{F_3}^2 = 1.8\chi_{F_2}^2$ indicating that either fit is as good as the other. The value of $\chi^2$ can also be used to see how well the data, in the regime where the correction to Darcy's law is cubic in the average velocity, is fitted by $F_3$ compared with the fit obtained using $F$. The corresponding values of $\chi^2$ for each case are shown in the captions of Fig.-3.19 through Fig.-3.24. As can be seen, $\chi_{F_3}^2$ is approximately $10\chi_F^2$ or less. This suggest that $F_3$ is a good model for the data in that regime and that the contribution of the quadratic term in the fit given by $F$ is not very significant.

In Table-3.2 on page 42, there are collected the values of the dimensionless coefficients $(\frac{\mu}{\rho^2})C$ and $\sqrt{k}b$ that appear in equation (3.7*a*) defining $F_3$ and equation (3.7*b*) defining $F_2$ respectively. As can be seen, the average of $b\sqrt{k} \cong 0.078$. This number is very close to the experimental value of such parameter found by Beavers and Sparrow (1969).

Finally, Fig.-3.34 shows a Log-Log plot of the conductivity $(\sigma/\sigma_f)$ Vs the porosity $(\phi)$ indicating a power law relating both quantities according to Archie's law $\sigma \propto \sigma_f\phi^m$, with $m \cong 2$ and the proportionality constant close to one, in agreement with many experimental cases. However, these values are not entirely universal (Wong *et al.* 1984). A plot of the permeability $(k/L^2)$ Vs the porosity is shown in Fig.-3.36. No evidence of a power law relating this two quantities was found. Nevertheless, it was possible to find some agreement with the theoretical work of Sangani and Acrivos (1982) who discuss slow flow through a periodic array of infinitely long circular cylinders. They provide an equation for the dimensionless drag force per unit length of a cylinder which, after using Darcy's law, can be written in the following form:

$$F' \equiv \frac{a}{c}\left(\frac{1}{\mu V}\right)\left(-\frac{\Delta P}{\Delta X}\right) = \frac{a}{ck} \tag{3.10}$$

where $c$ is the solid fraction $(1-\phi)$ and $(a)$ is the area of one obstacle, $(\pi r^2)$ for cylinders, $\frac{a}{c}$ is the number of obstacles per unit area, and $F'$ is given by (Sangani and Acrivos (1982)):.

$$F' = \frac{4\pi}{-\frac{1}{2}Ln(c) - 0.738 + c - 0.887c^2 + 2.039c^3} \tag{3.11}$$

In Fig.-3.38 it is shown a plot of $\frac{a}{ck}$ and $F'$ according to equation (3.11) versus the solid fraction (c). As parameter $(a)$, we use the crossectional area of the square obstacles used in our simulations. The length of each obstacle is shown in Table-3.1, on page 42. One can appreciate that the points are displaced by a fairly constant amount in the vertical direction. Consequently in Fig.-3.39 and Fig.-3.40 we show plots were $\frac{a}{ck}$ was multiplied by 0.7 and 0.175 respectively. In this way we were able to "fit" the data according to equation (3.11). The multiplicative constant correction perhaps represents a geometric correction, reflecting the difference between circular and square solid regions.

It should be mentioned that equation (3.11) was also used by Koch and Ladd (1997) to analyze the results of their work about fluid flow through periodic and random arrays of aligned cylinders. They found very good agreement between the dilute asymptote of equation (3.11) and their data.

## 3.4 Numerical Precision

As indicated before, we carried out our computations using the commercial Fluid Dynamics Packages (CFD) called NEKTON based on the spectral element method, a

| Geometry | $\phi$ | $k(cm^2)$ | $\sigma(\sigma_f)$ | obst. length(cm) |
|---|---|---|---|---|
| Fig.-3.1 | 0.76172 | 1.14450E-4 | 0.56642 | 0.05000 |
| Fig.-3.2 | 0.71556 | 1.27961E-4 | 0.52169 | 0.05333 |
| Fig.-3.3 | 0.46387 | 4.83278E-6 | 0.24527 | ——- |
| Fig.-3.4 | 0.82422 | 2.10859E-4 | 0.67687 | 0.05000 |
| Fig.-3.5 | 0.88750 | 3.52703E-4 | 0.78051 | 0.04000 |
| Fig.-3.6 | 0.90112 | 3.98188E-4 | 0.80449 | 0.03750 |
| Fig.-3.7 | 0.92188 | 4.83736E-4 | 0.84233 | 0.03333 |
| Fig.-3.8 | 0.95606 | 7.07157E-4 | 0.90798 | 0.02500 |
| Fig.-3.9 | 0.98047 | 1.03882E-3 | 0.95795 | 0.01667 |
| Fig.-3.10 | 0.99297 | 1.44105E-3 | 0.98414 | 0.01000 |

Table 3.1: Parameters characterizing the simulated porous media samples used in this work.

| Geometry | $(\frac{\mu}{\rho^2})C$ | $b\sqrt{k}$ |
|---|---|---|
| Fig.-3.1 | 0.06269 | 0.17044 |
| Fig.-3.2 | 0.02063 | 0.03273 |
| Fig.-3.3 | 0.62826 | ——- |
| Fig.-3.4 | 0.04811 | 0.10069 |
| Fig.-3.5 | 0.03768 | 0.08999 |
| Fig.-3.6 | 0.03487 | 0.08706 |
| Fig.-3.7 | 0.03284 | 0.08237 |
| Fig.-3.8 | 0.02776 | 0.07415 |
| Fig.-3.9 | 0.02407 | 0.06198 |
| Fig.-3.10 | 0.01800 | 0.05053 |
| | | ave = 0.078 |

Table 3.2: Coefficients of the fit according to equations (3.7$a$) and (3.7$b$).

high order finite element technique for solution of partial differential equations. The accuracy of this package has been tested by comparing its solution of many benchmark problems with published experimental and/or analytical results (NEKTON v2.85 manual vol. 2).

Basically, there are two steps that need to be carried out to establish a converged accurate result with NEKTON. First the result needs to be mesh-independent. This is accomplished by revising the grid and increasing the number of macroelements (M). Second, the numerical value of the obtained result is improved by using higher polynomial order (N) to approximate the solution. In the first case the error decrease as $M^N$, while in the second case the error decrease exponentially sa $e^{-\alpha N}$.

Our calculations were carried out until the results were essentially independent of the number of macroelements used in defining the sample geometry, and of the number of internal nodes defined by NEKTON when defining the computational domain on each macroelement. The final grid for each computation was about 400 macroelements. Some illustrations are given in Fig.-3.41 through Fig.-3.43. The refinement of the grid was done using NORDER = 5. This means that each macroelement (4 corner element) entered by the user is divided by NEKTON into 5 × 5 nodes (including the corners) located at places that correspond to the zeros of the normalized Legendre polynomial of order $N - 1$. Then we increase the NORDER to 7, and, after comparing results (like numerical value of the pressure at both end of the channel, numerical value of the components of the velocity (Ux,Uy) and pressure (P) at some points inside the porous media, and verifying that the stream lines were continuous) with corresponding values obtained using NORDER = 5 calculations, it was found that with NORDER = 5 we were obtaining sufficiently accurate results. Nevertheless, all the calculation were done using NORDER = 7, and, to be sure, a few cases were done using NORDER = 9. Table-3.3, on page 45, show some of these results.

In addition, NEKTON provides parameters that can be varied by the user to control the numerical precision of the computation. Once specified, NEKTON uses those parameters together with length scales, computed eigenvalues, and material properties to convert this physical criterion into numerical convergence criteria for the iterative loops inside the NEKTON solvers. This ensures optimal efficiency in the NEKTON solvers.

| Geometry | Re | NORDER | $P_{out}$ | $P_{in}$ |
|---|---|---|---|---|
| Fig.-3.4 | 8.712E-4 | 7 | -0.11710755E+03 | 0.11773073E+03 |
| | 8.712E-4 | 9 | -0.11721326E+03 | 0.11783702E+03 |
| | 3.000 | 7 | -0.49220066E+06 | 0.49682578E+06 |
| | 3.000 | 9 | -0.49323766E+06 | 0.49709484E+06 |
| | 4.840 | 7 | -0.91241156E+06 | 0.92382569E+06 |
| | 4.840 | 9 | -0.91649025E+06 | 0.92267850E+06 |
| Fig.-3.7 | 3.665E-3 | 5 | -0.14542390E+03 | 0.14582835E+03 |
| | 3.665E-3 | 7 | -0.14761411E+03 | 0.14802690E+03 |
| | 3.665E-3 | 9 | -0.14770090E+03 | 0.14811414E+03 |
| | 2.932E-1 | 5 | -0.11672884E+05 | 0.11705500E+05 |
| | 2.932E-1 | 7 | -0.11845116E+05 | 0.11878952E+05 |
| | 2.932E-1 | 9 | -0.11852117E+05 | 0.11886082E+05 |
| | 1.759 | 5 | -0.75849695E+05 | 0.75862977E+05 |
| | 1.759 | 7 | -0.76495234E+05 | 0.76523125E+05 |
| | 1.759 | 9 | -0.76539305E+05 | 0.76565609E+05 |
| | 4.399 | 5 | -0.22885420E+06 | 0.22841634E+06 |
| | 4.399 | 7 | -0.22729022E+06 | 0.22671700E+06 |
| | 4.399 | 9 | -0.22774922E+06 | 0.22659086E+06 |
| Fig.-3.9 | 2.256 | 7 | -0.33790219E+05 | 0.33501816E+05 |
| | 2.256 | 9 | -0.33788258E+05 | 0.33497473E+05 |
| | 4.297 | 7 | -0.71440656E+05 | 0.70100164E+05 |
| | 4.297 | 9 | -0.71429352E+05 | 0.70013438E+05 |

Table 3.3: This table show values of the pressure obtained by using increasing values of the parameter NORDER. This should be be done in NEKTON to obtain a converged solution. At this point we already had verified independence of the results with the refinement of the computational domain. Notice that variations in the numerical values occur after the second significant digit. This implies a relative error of less than 1% between the value with high NORDER and the value with low NORDER. Here $P_{in}$ refers to the pressure at the left end of the channel, while $P_{out}$ refers to the pressure at the right end of the channel. Fluid is flowing from left to right.

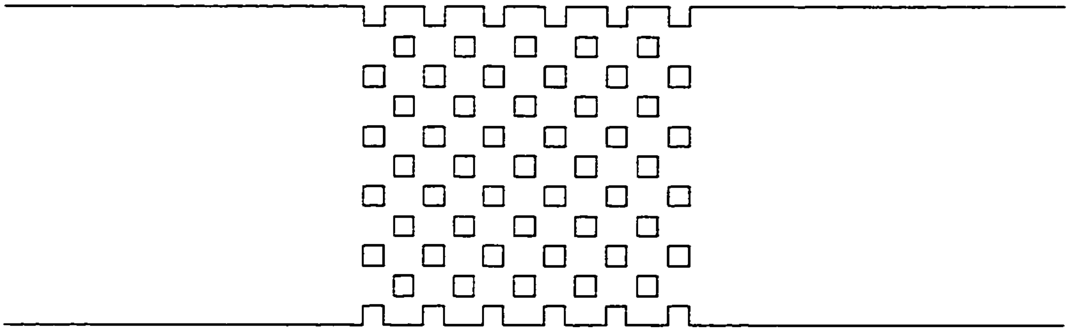

Figure 3.1: Quasiperiodic porous sample with $\phi = 0.7617$ and $k = 1.14450 \times 10^{-4}\ cm^2$

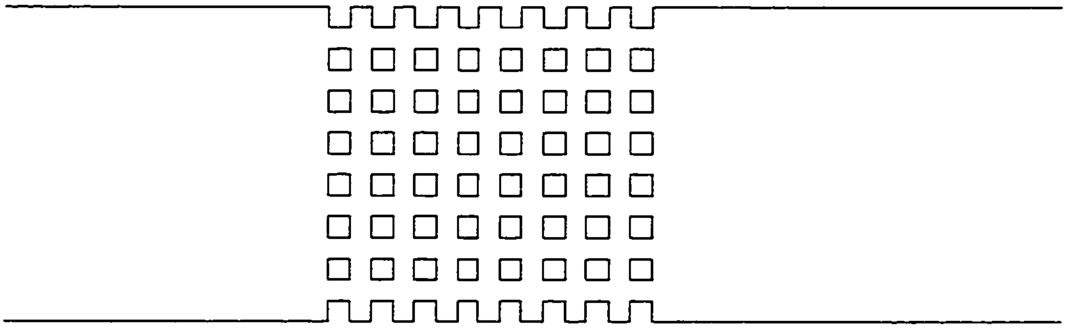

Figure 3.2: Quasiperiodic porous sample with $\phi = 0.7156$ and $k = 1.27961 \times 10^{-4}\ cm^2$

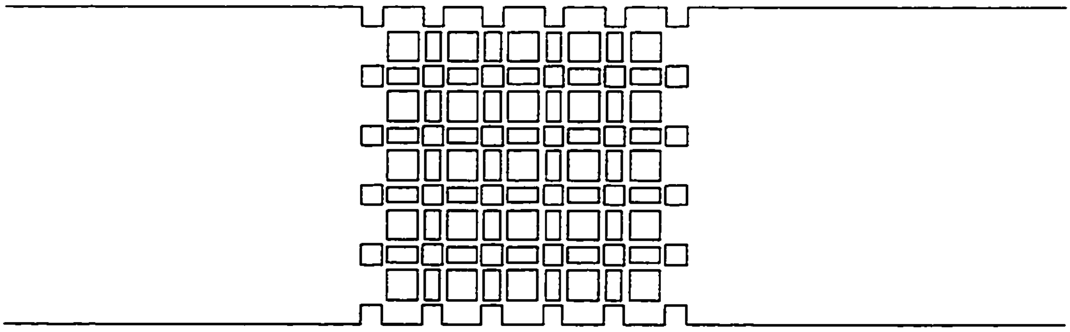

Figure 3.3: Quasiperiodic porous sample with $\phi = 0.4638$ and $k = 4.83278 \times 10^{-6}\ cm^2$

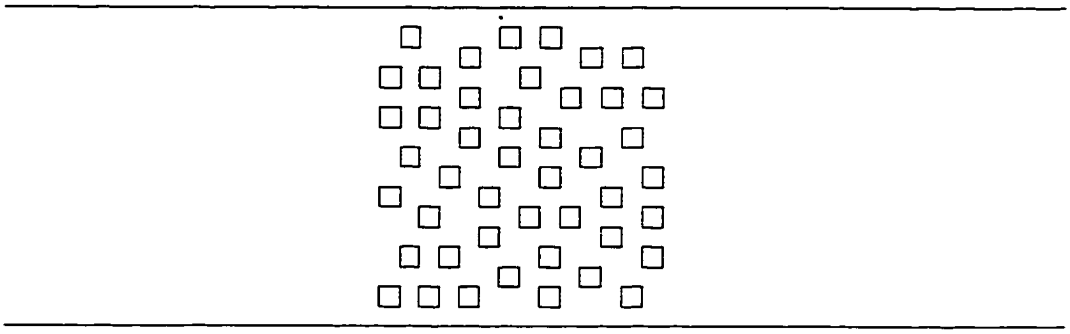

Figure 3.4: Random sample with $\phi = 0.8242$, $k = 2.10859 \times 10^{-4}\ cm^2$, $\sigma = 0.67687\,\sigma_f$

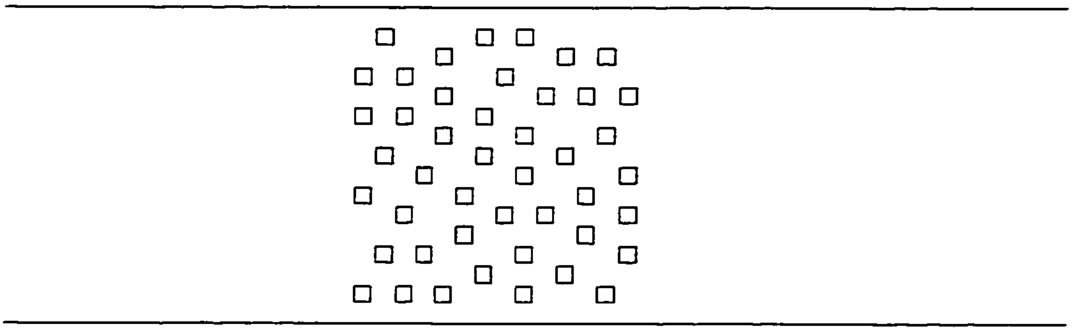

Figure 3.5: Random sample with $\phi = 0.8875$, $k = 3.52703 \times 10^{-4}\ cm^2$, $\sigma = 0.78051\,\sigma_f$

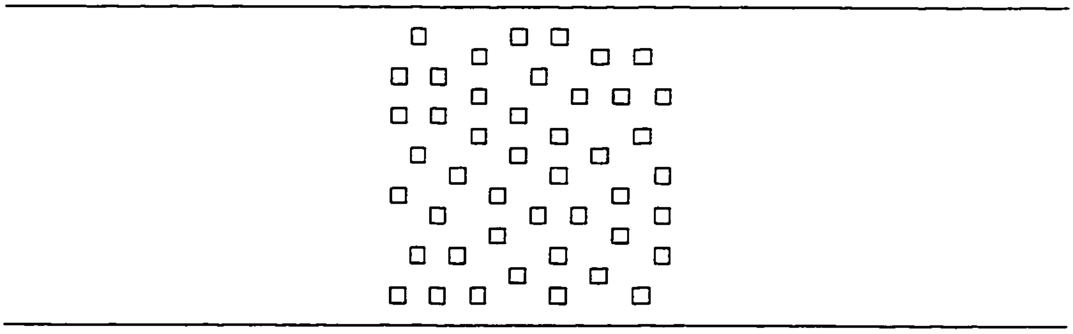

Figure 3.6: Random sample with $\phi = 0.9011$, $k = 3.98188 \times 10^{-4}\ cm^2$, $\sigma = 0.80449\,\sigma_f$

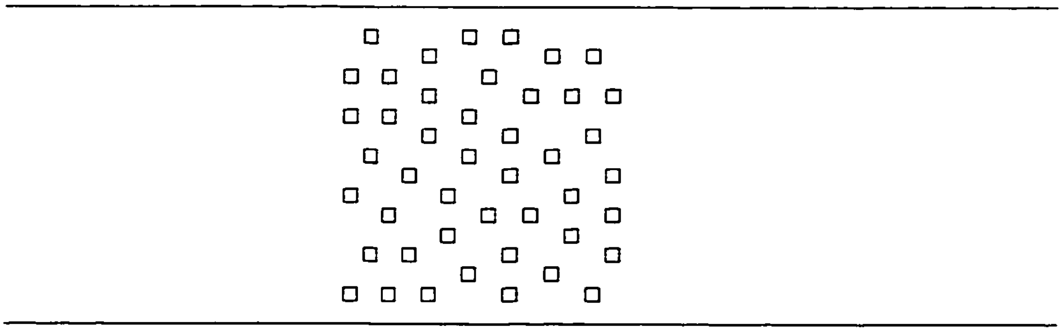

Figure 3.7: Random sample with $\phi = 0.9219$, $k = 4.83736 \times 10^{-4}\ cm^2$, $\sigma = 0.84233\,\sigma_f$

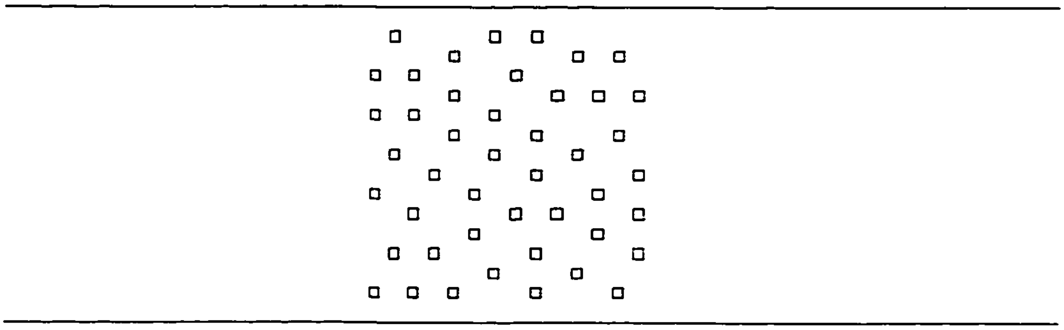

Figure 3.8: Random sample with $\phi = 0.9561$, $k = 7.07157 \times 10^{-4}\ cm^2$, $\sigma = 0.90798\,\sigma_f$

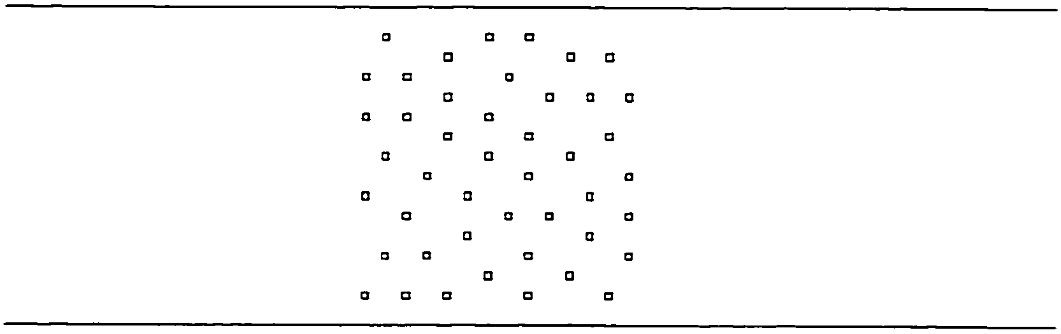

Figure 3.9: Random sample with $\phi = 0.9804$, $k = 1.03882 \times 10^{-3}\ cm^2$, $\sigma = 0.95795\,\sigma_f$

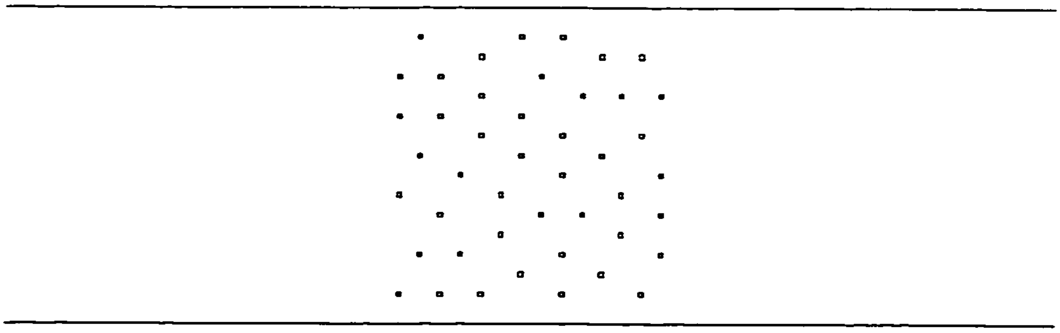

Figure 3.10: Random sample with $\phi = 0.9929$, $k = 1.44105 \times 10^{-3}\ cm^2$, $\sigma = 0.98414\,\sigma_f$

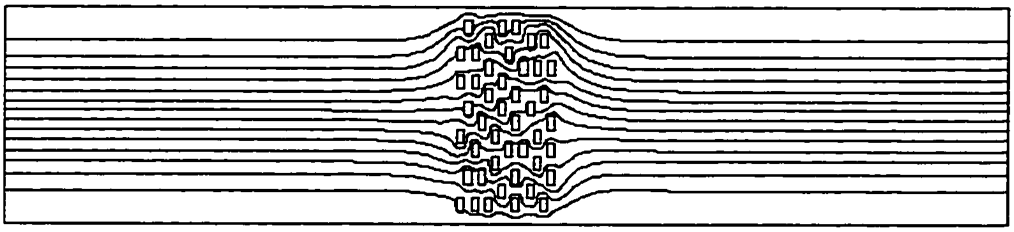

Figure 3.11: Example of stream lines pattern

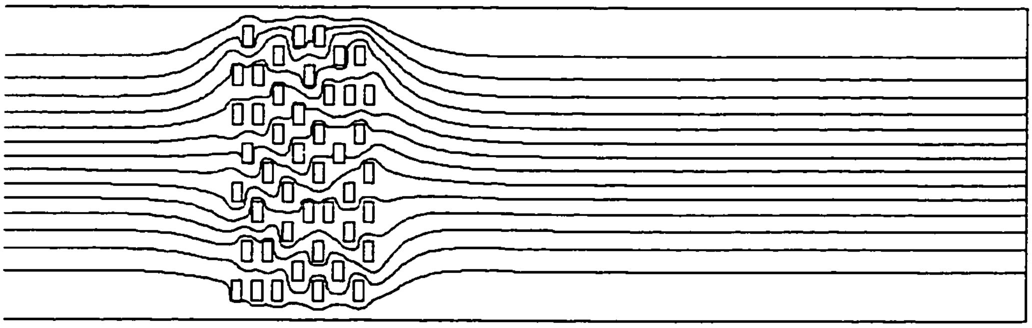

Figure 3.12: Magnified example of stream lines pattern

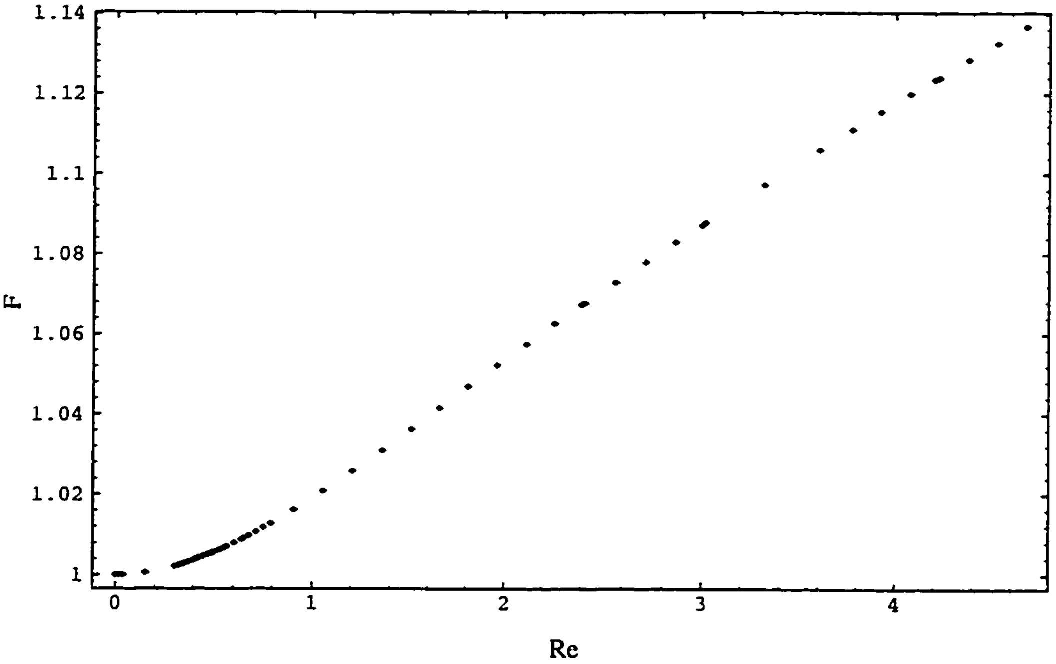

Figure 3.13: Typical behavior of $\frac{\rho \mathcal{L} k}{\mu^2 Re}(-\frac{\Delta P}{\Delta X})$, in the range of Reynolds number we were able to reach. This set of data corresponds to the simulation done using the geometry shown in Fig.-3.2 on page 46. Here, $\mathcal{L} = k^{1/2}$.

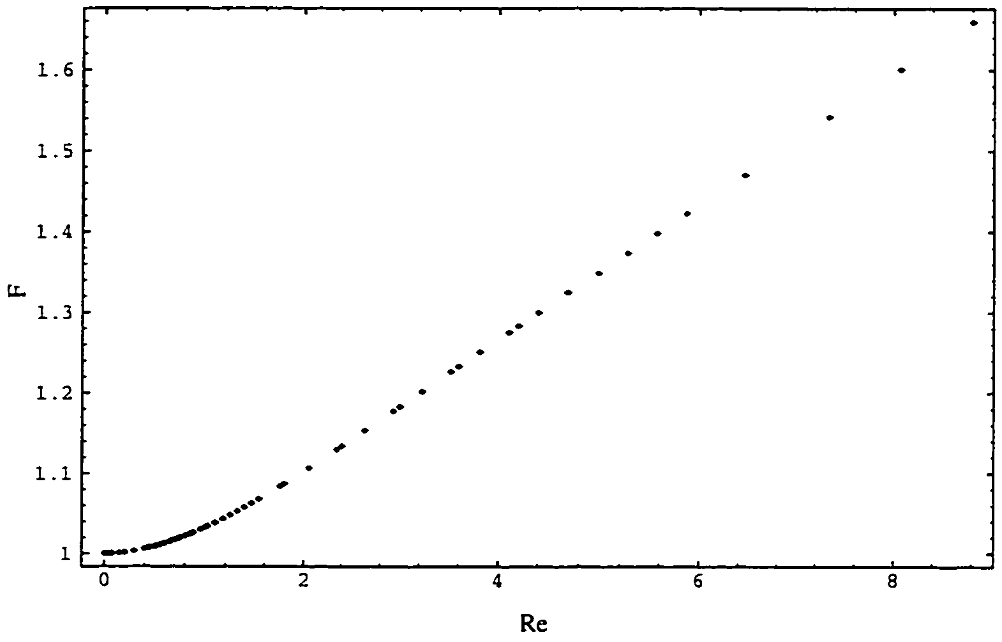

Figure 3.14: Typical behavior of $\frac{\rho \mathcal{L} k}{\mu^2 Re}(-\frac{\Delta P}{\Delta X})$, in the range of Reynolds number we were able to reach. This set of data corresponds to the simulation done using the geometry shown in Fig.-3.7 on page 48. Here, $\mathcal{L} = k^{1/2}$.

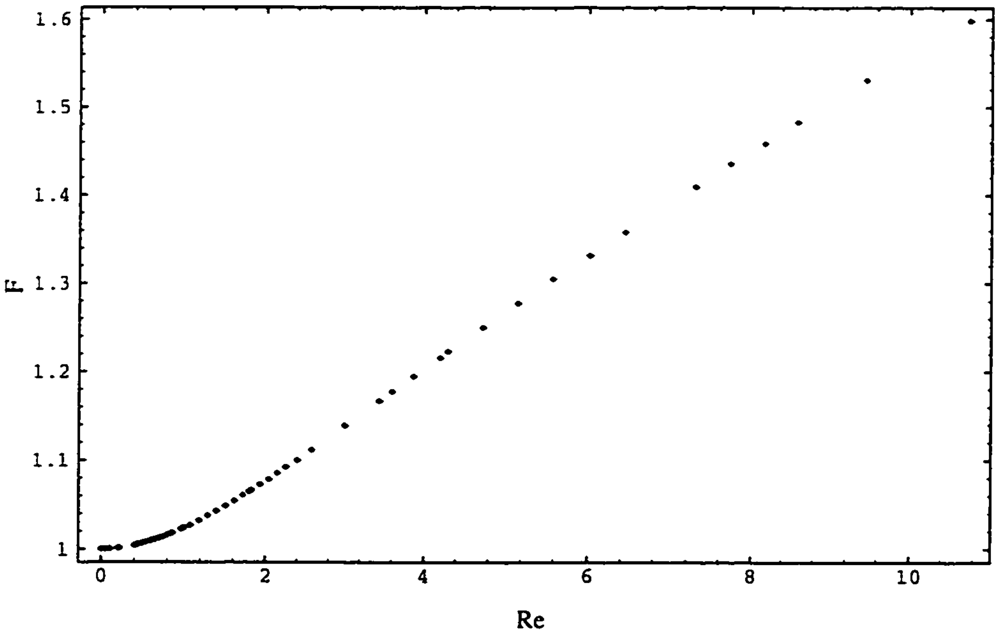

Figure 3.15: Typical behavior of $\frac{\rho \mathcal{L} k}{\mu^2 Re}(-\frac{\Delta P}{\Delta X})$, in the range of Reynolds number we were able to reach. This set of data corresponds to the simulation done using the geometry shown in Fig.-3.9 on page 49. Here, $\mathcal{L} = k^{1/2}$.

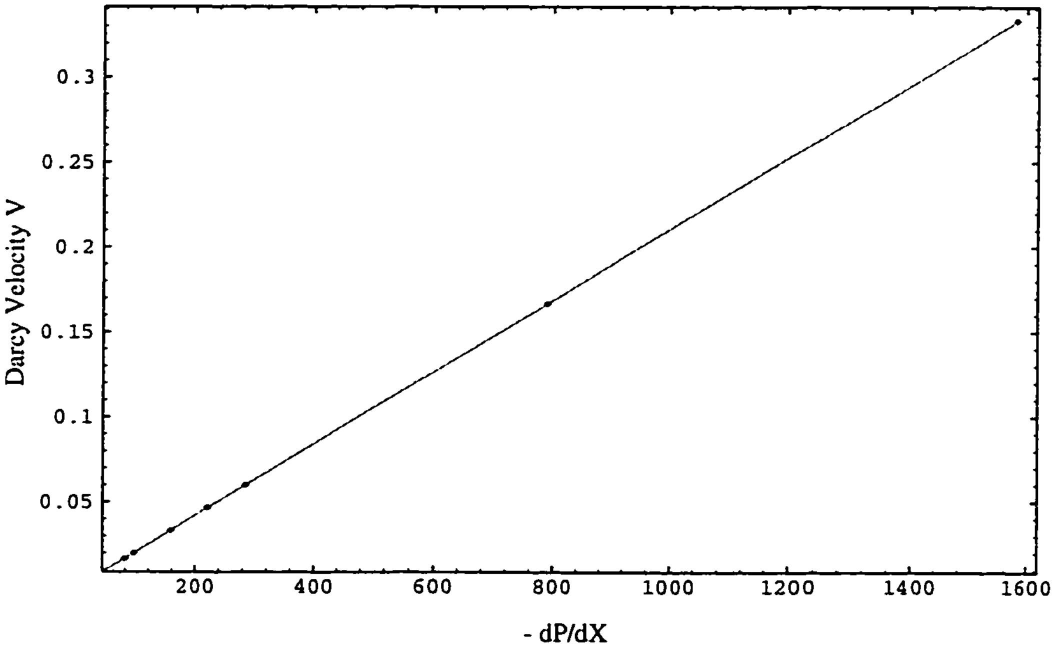

Figure 3.16: Example of straight line fitting low flow rate data (points). In this way, the permeability (k) of a porous media can be found by using Darcy's law, equation (1.1) on page 1.

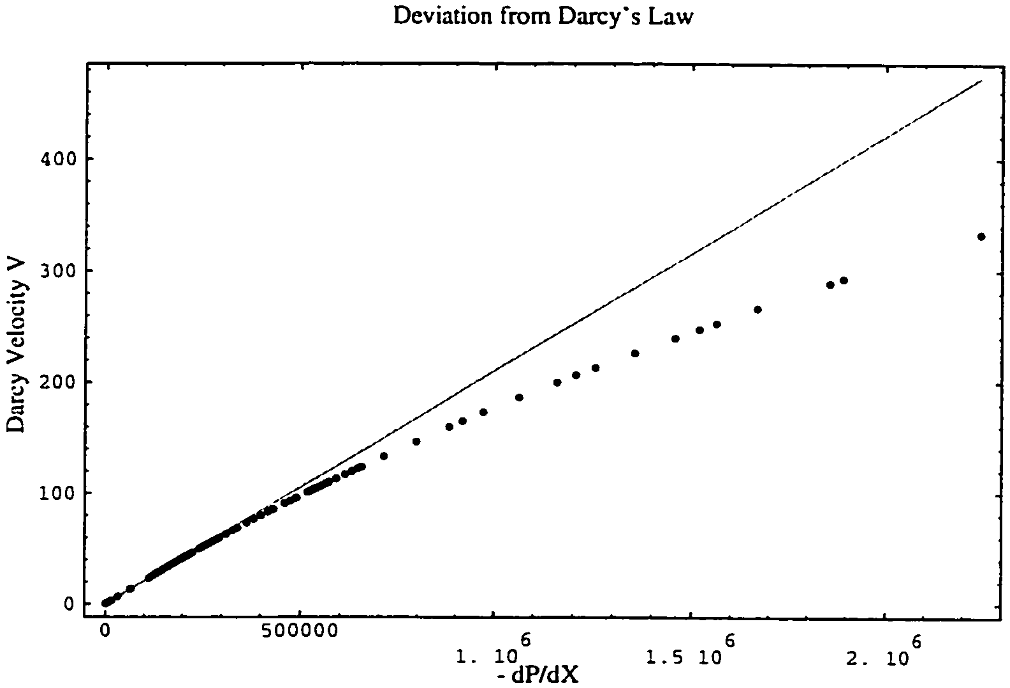

Figure 3.17: Typical deviation of data (points) from Darcy's law (solid line).

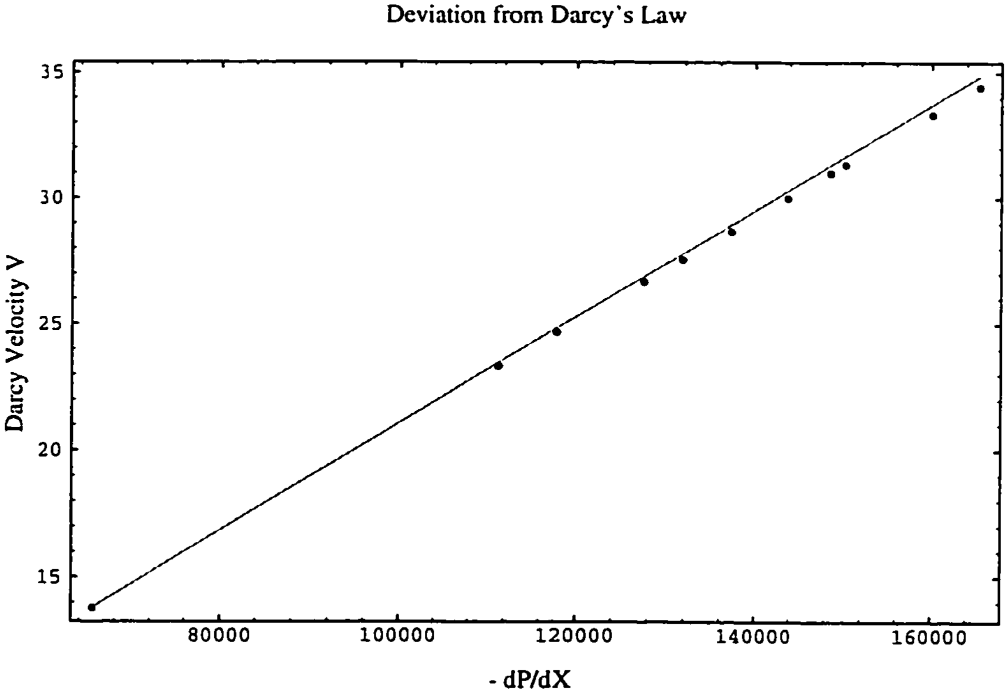

Figure 3.18: Plot of data (points) showing deviation from Darcy's law (solid line) at low flow rate.

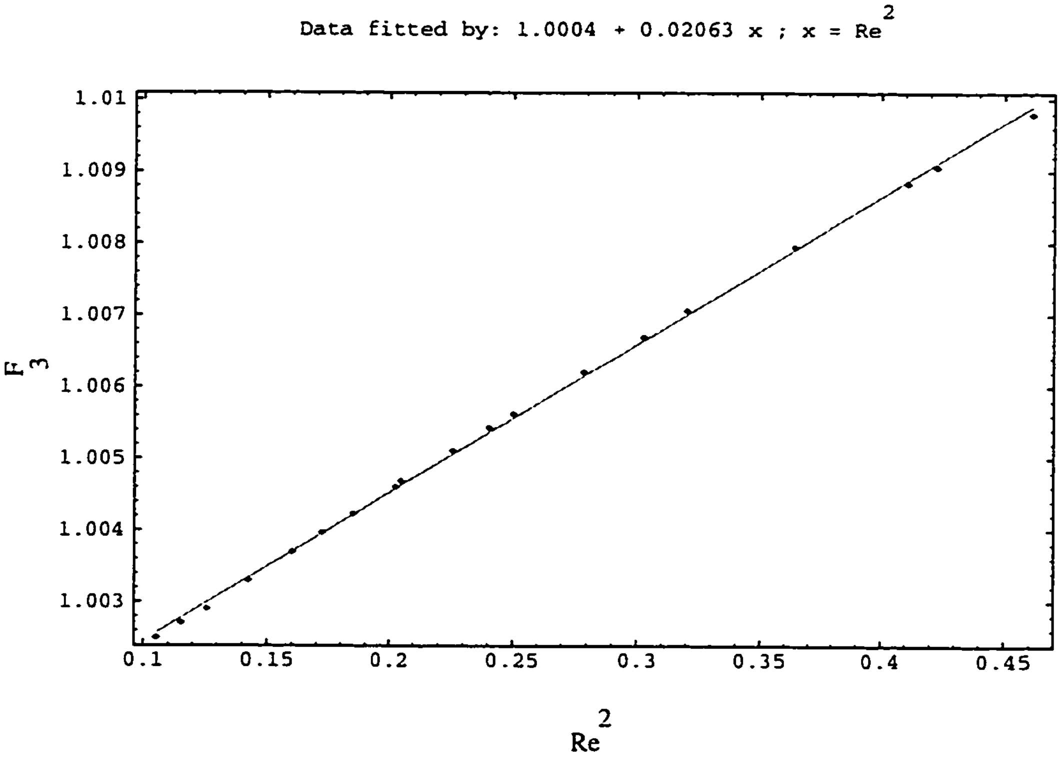

Figure 3.19: $\frac{\rho \mathcal{L} k}{\mu^2 Re}(-\frac{\Delta P}{\Delta X})$ (points) fitted by $F_3$ (solid line), equation (3.7$a$) on page 36. This set of data corresponds to the simulation done using the geometry shown in Fig.-3.2 on page 46. Here, $\mathcal{L} = k^{1/2}$. $\chi^2_{F_3} = \frac{6.23 \times 10^{-8}}{\sigma^2}$ computed according to equation (3.9) on page 39. See discussion below equation (3.9) for the meaning of this value.

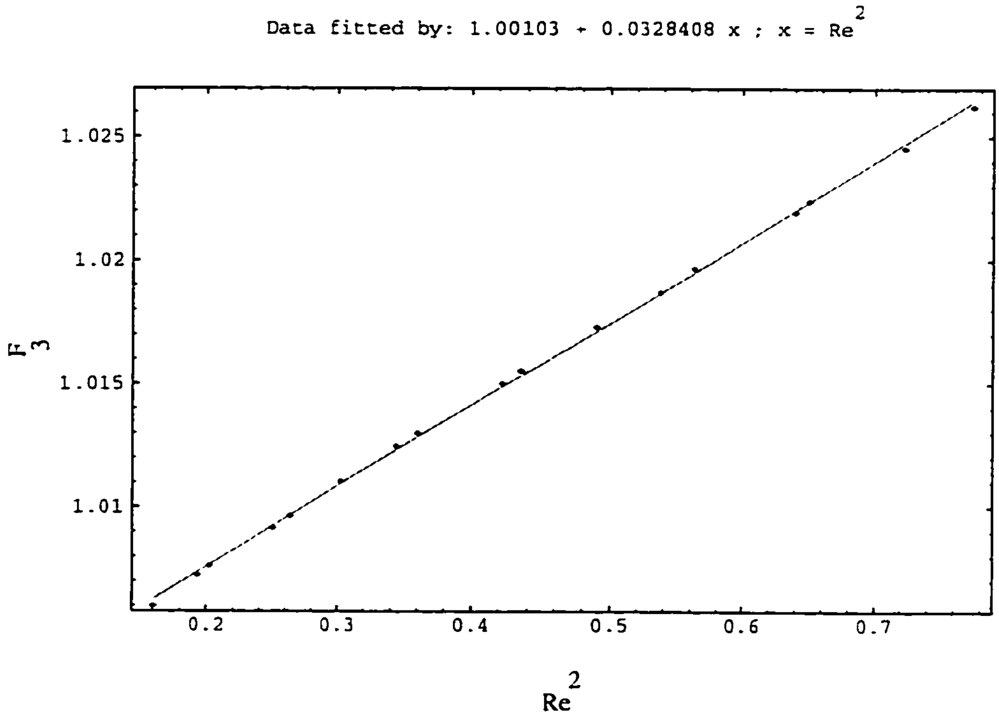

Figure 3.20: $\frac{\rho \mathcal{L} k}{\mu^2 Re}(-\frac{\Delta P}{\Delta X})$ (points) fitted by $F_3$ (solid line), equation (3.7$a$) on page 36. This set of data corresponds to the simulation done using the geometry shown in Fig.-3.7 on page 48. Here, $\mathcal{L} = k^{1/2}$. $\chi^2_{F_3} = \frac{3.79\times10^{-7}}{\sigma^2}$ computed according to equation (3.9) on page 39. See discussion below equation (3.9) for the meaning of this value.

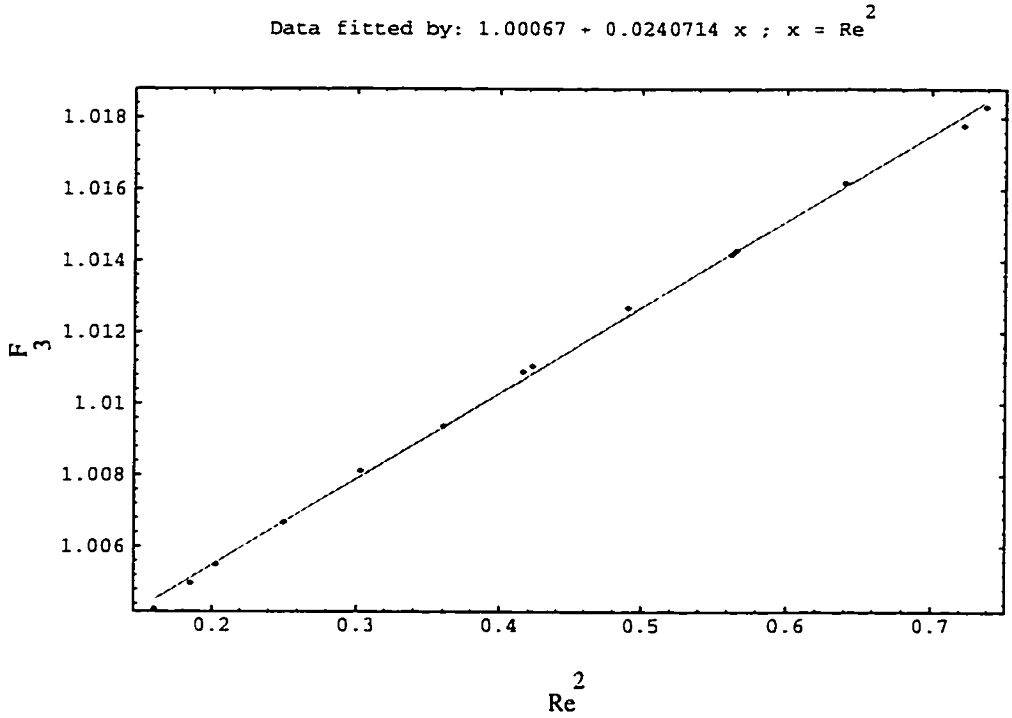

Figure 3.21: $\frac{\rho \mathcal{L} k}{\mu^2 Re}(-\frac{\Delta P}{\Delta X})$ (points) fitted by $F_3$ (solid line), equation (3.7*a*) on page 36. This set of data corresponds to the simulation done using the geometry shown in Fig.-3.9 on page 49. Here, $\mathcal{L} = k^{1/2}$. $\chi^2_{F_3} = \frac{3.81\times10^{-7}}{\sigma^2}$ computed according to equation (3.9) on page 39. See discussion below equation (3.9) for the meaning of this value.

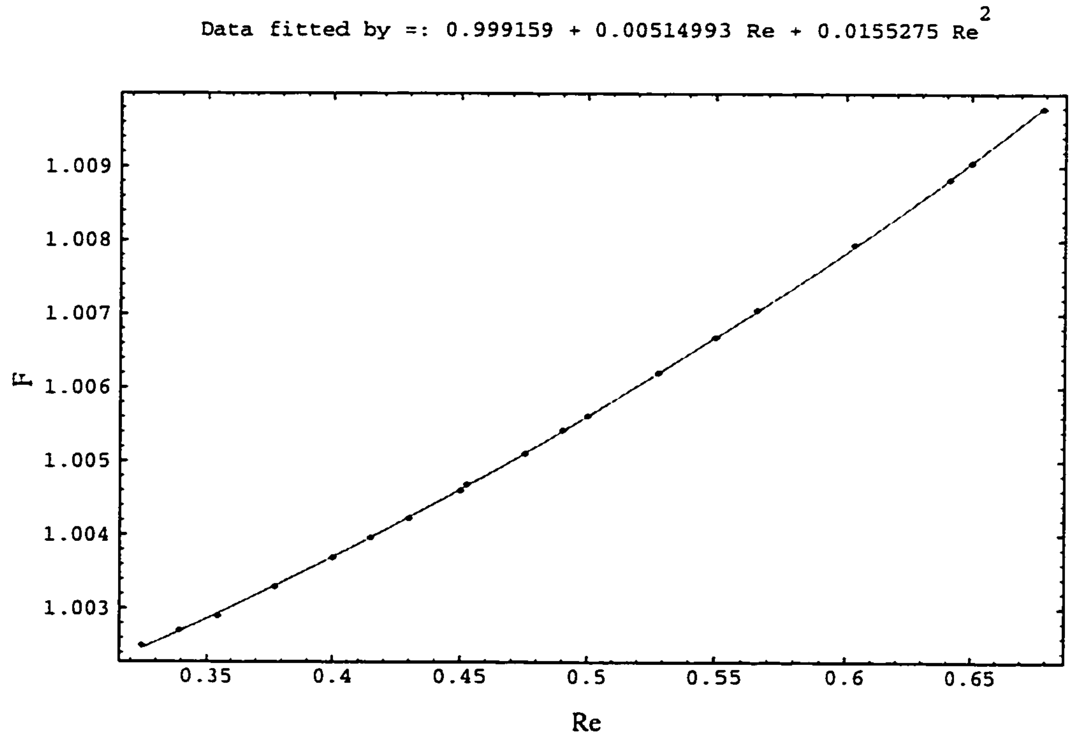

Figure 3.22: $\frac{\rho \mathcal{L} k}{\mu^2 Re}(-\frac{\Delta P}{\Delta X})$ (points) fitted by $F$ (solid line), equation (3.6) on page 36. This set of data corresponds to the simulation done using the geometry shown in Fig.-3.2 on page 46. Here, $\mathcal{L} = k^{1/2}$. $\chi_F^2 = \frac{5.70\times10^{-9}}{\sigma^2}$ computed according to equation (3.9) on page 39. See discussion below equation (3.9) for the meaning of this value.

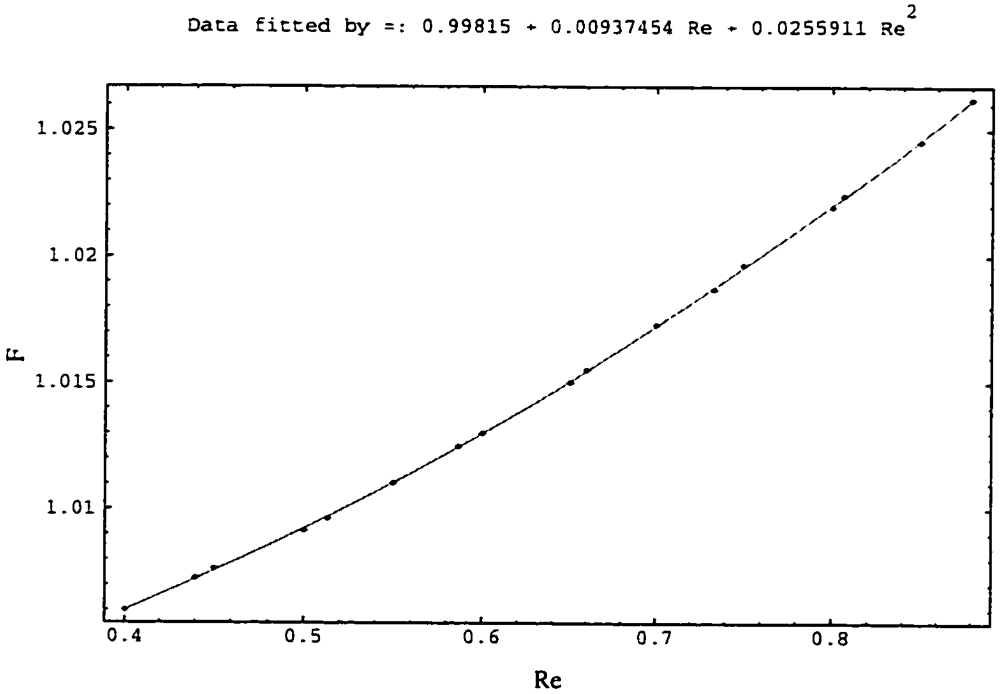

Figure 3.23: $\frac{\rho \mathcal{L} k}{\mu^2 Re}(-\frac{\Delta P}{\Delta X})$ (points) fitted by $F$ (solid line), equation (3.6) on page 36. This set of data corresponds to the simulation done using the geometry shown in Fig.-3.7 on page 48. Here, $\mathcal{L} = k^{1/2}$. $\chi_F^2 = \frac{5.29\times10^{-8}}{\sigma^2}$ computed according to equation (3.9) on page 39. See discussion below equation (3.9) for the meaning of this value.

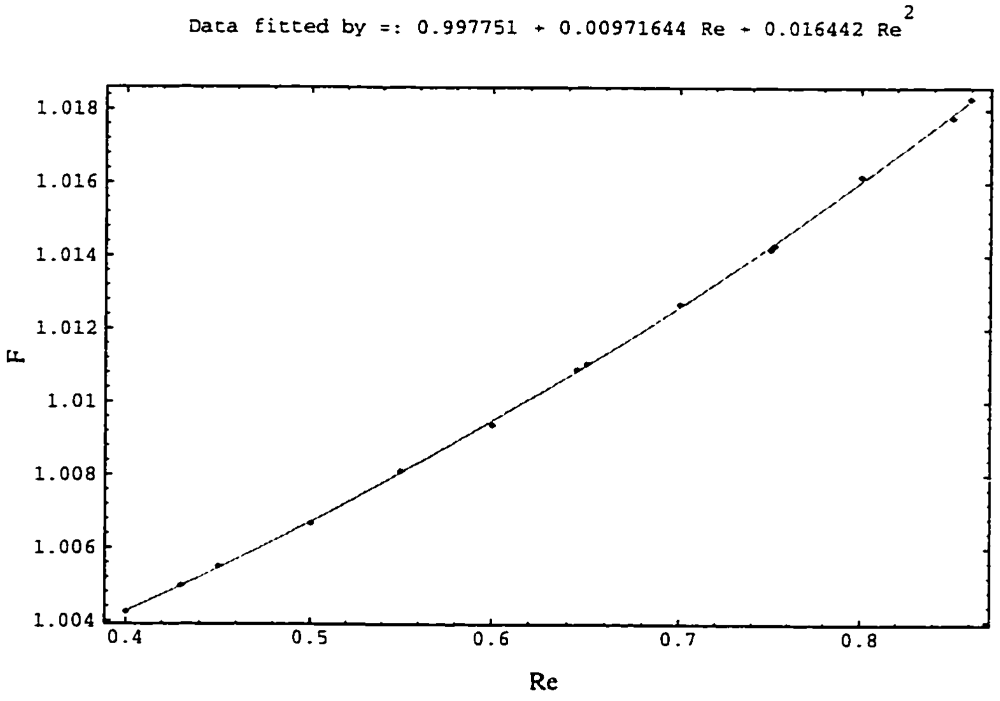

Figure 3.24: $\frac{\rho\mathcal{L}k}{\mu^2 Re}(-\frac{\Delta P}{\Delta X})$ (points) fitted by $F$ (solid line), equation (3.6) on page 36. This set of data corresponds to the simulation done using the geometry shown in Fig.-3.9 on page 49. Here, $\mathcal{L} = k^{1/2}$. $\chi_F^2 = \frac{7.93\times10^{-8}}{\sigma^2}$ computed according to equation (3.9) on page 39. See discussion below equation (3.9) for the meaning of this value.

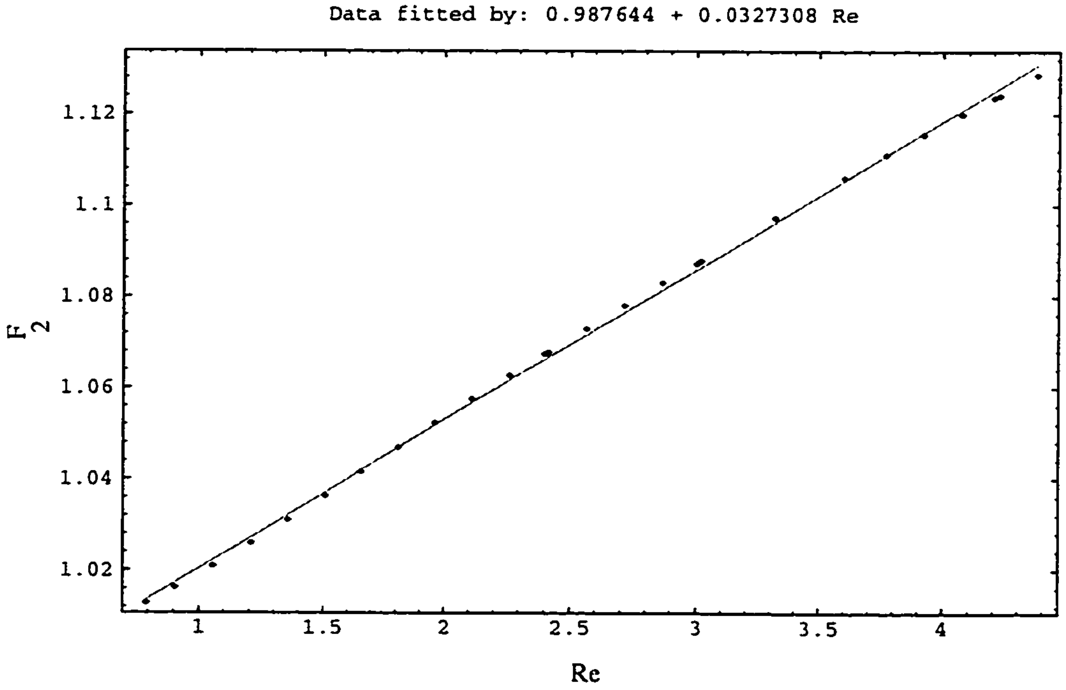

Figure 3.25: $\frac{\rho\mathcal{L}k}{\mu^2 Re}(-\frac{\Delta P}{\Delta X})$ (points) fitted by $F_2$ (solid line), equation (3.7*b*) on page 36. This set of data corresponds to the simulation done using the geometry shown in Fig.-3.2 on page 46. Here, $\mathcal{L} = k^{1/2}$.

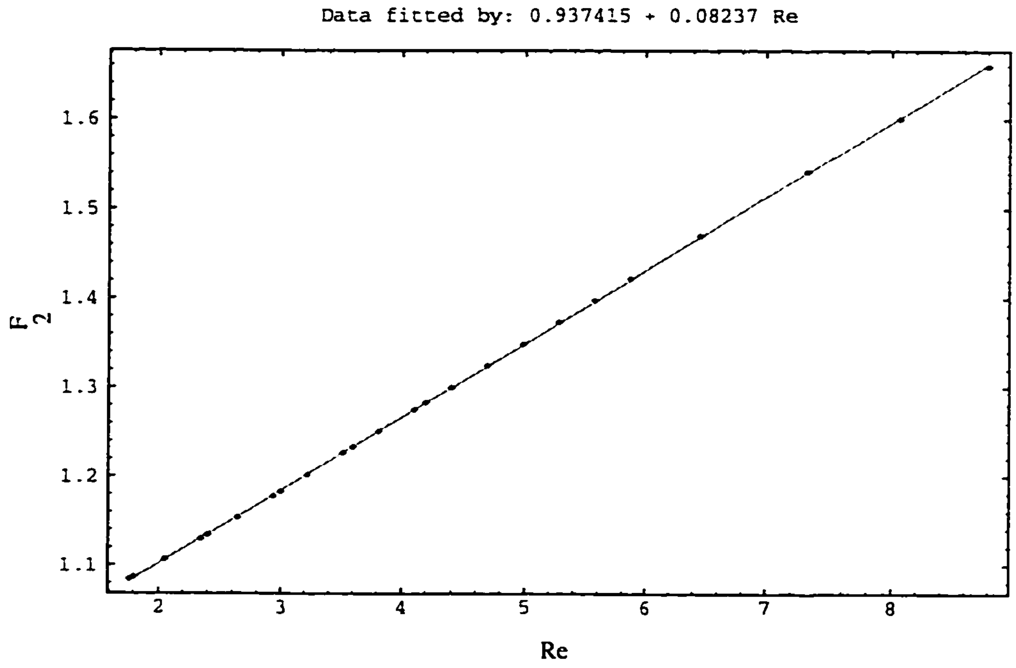

Figure 3.26: $\frac{\rho \mathcal{L} k}{\mu^2 Re}(-\frac{\Delta P}{\Delta X})$ (points) fitted by $F_2$ (solid line), equation (3.7*b*) on page 36. This set of data corresponds to the simulation done using the geometry shown in Fig.-3.7 on page 48. Here, $\mathcal{L} = k^{1/2}$.

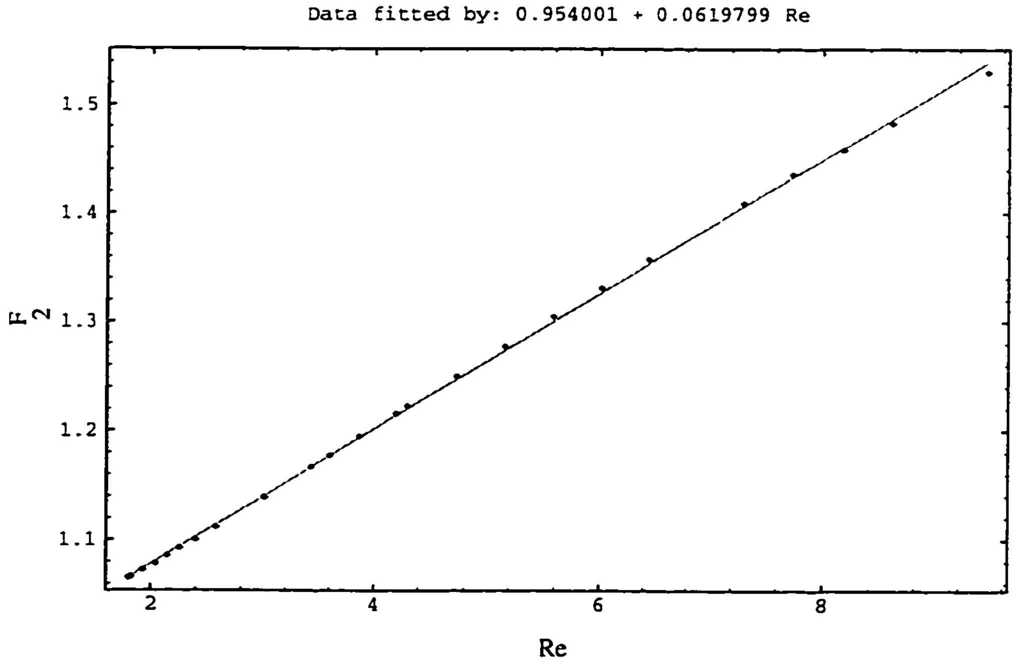

Figure 3.27: $\frac{\rho \mathcal{L} k}{\mu^2 Re}(-\frac{\Delta P}{\Delta X})$ (points) fitted by $F_2$ (solid line), equation (3.7*b*) on page 36. This set of data corresponds to the simulation done using the geometry shown in Fig.-3.9 on page 49. Here, $\mathcal{L} = k^{1/2}$.

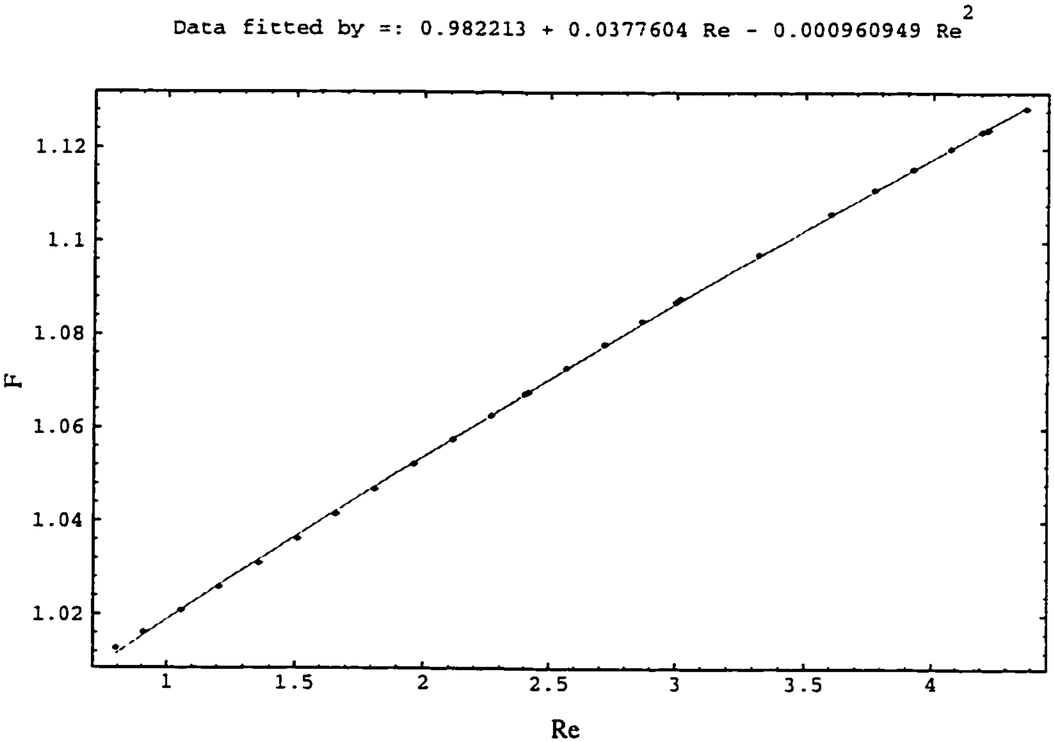

Figure 3.28: $\frac{\rho\mathcal{L}k}{\mu^2 Re}(-\frac{\Delta P}{\Delta X})$ (points) fitted by $F$ (solid line), equation (3.6) on page 36. This set of data corresponds to the simulation done using the geometry shown in Fig.-3.2 on page 46. Here, $\mathcal{L} = k^{1/2}$.

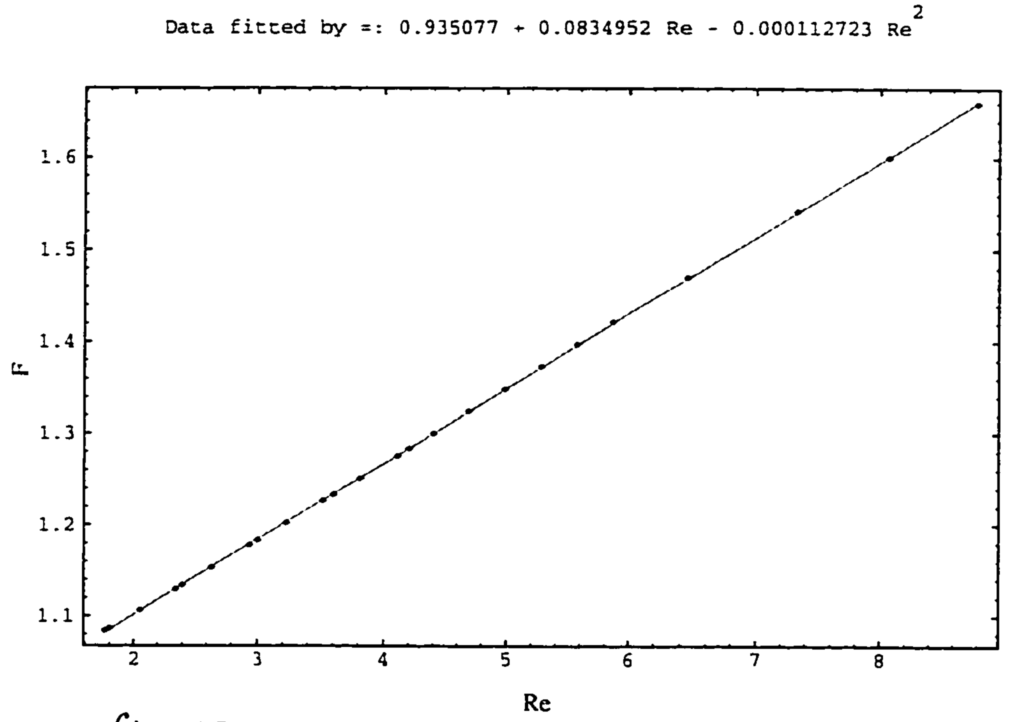

Figure 3.29: $\frac{\rho\mathcal{L}k}{\mu^2 Re}(-\frac{\Delta P}{\Delta X})$ (points) fitted by $F$ (solid line), equation (3.6) on page 36. This set of data corresponds to the simulation done using the geometry shown in Fig.-3.7 on page 48. Here, $\mathcal{L} = k^{1/2}$.

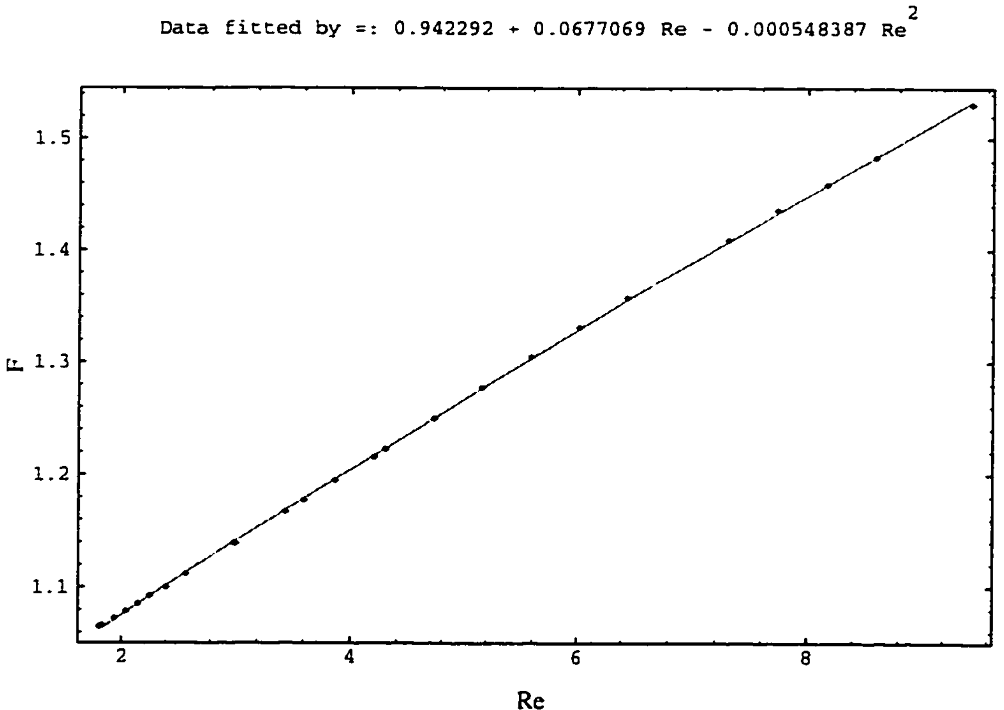

Figure 3.30: $\frac{\rho\mathcal{L}k}{\mu^2 Re}(-\frac{\Delta P}{\Delta X})$ (points) fitted by $F$ (solid line), equation (3.6) on page 36. This set of data corresponds to the simulation done using the geometry shown in Fig.-3.9 on page 49. Here, $\mathcal{L} = k^{1/2}$.

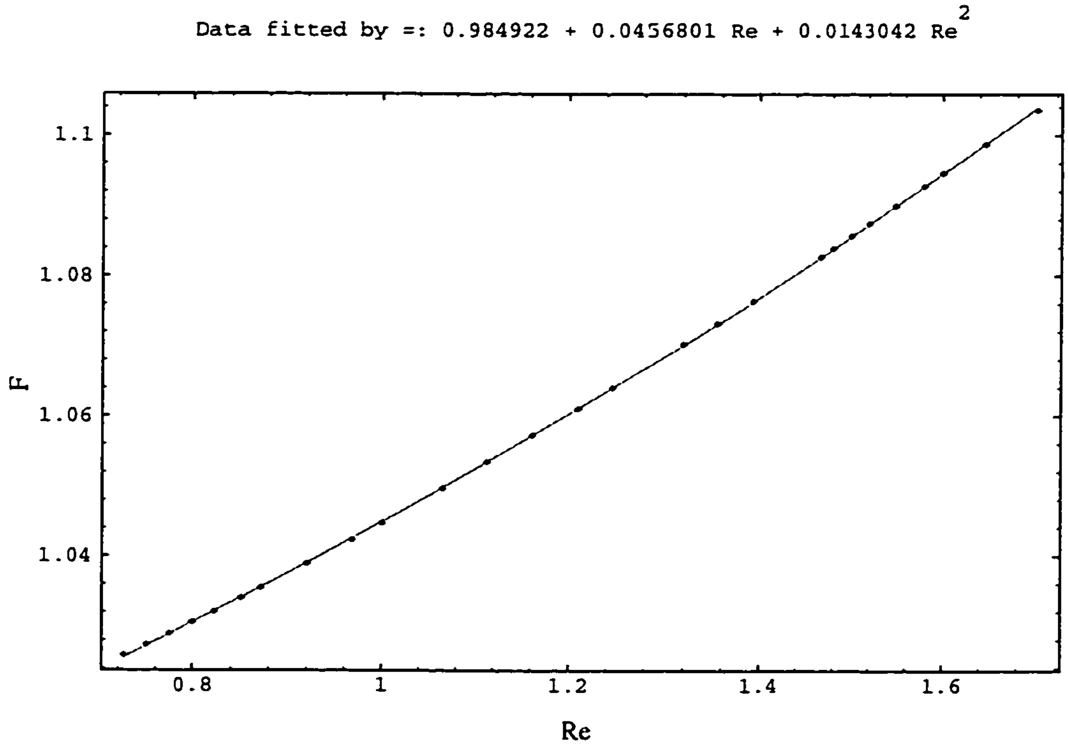

Figure 3.31: $\frac{\rho \mathcal{L} k}{\mu^2 Re}(-\frac{\Delta P}{\Delta X})$ (points) fitted by $F$ (solid line), equation (3.6) on page 36. This set of data corresponds to the simulation done using the geometry shown in Fig.-3.4 on page 47. The range of Reynolds number corresponds to the transition from the regime where the flow is dominated by $F_3$, equation (3.7*a*) on page 36, to the regime where the flow is dominated by $F_2$, equation (3.7*b*) on page 36. Here, $\mathcal{L} = k^{1/2}$. $\chi_F^2 = \frac{4.02 \times 10^{-7}}{\sigma^2}$ computed according to equation (3.9) on page 39.

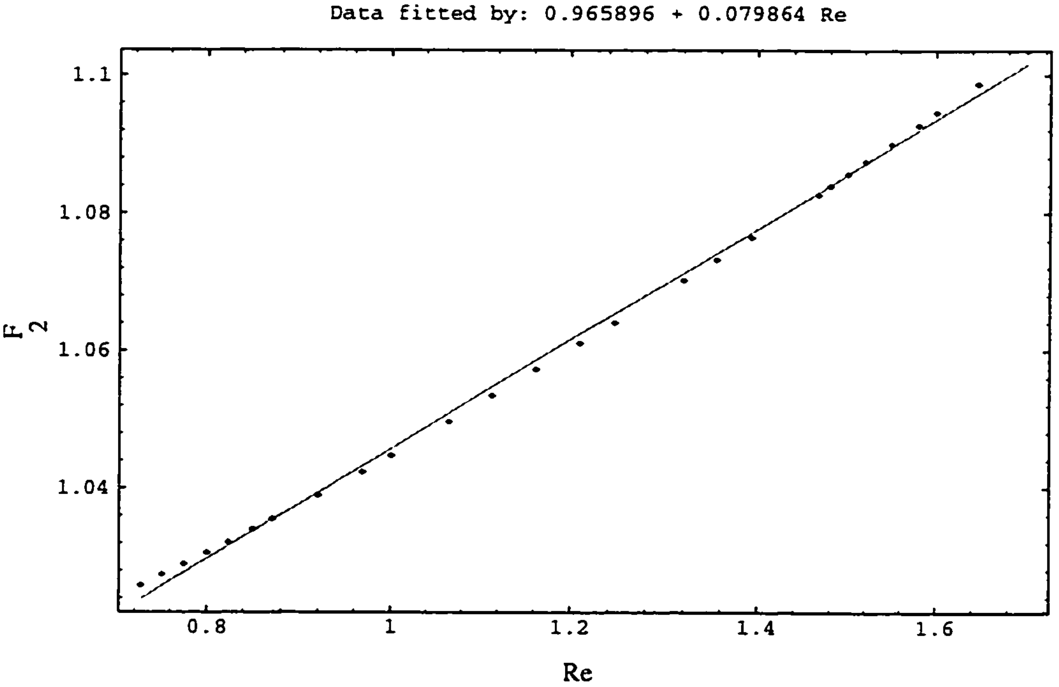

Figure 3.32: $\frac{\rho\mathcal{L}k}{\mu^2 Re}(-\frac{\Delta P}{\Delta X})$ (points) fitted by $F_2$ (solid line), equation (3.7*b*) on page 36. This set of data corresponds to the simulation done using the geometry shown in Fig.-3.4 on page 47. The range of Reynolds number corresponds to the transition from the regime where the flow is dominated by $F_3$, equation (3.7*a*) on page 36, to the regime where the flow is dominated by $F_2$, equation (3.7*b*) on page 36. Here, $\mathcal{L} = k^{1/2}$. $\chi^2_{F_2} = \frac{5.31\times 10^{-5}}{\sigma^2}$ computed according to equation (3.9) on page 39.

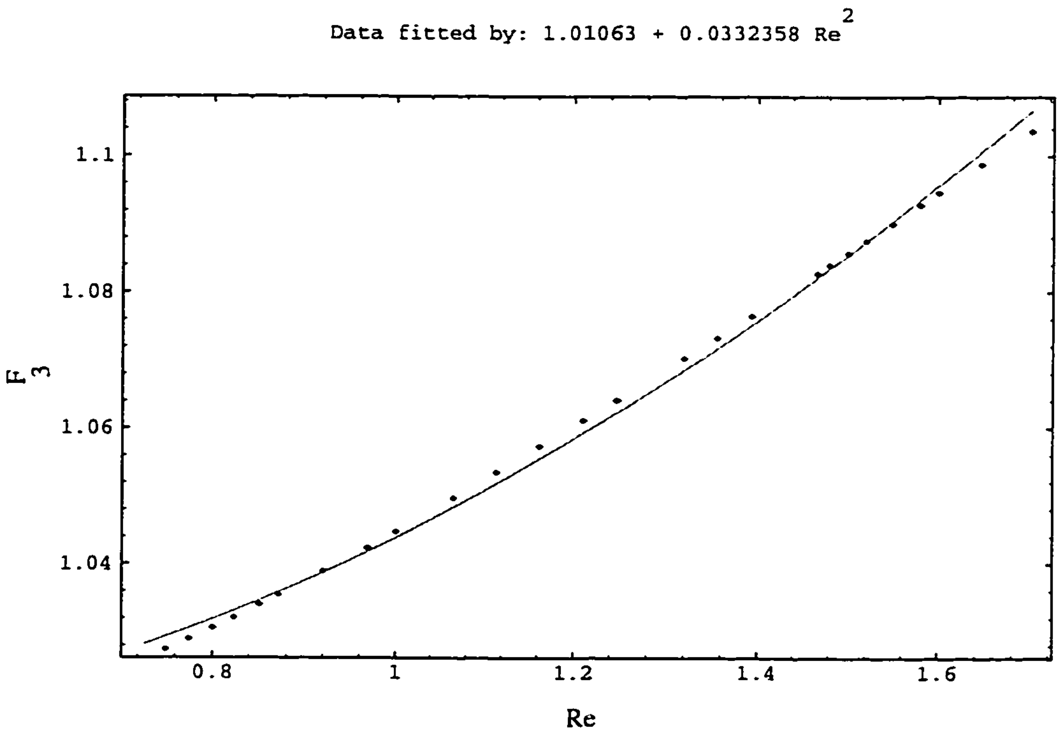

Figure 3.33: $\frac{\rho \mathcal{L} k}{\mu^2 Re}(-\frac{\Delta P}{\Delta X})$ (points) fitted by $F_3$ (solid line), equation (3.7$a$) on page 36. This set of data corresponds to the simulation done using the geometry shown in Fig.-3.4 on page 47. The range of Reynolds number corresponds to the transition from the regime where the flow is dominated by $F_3$, equation (3.7$a$) on page 36, to the regime where the flow is dominated by $F_2$, equation (3.7$b$) on page 36. Here, $\mathcal{L} = k^{1/2}$. $\chi^2_{F_3} = \frac{3.02 \times 10^{-5}}{\sigma^2}$ computed according to equation (3.9) on page 39.

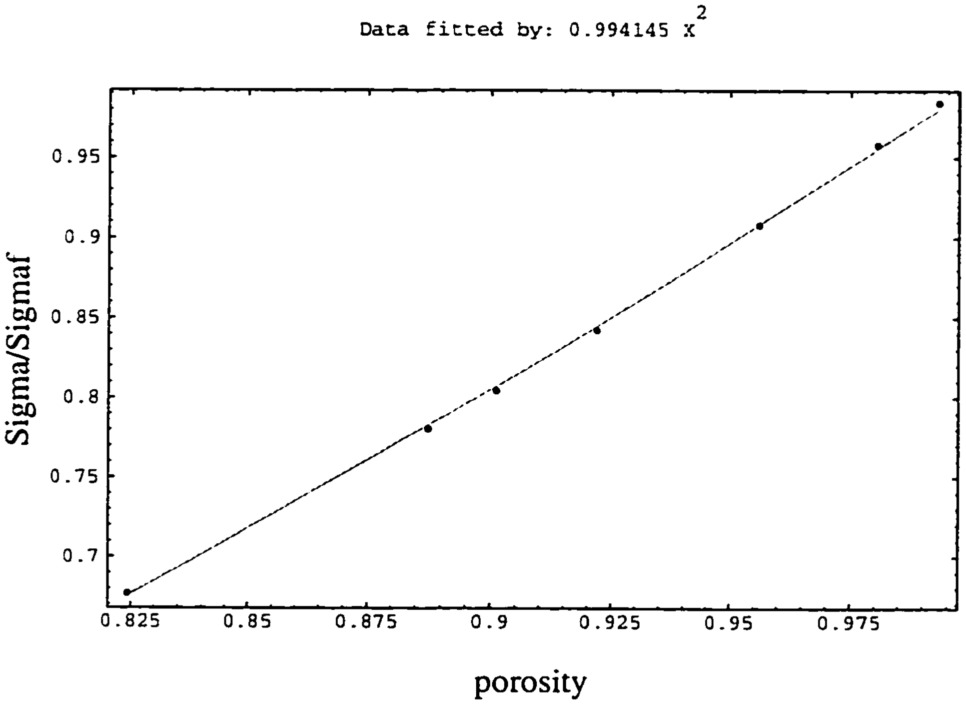

Figure 3.34: Conductivity ($\frac{\sigma}{\sigma_f}$) Vs porosity ($\phi$) following Archie's law (solid line): $\frac{\sigma}{\sigma_f} = a\,\phi^m$ with $a$ close to 1 and $m$ close to 2.

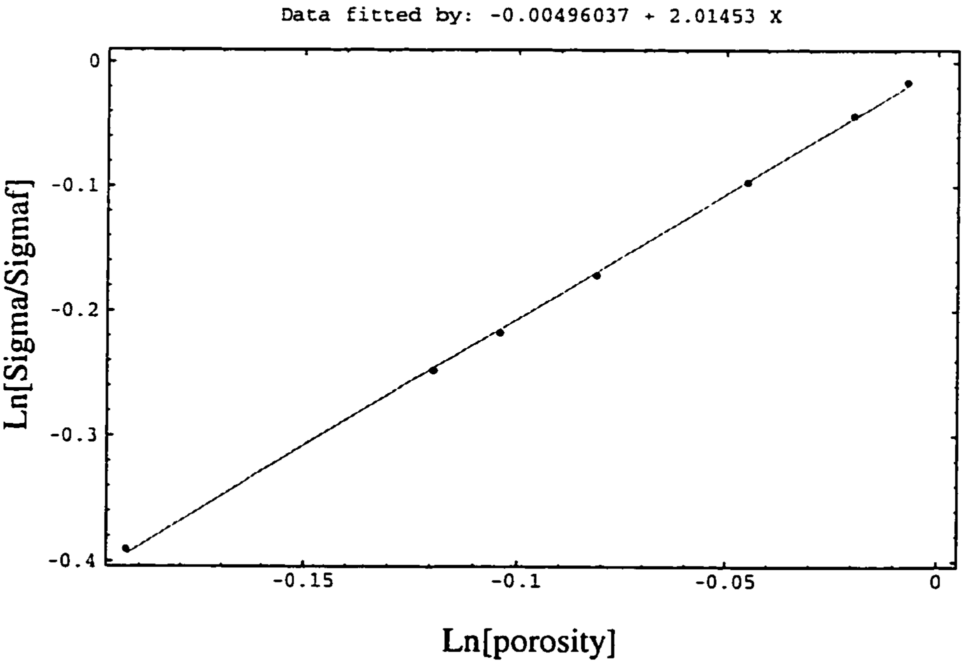

Figure 3.35: $Ln[\frac{\sigma}{\sigma_f}]$ Vs $ln[\phi]$ (points) following Archie's law (solid line): $Ln[\frac{\sigma}{\sigma_f}] = Ln[a] + m\,Ln[\phi]$ with $a$ close to 1 and $m$ close to 2.

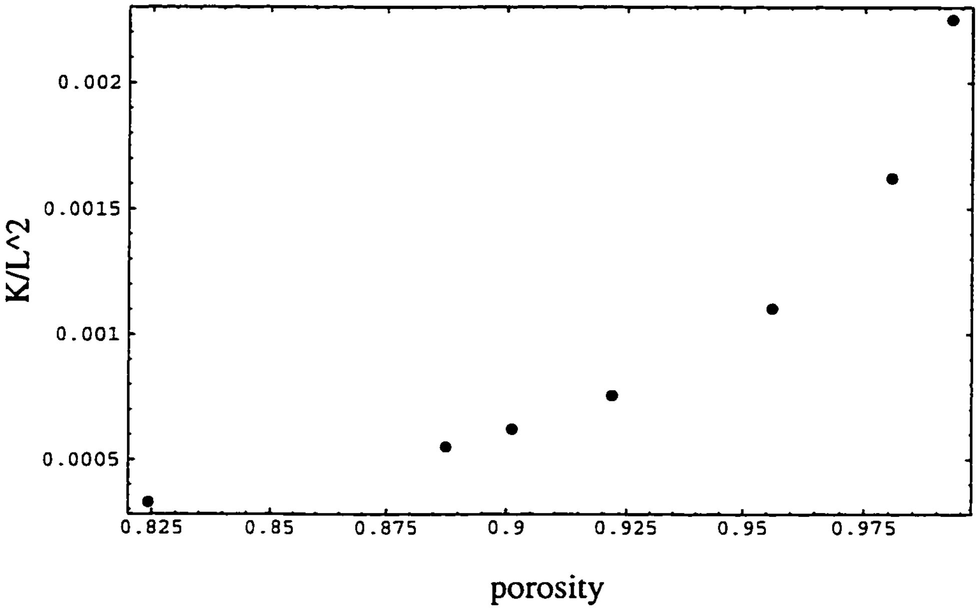

Figure 3.36: Permeability ($\frac{K}{L^2}$) Vs porosity ($\phi$). $L = 0.8\,cm^2$ is the length of the porous sample.

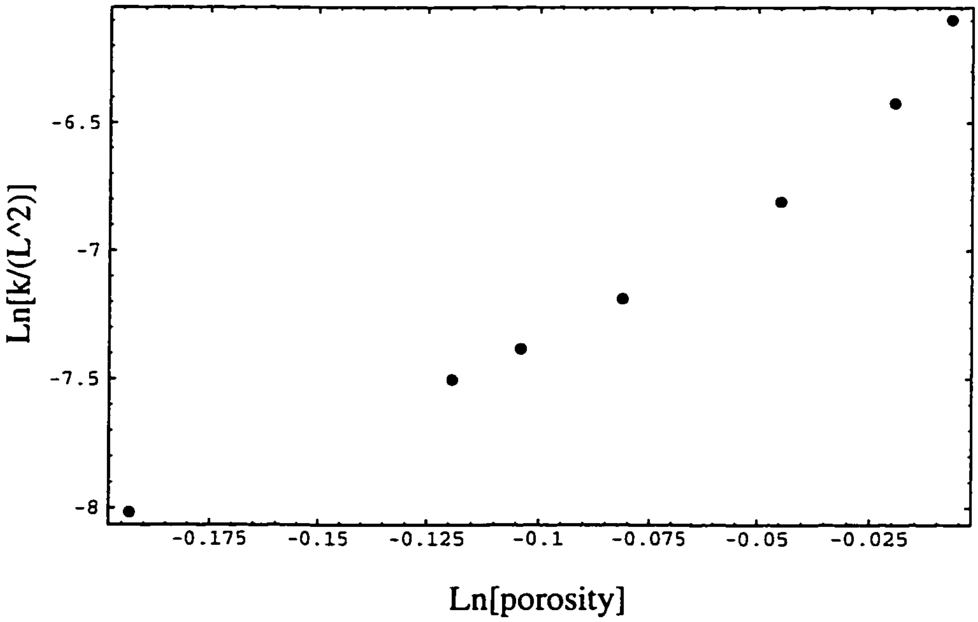

Figure 3.37: $Ln[\frac{K}{L^2}]$ Vs $Ln[\phi]$. $L = 0.8\,cm^2$ is the length of the porous sample.

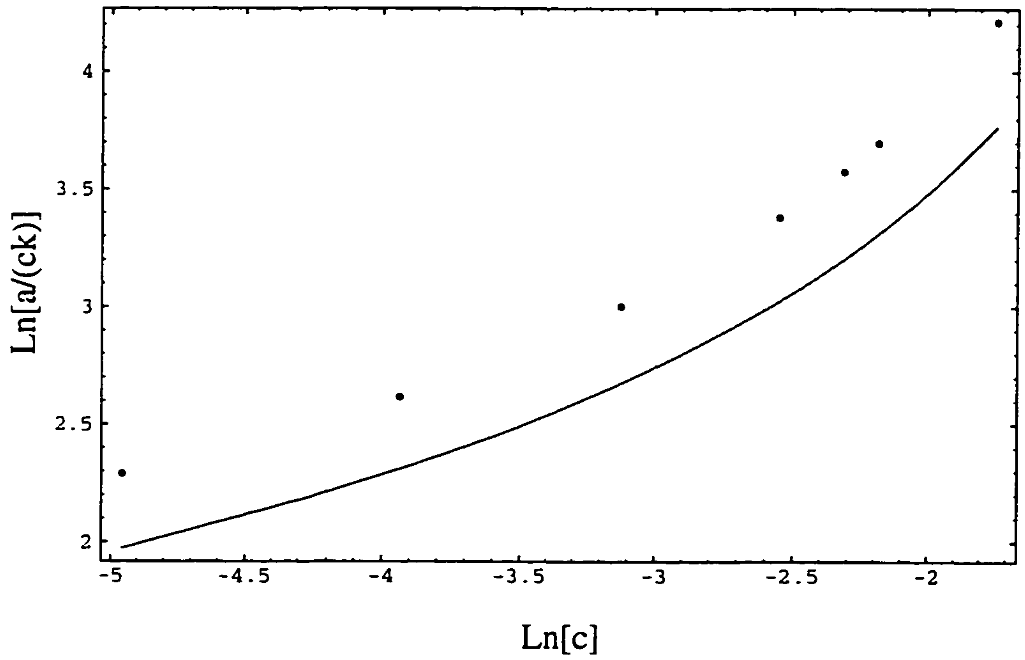

Figure 3.38: $Ln(\frac{a}{ck})$ Vs $Ln(c)$ (points) and $Ln(F')$ Vs $Ln(c)$ (solid line). $F'$ is given by equation (3.11) on page 41. $c$ is the solid fraction.

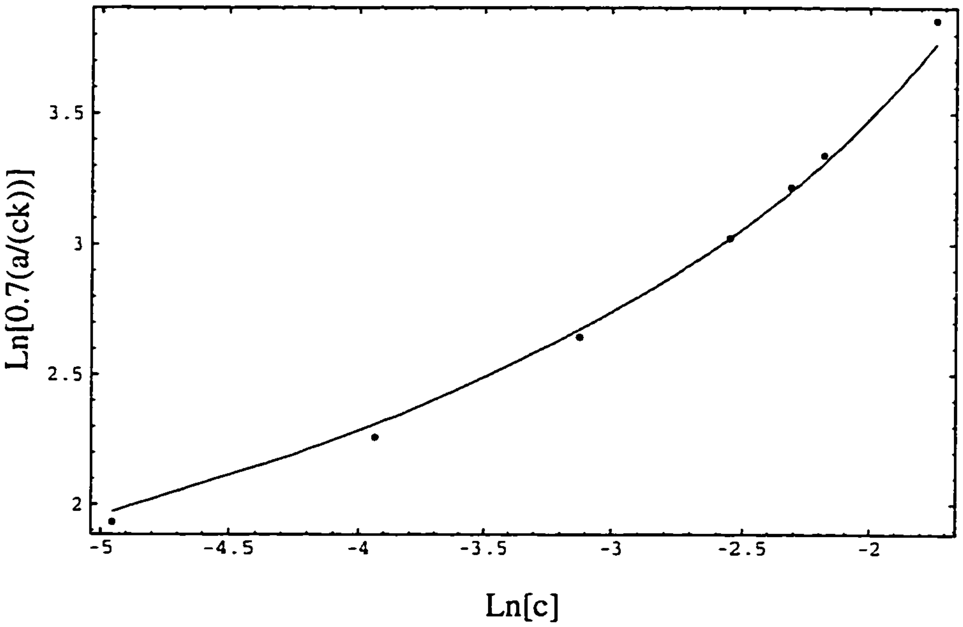

Figure 3.39: $Ln(\frac{0.7a}{ck})$ Vs $Ln(c)$ (points) and $Ln(F')$ Vs $Ln(c)$ (solid line). $F'$ is given by equation (3.11) on page 41. $c$ is the solid fraction.

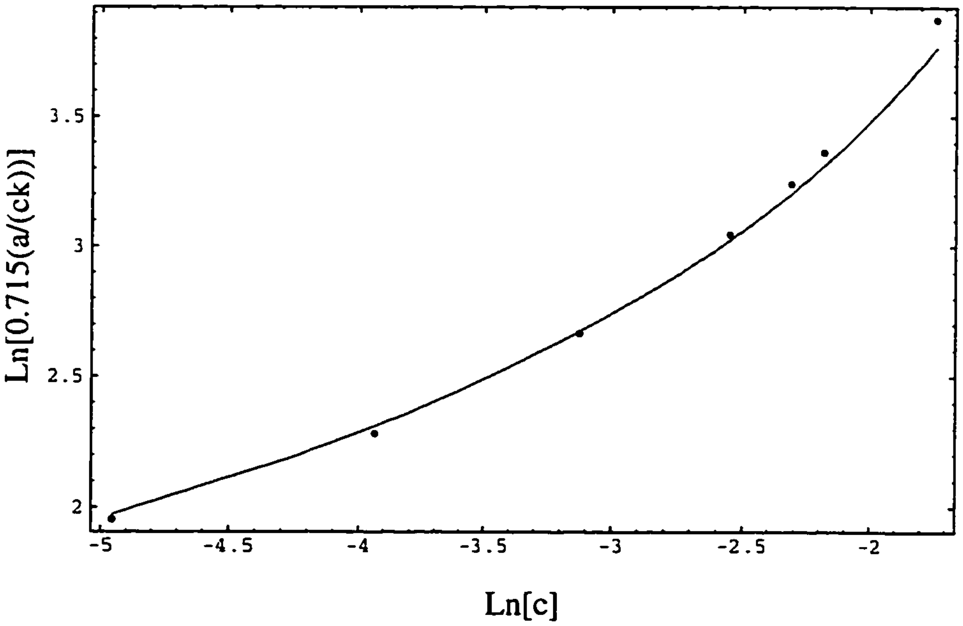

Figure 3.40: $Ln(\frac{0.715a}{ck})$ Vs $Ln(c)$ (points) and $Ln(F')$ Vs $Ln(c)$ (solid line). $F'$ is given by equation (3.11) on page 41. $c$ is the solid fraction.

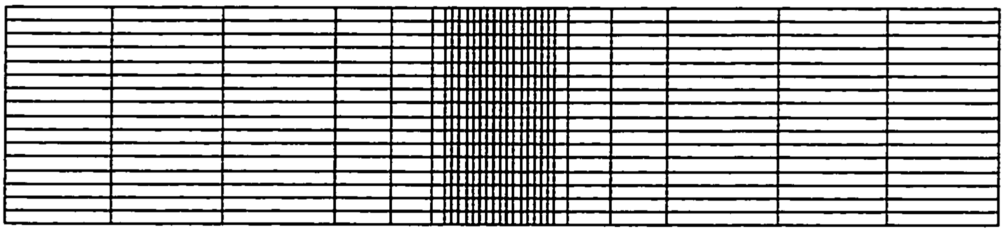

Figure 3.41: Mesh used for porous sample geometry shown in Fig.-3.4

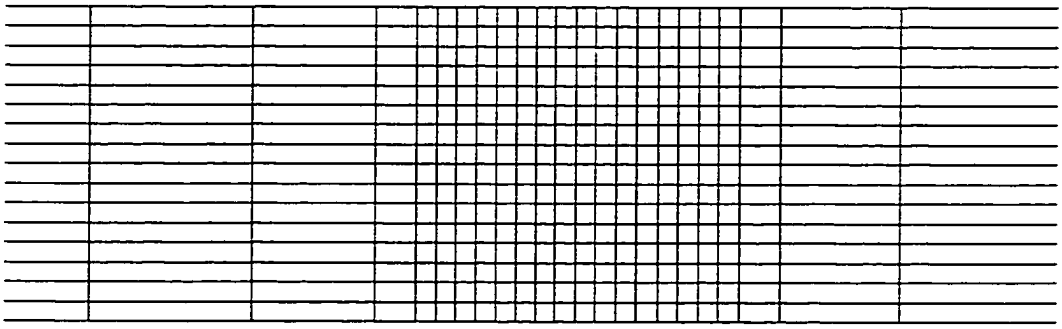

Figure 3.42: Expanded version of mesh used for geometry shown in Fig.-3.4

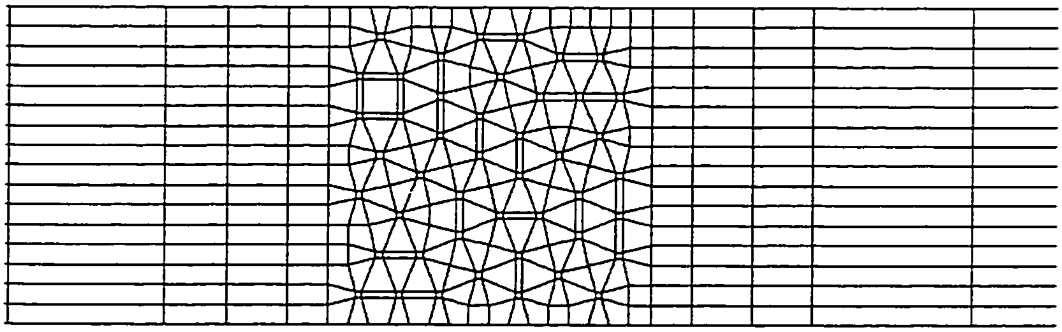

Figure 3.43: Mesh used for porous sample geometry shown in Fig.-3.9

# Chapter 4

# Summary

Computer solutions of the Navier Stokes equations were obtained in periodic and random arrays of long cylinders with square cross sections for low and moderate values of the Reynolds number based on the square root of the permeability of the porous samples, and the average (Darcy) velocity across the sample. The range of porosity covered can be considered to be in the dilute limit. At very low Reynolds numbers, we were able to fit our calculations of the permeability of the samples, based on Darcy's law, with analytical results obtained by Sangani and Acrivos (1982). The results show very good agreement with the theory provided that the data is properly scaled by a constant. Our results show that when the Reynolds number is less than one, the correction to Darcy's law is cubic in the average velocity throughout an *isotropic* and *homogeneous* porous media. This result is consistent with the theoretical conclusion of Mei and Auriault (1991) based on Homogenization theory. At moderate values of the Reynolds number, however, our results show that the first correction to Darcy's law becomes quadratic in the average velocity throughout the porous media, in agreement with Forchheimer relation, equation (1.2) on page 2. Though there is not strong theoretical justification for this behavior, there is considerable experimental evidence of it. These results can be summarized by the following equation:

$$-\nabla P = (\frac{\mu}{k})g(Re)\vec{V} \tag{4.1}$$

where the dimensionless function $g(Re)$ has the limiting behaviors:

$$g \rightarrow \begin{cases} 1 & \text{if } Re \rightarrow 0 \\ 1 + bRe^2 & \text{if } Re < 1 \\ 1 + cRe & Re \ finite \end{cases} \tag{4.2}$$

Also, in the limit of finite Reynolds numbers, our results are in very good agreement with the experimental results of Beavers and Sparrow (1969), and show that fluid through porous media of similar structure is well described by equation (3.8), with $\mathcal{L} = \sqrt{k}$ and $b\sqrt{k} \cong 0.07$. Furthermore, these results also support the idea of using the square root of the permeability as the characteristic dynamical length representing the pore scale. The use of other length scale would lead to different results, as may be obvious from equation (3.8), on page 37. Moreover, our results show that the cubic correction to Darcy's law is valid for Reynolds number greater than $\epsilon^{0.5}$ but less than one, while the quadratic regime was observed to occur at Reynolds number greater than $\epsilon^{-0.1}$. Recall that $\epsilon = \frac{\sqrt{k}}{L}$, with $L$ representing the porous sample length ($L = 0.8\,cm$ in this case). The fact that the flow regime is dominated by $F_3$ in Eq. (3.7$a$) for $\epsilon^{1/2} < Re < 1$, is in agreement with the assumption done by Mei and Auriault (1991) in their theoretical work. Many studies have been based on using rough estimations of the porous sizes, but as is discussed elsewhere (Scheidegger 1974, Dullien 1992), it leads to ambiguities in the range of validity of the different flow regimes characterizing fluid flow in porous media. This may be in part due to the fact that, in general, is expensive, both economically or computationally, the determination of permeabilities. In fact, finding the permeability of the sample used in this study was the most time-consuming part in cpu usage. On the other hand, we found that the conductivity of the random samples shown in Fig.-3.4 through Fig.-3.10 follows Archie's law with $m = 2$ as the exponent of the power law in the porosity. However, the permeability does not show any power behavior. Neither was a simple relation with the conductivity of the porous medium was found. Instead, it was found that the inverse of the product of the permeability and the solid fraction can be adjusted to follow an equation obtained by Sangani and Acrivos (1982) in the diluted approximation of a regular array of cylinders. We believe, that this result is not fortuitous, but instead, it shows that Sangani and Acrivos equation can be applied to random arrays of at less well defined cross section. Finally, though the derivation of Mei and Auriault 1991 was given by assuming periodic porous media, their validity to random structures is supported by this work, and its justification may be given in terms of ensemble-averages like in the work of Rubinsteins and Torquato (1989).

# Appendix A

# NEKTON

## A.1 About NEKTON

The numerical solutions of the Navier-Stokes equations were carried out by using version 2.9 of the commercial Computational Fluid Dynamics (CFD) software called NEKTON. This software can be used to obtain numerical solutions of the full incompressible, time-dependent Navier-Stokes and energy (heat transfer) equations, including subsets of such equations like steady and unsteady Stokes equations, heat conduction without fluid flow and vice versa, etc..

The spatial discretization used by the numerical computational engine of NEKTON is based in the so-called spectral element method, a high-order finite element method for partial differential equations, in complex 2-dimensional and 3-dimensional topology used to obtain numerical solution of the specified set of equations in the domain of interest. In this approach, the computational domain is represented as a set of macro-elements (defined by the user) with the solution and geometry being approximated (internally by the program) by high-order polynomial expansions within each macro-element. Specifically, a local Cartesian mesh, which corresponds to NxN(xN) (N=5,7,9,...,15) tensor-product Gauss-Lobatto Legendre collocation points (non-uniformly spaced by distances $\Delta x, \Delta y, (\Delta z)$) and clustered near the boundaries of the local macro-element, is constructed within each macro-element. The Gauss-Lobatto Legendre points were chosen because of their accurate approximation, interpolation, quadrature properties.

Within each macro-element, the dependent variables are expanded in terms of $(N-1)$th order tensor-product Lagrangian interpolant through the Gauss-Lobatto Legendre collocation points. For example, the temperature is expanded as: $T = \sum_{i=0}^{N} T_i h_i$ , where the $h_i$ are Lagrangian interpolant (polynomials that are unity at the $i^{th}$ Gauss-Lobatto node and zero at all others), and the $T_i$ are nodal values of the temperature.

Convergence to the exact solution is obtained either by increasing the number of macro-elements ($M$), which decreases the error by $M^{-N}$, or by increasing the order of the interpolant ($N$) in which case the error decrease as $e^{-\alpha N}$. Any solution should be verified to be converged (mesh-independent) by repeating the calculation with higher $M$ and/or $N$.

For time dependent simulations, NEKTON employs both explicit and implicit time-integration techniques, and the solution is updated to the new time level using various combinations of multisteps and multistage schemes.

NEKTON always ensures that the Courant stability restriction:

$$\Delta t < C \times MIN_{D_F} \left\{ \frac{\Delta x}{|u_x|}, \frac{\Delta y}{|u_y|}, \frac{\Delta x}{|u_x|} \right\} \tag{A.1}$$

is satisfied. $C$ represent the Courant number (specified by the user), $\Delta x$, $\Delta y$, $\Delta z$, are the distances between the spatial collocation points, $u_x$, $u_y$, $u_z$, are the $x$, $y$, and $z$ velocities respectively. $MIN_{D_F}$ refers to the minimum over the entire flow field.

## A.2 Using NEKTON

Basically, three steps are involved in the use of NEKTON. The first step is the PRENEK session, which is an interactive graphical package where the computational domain (stationary or moving) is defined. It involves the specification of the geometrical fluid-solid domain (or mesh generation), the specification of the physical parameters entering in the problem (material properties, boundary and initial conditions), and the definition of the numerical(discretization,solver,i/o) parameters. Material properties such as density, effective thermal expansion coefficients, volumetric latent heat of fusion at a front, the melting temperature at a front, and the unit vector in the gravitational field direction are taken to be time-independent and constant (uniform in space). Other material properties such as the dynamic viscosity, surface tension coefficient, body force, volumetric specific heat, thermal conductivity, volumetric heat generation, convection heat transfer coefficient, and the environment temperature can vary with time, space and temperature (if applicable). The boundary conditions can be specified either as constants or Fortran functions, and can be of the Dirichlet (essential) type, Neumann (natural) type, or mixed types. In addition, for the case of fluid flow, the non-slip and non penetration boundary conditions are assumed at any fluid-solid interface. For time dependent problems initial conditions in the velocity and temperature fields can be specified as zero initial conditions or in the form of a Fortran function. Also, it is possible to read results from an earlier simulation, and use these as initial conditions. All this information is stored as Fortran codes, in files generated automatically by PRENEK. The next step, called NEKTON, is to use the computational engine that performs the numerical integration of the Navier-Stokes and energy equations employing the information generated in the PRENEK session. There is little influence of the user in NEKTON operation, except by the selection, in the PRENEK session, of the specific routines that should be invoked in order to solve a particular problem by using a particular formulation. Basically two formulations are available: SPLIT formulation, which determines whether the Navier-Stokes equations will be solved using the classical first-order splitting scheme (fractional step method), and the STRESS formulation which determines whether the stress formulation of the fluid flow equations will be used. The user can select whether or not to use a particular formulation, although each one of them is recommended for specific problems. For instance, the SPLIT formulation should be used in time-dependent problems involving high Reynolds number ($Re > 25$) because the splitting errors are of order $\nu\Delta t$ ($\nu$ being the dynamic viscosity and $t$ time step). At high $Re$ the viscosity is low and the time step is small due to stability restrictions. The non-STRESS formulation can be used for flows ranging from stokes flows (where $Re = 0$) through transition flows. However, it is slower than the SPLIT formulation by a factor of approximately four. It is worth mentioning that a general knowledge of the finite element method would be of value for an efficient application of the package or for a correct interpretation of diagnostics. Finally, an interactive graphical package can be used by the user in order to inspect and analyze the results. This is called the POSTNEK session (more details can be found in the NEKTON reference manual).

NEKTON can be obtained from:

FLUENT, INC.
10 Cavendish Court
Lebanon, NH 03766
USA

# Bibliography

[1] Adler, P. M. (1992). Porous Media, Geometry and Transports. Butterworth-Heinemann.

[2] Ahmed, N., & Sunada, D.K. (1969). J. Hydraul. Div. Proc. ASCE. **95**, 1847.

[3] Allaire, G. (1992). SIAM j. Math. Anal. **23**, 1482.

[4] Auriault, J.L. (1991). Int. J. Engng. Sci. **29**, 785.

[5] Batchelor, G.K. (1967). An Introduction to Fluid Dynamics. Cambridge Univ. Press.

[6] Bakhvalov, N., & Panasenko, G. (1989). Homogenization: Averaging Processes in Periodic Media. Kluwer Academic.

[7] Bender, C.M., & Orszag, S.A. (1978). Advanced Mathematical Methods for Scientists and Engineers. McGraw-Hill, New York.

[8] Bear, J. (1972). Dynamics of fluids in porous media. Elsevier.

[9] Beavers, G.S. & Sparrow, E.M. (1969). J. Appl. Mech. **36**, 711.

[10] Beavers, G.S., Sparrow, E.M., & Rodenz, D.E. (1973). J. Appl. Mech. **40**,655.

[11] Bensoussan, A., Lions, J. L., & Papanicolaou, G. (1978). Asymptotic Analysis for periodic structures, North-Holland, Ansterdam.

[12] Berkowitz, B., & Balberg, I. (1993). Water Resour. Res. **29**, 775.

[13] Broadbent, S.R., & Hammersley, J.M. (1957). Proc. Cambridge Philos. Soc. **53**, 629.

[14] Bryant, S.L., Mellor, D.W., & Cade, C.A. (1993). AICHE J. **39**, 387.

[15] Bunde, A. & Havlin, S. (Eds.) (1996). Fractals and Disordered Systems, $2^{nd}$ Edition, Springer.

[16] Burke, S.P., & Plummer, W.B. (1928). Ind. Eng. Chem. **20**, 1196.

[17] Canuto, C., Hussaini, M.Y., Quarteroni, A., & Zang, T.A. (1988). Spectral Methods in Fluid Dynamics, Springer-Verlag, Series in Computational Physics.

[18] Chandler, R., Koplik, J., Lerman, K. & Willemsen, J.F. (1982). J. Fluid Mech. **119**, 249.

[19] Chen, J.D., & Koplik, J. (1985). J. Colloid. Sci. **108**, 304.

[20] Cole, J. D. (1968). Perturbation Methods in Applied Mathematics. Blaisedell, Waltham, Mass.

[21] Cvetkovic, V. D. (1986). Transport in porous media **1**, 63.

[22] Domb, C., Green, M.S., & Lebowitz, J.L. (1972-1988). Phase Transitions and Critical Phenomena, vols. 1-12, Academic.

[23] Dullien, F.A.L. (1992). Porous Media, Fluid Transport and Pore Structure. Academic Press.

[24] Dybbs, A. & Edwards, R. V. (1984). in Fundamentals of Transport Phenomena in Porous Media, eds. Bear, J. & Corapcioglu, M. Y., Martinus Nijhoff Publishers (1984).

[25] Ergun, S. (1952). Chem. Eng. Prog. **48**, 88.

[26] Essam, J. W. (1980). Rep. Prog. Phys. **43**, 833.

[27] Fatt, I. (1956). Trans. Am. Inst. Min. Metall. Pet. Eng. **207**, 144.

[28] Fatt, I. (1956). Trans. Am. Inst. Min. Metall. Pet. Eng. **207**, 160.

[29] Fatt, I. (1956). Trans. Am. Inst. Min. Metall. Pet. Eng. **207**, 164.

[30] Gouyet, J.F. (1997). Physics and Fractal Structures, Springer.

[31] Happel, J. & Brenner, H. (1983). Low Reynolds Number Hydrodynamics, Kluwer Academic Publishers.

[32] Herrmann, H. J. (1986). Phys. Rep. **136**, 153.

[33] Hornung, U. (1996). Homogenization and Porous Media, Springer.

[34] Huang, K. (1987). Statistical Mechanics, $2^{nd}$ Edition, Wiley.

[35] Isichenko, M.B. (1992). Rev. Mod. Phys. **64**, 961.

[36] Jaeger, H.M., Nagel, S.R. & Behringer, R.P. (1996). Rev. Mod. Phys. **68**, 1259.

[37] Keller, J. B. (1980). in non-linear P.D.E.s in Engineering and Applied Science, ed. Sternberg et al., Marcel Dekker, New York (1980).

[38] Kikuchi, R. (1970). J. Chem. Phys. **53**, 2713.

[39] Kirkpatrick, S. (1971). Phys. Rev. Lett. **27**, 1722.

[40] Kirkpatrick, S. (1973). Rev. Mod. Phys. **45**, 574.

[41] Kirkpatrick, S. (1979). In Ill-Condensed Matter: Les Houches Lectures p. 423. Edited by Balian, R., Maynard, R., & Toulouse, G., North-Holland.

[42] Koplik, J. (1981). J. Phys. C **14**, 4821.

[43] Koplik, J. (1982). J. Fluid Mech. **119**, 219. See also ADDENDUM, Koplik, J. (1983), J. Fluid Mech. **130**, 468.

[44] Koplik, J. (1983). J. Fluid Mech. **130**, 468.

[45] Koplik, J., Lin, C., & Vermette, M. (1984). J. Appl. Phys. **56**, 3127.

[46] Koplik, J., & Lasseter, T.J. (1985). Soc. Pet. Eng. J. **25**, 89.

[47] Koplik, J., Redner, S., & Wilkinson, D. (1988). Phys. Rev. A **37**, 2619.

[48] Koplik, J. (1990). Lecture presented at the Les Houches Winter School "Physics of Granular Media" 20 February - 1 March.

[49] Kostek, S., Schwartz, M., & Johnson, D.L. (1992). Phys. Rev. B **45**, 186.

[50] Kyazym-zade, A.G. (1992). Sov. Phys. Semicond. **26**, 95.

[51] Ladyzhenskaya, O. A. (1963). The Mathematical Theory of Viscous Incompressible Flow, Gordon & Breach, New York.

[52] Lin, C., Pirie, G., & Trimmer, J. (1986). Geophys. Res. **91**, 2173.

[53] Lenormand, R. & Boris, S. (1980). C. R. Acad. Sci. (Paris). **291**, 279.

[54] Macdonald, I.F., El-Sayed, M.S., Mow, K., & Dullien, F.A.L. (1979). Ind. Eng. Chem. Fundam. **18**, 199.

[55] Martys, N., & Garboczi, E.J. (1992). Phys. Rev. B **46**, 6080.

[56] Matthews, G.P., Moss, A.K., Spearing, M.C., & Voland, F. (1993). Powder Technol. **76**, 95.

[57] Mei, C. C. & Auriault, J. L. (1991). J. Fluid Mech. **222**, 647.

[58] Murdock, J.A. (1991). Perturbations: Theory and Methods. Jhon Wiley & Sons, INC.

[59] Nayfeh, A. H. (1981). Introduction to Perturbation Techniques. Wiley, New York.

[60] Nayfeh, A. H. (1973). Perturbation Methods. Wiley, New York.

[61] Nekton Reference Manuals Vol. I(User's Guide) & Vol. II(Theory, Tutorials and Validation Problems) (1994). Fluent, Inc.

[62] Newman, L.M., & Schulman, L.S. (1981). J. Phys. A **14**, 1735.

[63] Press, H.W., Teukolsky, S.A., Vetterling, W.T., & Flannery, B.P. (1992). Numerical Recipes in FORTRAN, $2^{nd.}$ Edition, Cambridge University Press.

[64] Proudman, I. & Pearson, J.R.A. (1956). J. Fluid Mech. **2**, 237.

[65] Rubenstein, J. & Torquato, S. (1989). J. Fluid Mech. **206**, 25.

[66] Reddy, J.N. (1993). An Introduction to the Finite Element Method, $2^{nd.}$ Edition, McGraw-Hill.

[67] Sangani, A.S. & Acrivos, A. (1982). Int. J. Multiphase Flow. **8**, 343.

[68] Sahimi, M. (1993). Rev. Mod. Phys. **65**, 1393.

[69] Sahimi, M. (1994). Applications of Percolation Theory (Taylor and Francis, london)

[70] Sanchez-Palencia, E. (1980). Nonhomogeneous Media and Vibration Theory. Lectures Notes in Physics **127**, Springer.

[71] Scheidegger, A. E. (1974). The physics of flow through porous media, $3^{rd}$ Edition, University of Toronto Press.

[72] Sedov, L.I. (1993). Similarity and Dimensional Methods in Mechanics, $10^{th}$ Edition, CRC Press.

[73] Shante, V.K.S., & Kirkpatrick, S. (1971). Avd. Phys. **20**, 325.

[74] Stauffer, D., & Aharony, A. (1992). Introduction to Percolation Theory, $2^{nd}$ Edition, Taylor and Francis (London).

[75] Thompson, A.H., Katz, A.J., & Krohn, C.E. (1987). Adv. Phys. **36**, 625.

[76] Tritton, D. J. (1992). Physical Fluid Dynamics, $2^{nd}$ Edition, Clarendon Press (Oxford).

[77] Wilson, K.G. (1979). Sci. Am. **241**, 158.

[78] Wong, P., Koplik, J., & Tomanic, J.P. (1984). Phys. Rev. B **30**, 6606.

[79] Zick, A.A. & Homsy, G. M. (1982). J. Fluid Mech.**115**,13.

[80] Ziman, J.M. (1968). J. Phys. C **1**,1532.

# IMAGE EVALUATION
# TEST TARGET (QA-3)

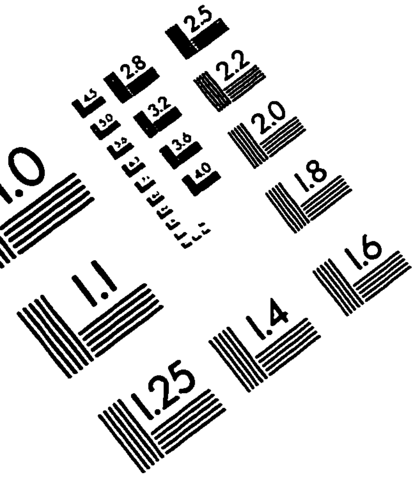

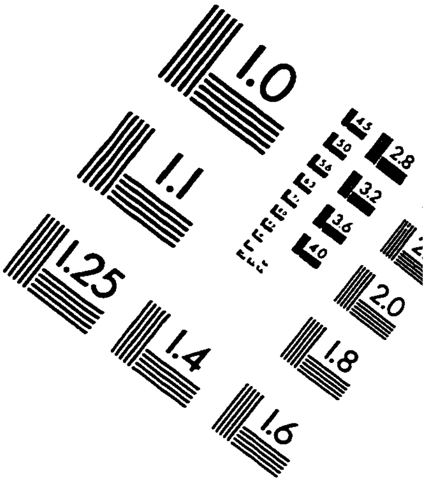

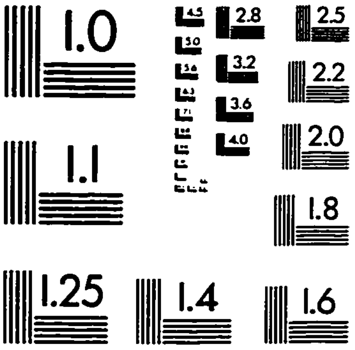

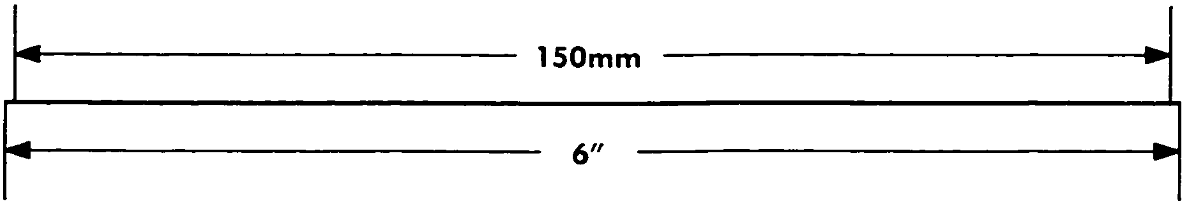

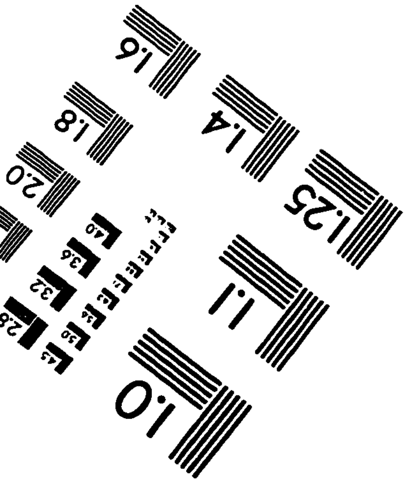

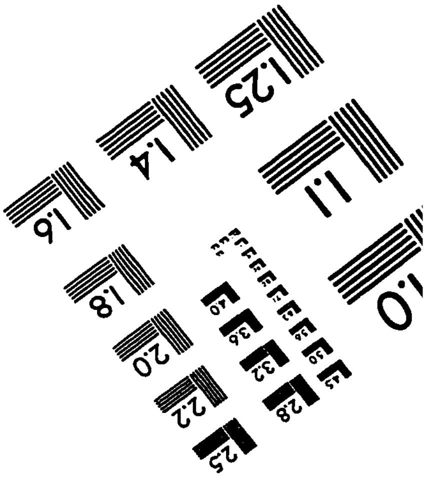

APPLIED IMAGE . Inc
1653 East Main Street
Rochester, NY 14609 USA
Phone: 716/482-0300
Fax: 716/288-5989